



# KOCAELI JOURNAL OF SCIENCE AND ENGINEERING

## Owner

Prof. Dr. Sadettin HÜLAGÜ - (Kocaeli University)

## Editor in Chief

Prof. Dr. K. Süleyman YİĞİT - (Kocaeli University)

## Editors

Prof. Dr. Murat HOŞÖZ - (Kocaeli University)  
Assoc. Prof. Dr. H. Hakan GÜREL - (Kocaeli University)  
Assoc. Prof. Dr. Mihriban CİVAN - (Kocaeli University)  
Asst. Prof. Dr. Recep Kaya GÖKTAŞ- (Kocaeli University)

## Production Editors

R.A. Abdurrahman GÜN - (Kocaeli University)  
Lecturer Yusuf YAĞCI - (Kocaeli University)

## Copy Editor (English)

Lecturer İsmail Hakkı PASLI - (Kocaeli University)

## Asistant Editors

Asst. Prof. Dr. Alp Eren ŞAHİN - (Kocaeli University)  
R.A. Abdurrahman GÜN - (Kocaeli University)

## Secretary

Durmuş İMAT - (Kocaeli University)

## Section Editors

Prof. Dr. Adem TEKİN (İTU)  
Prof. Dr. Adnan SÖZEN (Gazi University)  
Assoc. Prof. Dr. Ahmet SAYAR (Kocaeli University)  
Prof. Dr. Ahmet Ziyaettin ŞAHİN (KFUPM, S.A.)  
Prof. Dr. Aleksandrs SOSTAKS (University of Latvia)  
Assoc. Prof. Dr. Ali TÜRKCAN (Kocaeli University)  
Asst. Prof. Dr. Atakan ALKAN (Kocaeli University)  
Assoc. Prof. Dr. Başar UYAR (Kocaeli University)  
Prof. Dr. Beyhan PEKEY (Kocaeli University)  
Prof. Dr. Bülent ORUÇ (Kocaeli University)  
Prof. Dr. Cihan KARAKUZU (Bilecik Şeyh Edebali University)  
Prof. Dr. Dilek ODAÇI DEMİRKOL (Ege University)  
Asst. Prof. Dr. Dilek OKUYUCU (Erzurum Technical University)  
Asst. Prof. Dr. Ekin EKİNCİ (Sakarya University of Applied Sciences)  
Prof. Dr. Engin ÖZDEMİR (Kocaeli University)  
Prof. Dr. Fatma GÜLTEKİN (Karadeniz Technical University)  
Prof. Dr. Fatma KANCA (Fenerbahçe University)  
Prof. Dr. Günay ÖZTÜRK (İzmir Demokrasi University)  
Prof. Dr. Hakan PEKEY (Kocaeli University)  
Assoc. Prof. Dr. Halil YİĞİT (Kocaeli University)  
Assoc. Prof. Dr. Halim Aytekin ERGÜL (Kocaeli University)  
Prof. Dr. Hamid EL-QARNIA (Cadi Ayyad University)

Dr. Helena AZEVEDO (Queen Mary University of London)  
Prof. Dr. Hüseyin Metin ERTUNÇ (Kocaeli University)  
Prof. Dr. İulian STANASEL (University of Oradea)  
Asst. Prof. Dr. İbrahim MUTLU (Kocaeli University)  
Prof. Dr. Kerem KÜÇÜK (Kocaeli University)  
Asst. Prof. Dr. Mehlika KOCABAŞ AKAY (Kocaeli University)  
Asst. Prof. Dr. Mehmet Aytaç ÇINAR (Kocaeli University)  
Prof. Dr. Mehmet BAYRAK (Sakarya University)  
Prof. Dr. Mustafa ÇANAKCI (Kocaeli University)  
Asst. Prof. Dr. Mustafa Hikmet Bilgehan UÇAR (Kocaeli University)  
Assoc. Prof. Dr. Müslüm ARICI (Kocaeli University)  
Assoc. Prof. Dr. Oana Delia STANASEL (University of Oradea)  
Prof. Dr. Özer YILMAZ (Bursa Uludağ University)  
Prof. Dr. Semra BORAN (Sakarya University)  
Asst. Prof. Dr. Suhap ŞAHİN (Kocaeli University)  
Asst. Prof. Dr. Şaban Hakan ATAPEK (Kocaeli University)  
Prof. Dr. Tamer SINMAZÇELİK (Kocaeli University)  
Prof. Dr. Recep Taygun GÜRDAY (Kocaeli University)  
Prof. Dr. Yunus Emre ERDEMLİ (Kocaeli University)  
Prof. Dr. Zerrin ALADAĞ (Kocaeli University)  
Asst. Prof. Dr. Zeynep Hilal KİLİNCİ (Kocaeli University)

## Advisory Board

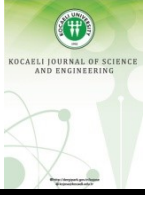
Assoc. Prof. Dr. Ahmet KARAKAŞ (Kocaeli University)  
Prof. Dr. Ali KILIÇARSLAN (Hitit University)  
Prof. Dr. Ali SÜRMEK (Uludağ University)  
Prof. Dr. Ata ATUN (Cyprus Science University)  
Asst. Prof. Dr. Ayşe Arzu ARI (Kocaeli University)  
Prof. Dr. Ayşe Nilgün AKIN (Kocaeli University)  
Assoc. Prof. Dr. Burcu ONAT (İstanbul University)  
Asst. Prof. Dr. Canan Dilek EREN (Kocaeli University)  
Prof. Dr. Cenk SAYIN (Marmara University)  
Prof. Dr. Dong LI (Northeast Petroleum University)  
Asst. Prof. Dr. Emre KİSHALI (Kocaeli University)  
Prof. Dr. Erhan PULAT (Bursa Uludağ University)  
Prof. Dr. Fadime SERTÇELİK (Kocaeli University)  
Prof. Dr. Hasan KÜRÜM (Firat University)  
Assoc. Prof. Dr. Hikmet SÜRMEK (Mersin University)  
Assoc. Prof. Dr. İlyas KANDEMİR (Gebze Technical University)  
Prof. Dr. Kamaruzzaman SOPIAN (The National University of Malaysia)  
Assoc. Prof. Dr. Kasım BAYNAL (Kocaeli University)  
Prof. Dr. Mehmet YILMAZ (Kocaeli University)  
Prof. Dr. Mehmet ARIK (Özyeğin University)

Assoc. Prof. Dr. Mehmet Ufuk KASIM (Kocaeli University)  
Assoc. Prof. Dr. Murat Selim ÇEPNİ (Kocaeli University)  
Prof. Dr. Nevim GENÇ (Kocaeli University)  
Prof. Dr. Nil Pembe ÖZER (Kocaeli University)  
Prof. Dr. Nilgün FİĞLALİ (Kocaeli University)  
Prof. Dr. Nurhan Turgut DUNFORD (Oklahoma State University)  
Prof. Dr. Oğuzhan URHAN (Kocaeli University)  
Assoc. Prof. Dr. Onur ÇOBAN (Kocaeli University)  
Prof. Dr. Oscar CASTILLO (Tijuana Institute of Technology)  
Prof. Dr. Özcan GÜNDOĞDU (Kocaeli University)  
Prof. Dr. Raşit KÖKER (Sakarya University)  
Prof. Dr. Rezzan KASIM (Kocaeli University)  
Prof. Dr. Safa Bozkurt ÇOŞKUN (Kocaeli University)  
Prof. Dr. Serdar İPLİKÇİ (Pamukkale University)  
Prof. Dr. Sezai TOKAT (Pamukkale University)  
Prof. Dr. Şeref Naci ENGİN (Yıldız Technical University)  
Prof. Dr. Tahsin ENGİN (Sakarya University)  
Assoc. Prof. Dr. Vildan ÇETKİN (Kocaeli University)  
Assoc. Prof. Dr. Wang FUQIANG (Harbin Institute of Technology)

## Printed By

Kocaeli University - Graduate School of Natural and Applied Sciences - Umuttepe Campus 41001, Kocaeli / TURKEY

Tel: +090 (262) 303 35 56 Fax: +090 (262) 303 30 33 E-mail: kojose@kocaeli.edu.tr



**COVER PAGE..... I**

**EDITORIAL AND ADVISORY BOARDS ..... II**

**TABLE OF CONTENTS..... III**

**Fusun YALCIN, Ahmet Mustafa TEPE, Güray DOĞAN, Nurfer ÇİZMECİ**

Spatial Regression Models for Explaining AQI Values in Cities of Turkey ..... 1-15

*(Research Paper)*

**Cevher Yusuf İNAN, Akın OKTAV**

Model Updating of a Euler-Bernoulli Beam Using the Response Method ..... 16-23

*(Research Paper)*

**Levent AYDIN, Sumeyya İLKİN, Mehmet Onur ARICAN, Ayfer PEKER,**

**Suhap ŞAHİN, Güralp ÖZKOÇ, Maksut Görkem AKSU, Serdar KÜÇÜK,**

**Özcan GÜNDOĞDU**

Development of Personal Protective Respirator Based on Additive

Manufacturing Technologies in Fighting Against Pandemic ..... 24-38

*(Research Paper)*

**Melda Güliz ATEŞ, Yıldız ŞAHİN**

Evaluation of Industry 4.0 Applications for Agriculture using AHP Methodology ..... 39-45

*(Research Paper)*

**Berrak ÖZGÜR**

Investigation Of Stability Changes In A Neural Field Model..... 46-50

*(Research Paper)*

**Ufuk YILDIZ**

Synthesis and Antioxidant Activities of Novel Naphthalimide Derivatives..... 51-58  
*(Research Paper)*

**Mert ÖKTEN**

An Investigation on Provincial Production & Consumption of Electric Energy:  
A Case Analysis for Ankara..... 59-68  
*(Research Paper)*

**Gökmen HASANÇEBİ, E. Mustafa YEĞİN, Korhan KARAARSLAN**

Fault Maintenance and Repair Application Based on Augmented Reality  
Technology in Electrical Distribution Systems ..... 69-78  
*(Research Paper)*

**Mehmet Furkan ÖZBEY, Cihan TURHAN**

A Case Study on the Assumption of Mean Radiant Temperature  
Equals to Indoor Air Temperature in a Free-Running Building..... 79-85  
*(Research Paper)*





## Spatial Regression Models for Explaining AQI Values in Cities of Turkey

Fusun YALCIN<sup>1,\*</sup> , Ahmet Mustafa TEPE<sup>2</sup> , Güray DOĞAN<sup>3</sup> , Nurfer CIZMECI<sup>4</sup> 

<sup>1</sup> Akdeniz University, Department of Mathematics, Antalya, 07058, Turkey, **ORCID:** 0000-0002-2669-1044

<sup>2</sup> Akdeniz University, Department of Environment Sciences, Antalya, 07058, Turkey, **ORCID:** 0000-0002-5210-6291

<sup>3</sup> Akdeniz University, Department of Environment Sciences, Antalya, 07058, Turkey, **ORCID:** 0000-0003-0481-8080

<sup>4</sup> Ministry of Education, Antalya, 07058, Turkey, **ORCID:** 0000-0002-5275-6120

### Article Info

#### Research paper

Received : October 01, 2020

Accepted : December 01, 2020

#### Keywords

Exploratory Spatial Data Analysis (ESDA)

Air Quality Index (AQI)

Spatial Regression Models

Moran's I

Local Indicators of Spatial

Association (LISA)

### Abstract

The aim of this study is to determine the natural and anthropogenic factors affecting the air quality index (AQI) and to create a model that shows the effects of these factors on AQI values in cities of Turkey. Natural and anthropogenic factors, which are thought to have an effect on AQI, were determined and interpreted with kriging maps. The effects of these factors on AQI were examined by explanatory spatial data analysis (ESDA). Global Moran's I and local Moran's I (LISA) indices were examined for the presence of spatial relation. Spatial lag model (SLM) was proposed for parameter estimation instead of ordinary least squares method (OLS) and the average AQI values for 2014 and 2015 were compared. It was also concluded that the average AQI values of 2014 and 2015 were in a strong correlation relationship (Pearson correlation coefficient of 0.914). On the Southern Anatolia, desert dust transport decreases the air quality of the region, however on the Black Sea coast, meteorological factors have a strong effect on air quality. Both SLM and OLS models showed that higher wind speed increases air quality in the cities while increase in GDP increases AQI.

## 1. Introduction

Low air quality has a negative effect on human health, vegetation, structures, ecosystem, and climate. Worldwide, 3.8 million premature deaths annually are attributed to ambient air pollution. Average particulate air pollution levels in many developing cities can be 4-15 times higher than World Health Organization (WHO) air quality guideline levels [1]. Ozone, which is formed as a result of the reaction of volatile organic compounds and nitrous oxides through sun rays in the troposphere, has a negative effect on human health and harms agricultural products and ecosystems [2-4]. Sulfur dioxide, another important anthropogenic pollutant, is released as a result of the burning of fossil fuels containing sulfur and causes acid

rains to occur in case of long-distance transport [5].

The air quality index (AQI) was developed to evaluate all atmospheric pollutants together in the urban environment and to easily share air quality with people. AQI, which was developed primarily in the USA, was used similarly in almost all of the world. AQI is generally calculated for particulate matter, carbon monoxide (CO), Sulfur dioxide (SO<sub>2</sub>), Nitrogen dioxide (NO<sub>2</sub>) and Ozone (O<sub>3</sub>) [6].

There are lots of studies carried out on the parameters affecting the air quality in the urban atmosphere in various parts of the worlds [7-11] and in Turkey [12-20]. These studies generally focused on the effects of urban pollution sources. However, the effects of regional processes and regional sources on AQI were not emphasized. Therefore, in those studies, regional drivers of urban air pollution are underestimated. In order to understand the spatial dependence in air quality, Local indicators of spatial association (LISA) analysis can be used. This analysis,

\* Corresponding Author: [fusunyalcin@akdeniz.edu.tr](mailto:fusunyalcin@akdeniz.edu.tr)



which assumes a spatial dependence, has been used in many areas where the local impact is considered in recent years [21-24].

In this study, it is aimed to identify the important parameters that have a negative and positive impact on air quality of urban atmospheres of Turkey for the year 2015. With the use of the results of the analysis, regional associations and differences in AQI were also investigated. In addition, the results of this research were helpful for the identification of the regionally effective parameters on AQI. These data for 2015 are compared with the data for 2014 that have been previously published [25]. The MATLAB, ArcGIS 10.2 and GeoDA programs were used to create the exploratory spatial data analysis (ESDA), global Moran's I and local Moran's I index calculation, ordinary least squares (OLS), spatial lag model (SLM) and spatial error model (SEM), which we use to estimate the spatial distribution of the air quality index and the factors affecting it.

## 2. Materials and Methods

### 2.1. Study Area

Turkey is located on Eastern Mediterranean basin. Turkey is the 37th largest country, with a total area of about 783 600 km<sup>2</sup> however, it is the 17th most populous country with a population of approximately 84 million. There are 81 cities in Turkey and 23 of these have populations above one million. The rainfall and temperature pattern of Turkey is controlled by four pressure centres located over Basra, Azor, Siberia and Iceland. In summer, meteorology of Turkey is under influence of Basra low pressure centre and Azor high pressure centre. However in winter, Siberia high pressure center and Iceland low pressure centers, which cause colder climatic conditions and more precipitation, respectively, are more effective in Turkey. The climatic conditions differ significantly due to existence of the mountains that run parallel to the coasts. The coastal regions areas have a milder climate and the inner plateau of Anatolia has hot summers and cold winters with limited rainfall [26].

### 2.2. Data

Air quality index values of the year 2015 were calculated from data obtained from air quality monitoring stations operated by Ministry of Environment and Urbanization. The AQI data for 2014 were taken from the previous study [25],[27]). The General Directorate of Meteorology provided daily, temperature, precipitation, wind speed and direction, relative humidity, atmospheric

pressure, sunshine duration, mixture height, intraday temperature change and cloudiness data. Then, some of these data were re-arranged as "annual average" and others as "annual total". Vehicle density, altitude, urban population, total population, population density, urbanization, per capita national income data were obtained from Turkey statistical institute (TSI). Descriptions of these data are given in Table 1.

**Table 1.** Descriptions of variables.

Independent variables	Unit	Brief descriptions of the variables
AQI		Air Quality Index
Wind Speed	m/s	Annual Average Wind Speed of Cities
Average Actual Pressure	kPa	Annual Average Pressure of Cities
Average Humidity		Annual Average Humidity of Cities
Google Altitude(M)	m	Cities' Altitudes Above Sea Level
Average Sunshine Duration	hour	Annual Average Sunbathing of Cities
Total Precipitation	mm	Annual Average Rainfall of Cities
Average Temperature	0C	Annual Average Temperature of Cities
Number of Automobiles Per Capita	car/person	Number of Cars Per Year Per Person in Cities
Number of People Per Car	person/car	Number of Cities Per Annual Car
Secon-Ind	TL	Gross Domestic Product by City (for industry) Branch of Economic Activity
GDP	TL	Gross National Product by City
Per capita GDP	TL	Gross Domestic Product per Capita by Province
Number of Vehicles		Annual Total Number of Vehicles in Cities
Total Population		Annual Total Population of Cities
Population Density	/km <sup>2</sup>	Annual Population Density of Cities
Urbanization Rate	%	Urban population / Total population

Data such as "gross annual product per capita", gross domestic product (GDP-S) for industry according to the economic activity branches on a provincial basis, gross domestic product per capita (GDP-K) and GDP-B for second level classification of statistical regional units, which are considered to have an impact on air quality, have been obtained from TSI.

Using the "Ordinary kriging spherical model", annual average humidity (Figure 1(a)), annual average pressure (Figure 1(b)), annual total precipitation (Figure 1(c)), annual average temperature (Figure 1(d)), and total population maps (Figure 1(e)) were prepared.

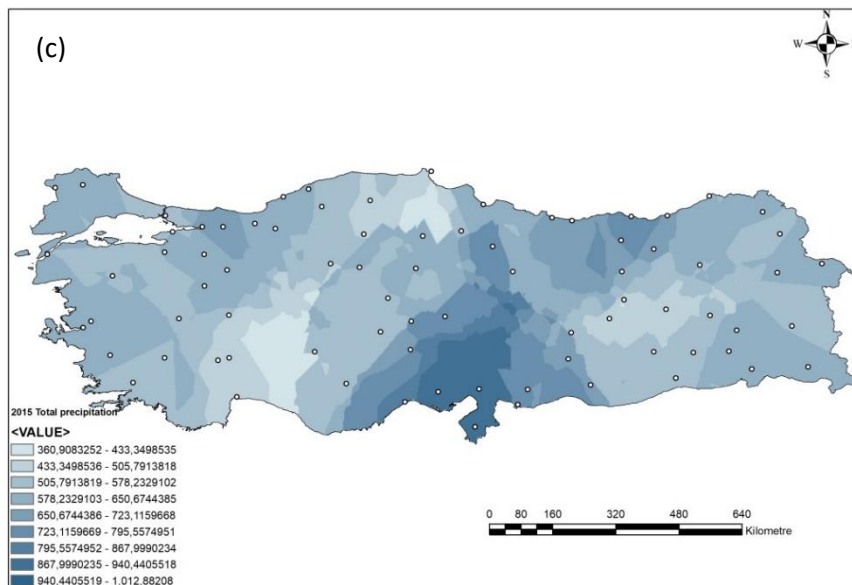
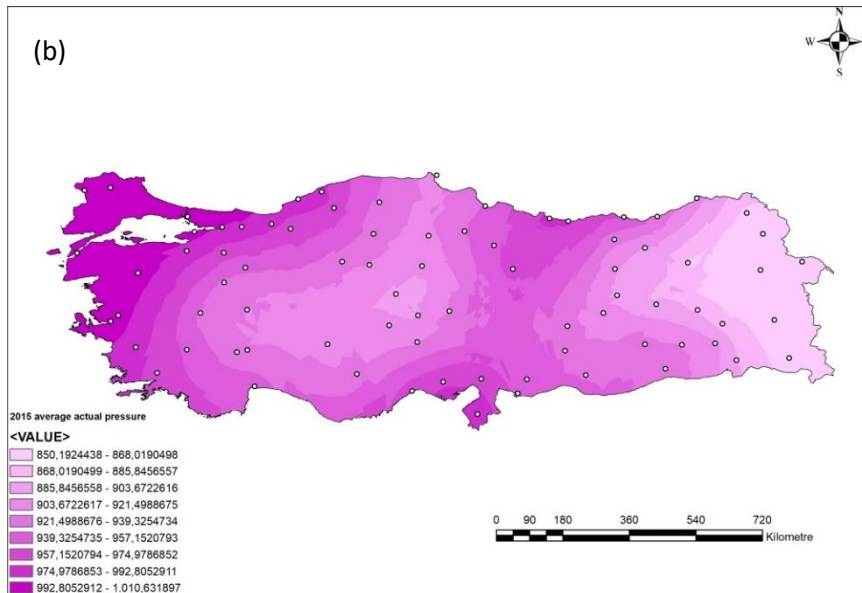
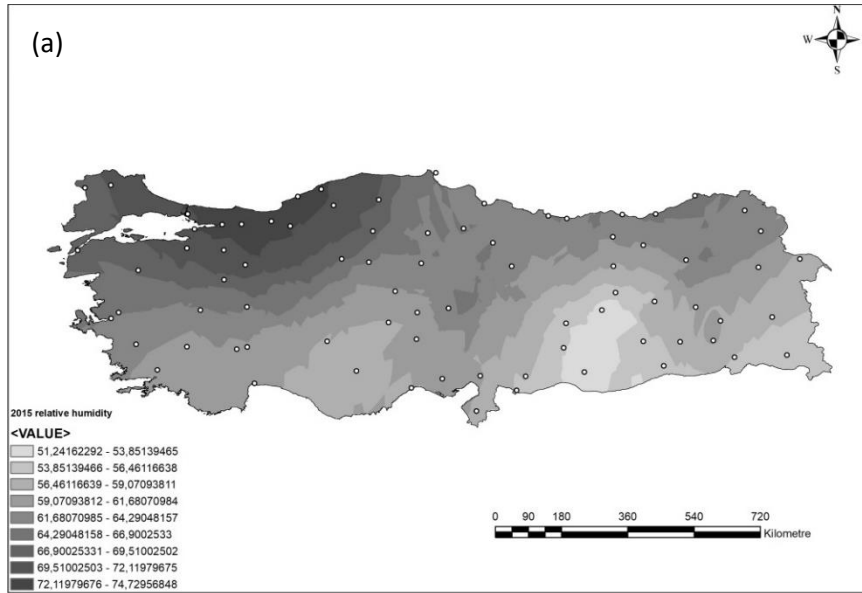


Figure 1. Location map and kriging maps.

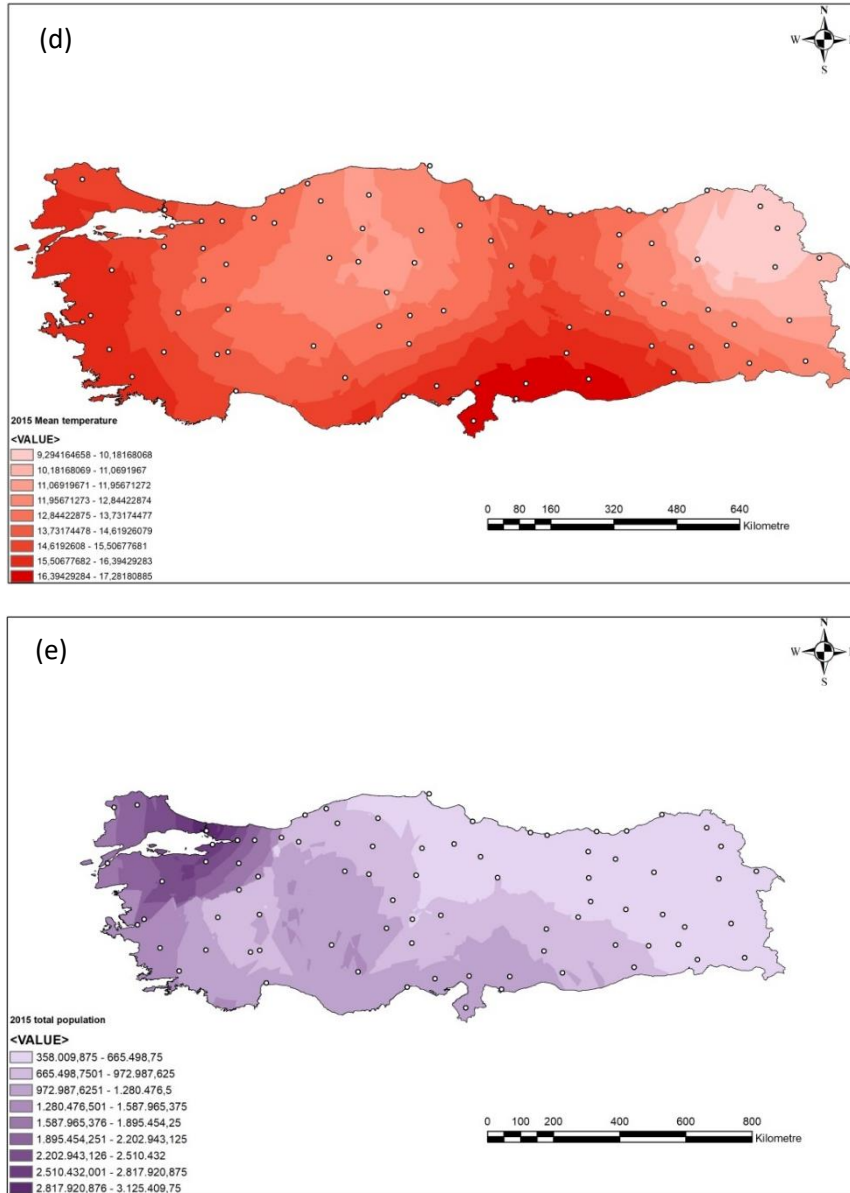


Figure 1. (Cont.) Location map and kriging maps.

Descriptive statistics of variables for spatial models are given in Table 2. In 2015, the lowest AQI value was calculated in Eskişehir with 64, the highest AQI value was 608 and was calculated in Bolu. Incomplete data in the average sunshine duration and total precipitation were completed with the series mean method. Variation Inflation Factor (VIF) related to linear multiple connection problem was investigated. Accordingly, variables with  $VIF > 10$  are not included in the model.

### 2.3. Air Quality Index Calculation

The air quality data used in this study were obtained from air quality monitoring stations operated by the Ministry of Environment and Civilization of Turkey [28]. There was at least one air quality monitoring station in

every city that measures at least  $PM_{10}$  and  $SO_2$ . If there were more than one monitoring station for a city, then the one that represents the urban background in the downtown area was selected and used in this study.

The data coverage was from January 2014 to December 2015. Before the use of the data, a quality control check was done based on the correlation of data with each other and extraordinary results were excluded from the data set. The AQI is an index for reporting daily air quality and its health effects by converting the observed concentrations to a number on a range of 0 to 500. An AQI level lower than 50 means that pollutants will not have any significant effect to anyone. If the AQI levels are at or higher 51, the air quality level defined as moderate, while values below 50 considered satisfactory. Table 3 shows the categories of AQI, the range of pollutant concentrations

and index values for each category.

The AQI values represent the maximum air quality sub-index of the following pollutants: PM<sub>10</sub>, O<sub>3</sub>, SO<sub>2</sub>, NO<sub>2</sub>, and CO. AQI is calculated, according to the Turkish standard, by using the pollutant concentration data from Eq. (1):

$$I_p = \frac{I_{Hi} - I_{Lo}}{BP_{Hi} - BP_{Lo}} (C_p - BP_{Lo}) + I_{Lo} \quad (1)$$

where  $I_p$  is the air quality index for pollutant  $p$ ,  $C_p$  is the monitored concentration of pollutant  $p$ ,  $I_{Hi}$  is the maximum air quality index value for color category that corresponds to  $C_p$ ,  $I_{Lo}$  is the minimum air quality index value for color category that corresponds to  $C_p$ ,  $BP_{Hi}$  is the maximum concentration of air quality index color category that

contains  $C_p$ ,  $BP_{Lo}$  is the minimum concentration of air quality index color category that contains  $C_p$ . Final AQI of a city is determined as the maximum  $I_p$  value for a given time. In almost all cases, AQI calculated for PM<sub>10</sub> was the maximum value. Therefore, daily AQI values of the cities were calculated for the years 2014 and 2015 and those AQI values were used for further analysis. There are 81 provinces in Turkey and except for Bolu, daily AQI was calculated for each province for the years 2014 and 2015. For Bolu, daily AQI values calculated using daily average values of SO<sub>2</sub> values because PM<sub>10</sub> data of Bolu was not available. Finally, the data was transformed into spatial data by adding the coordinates of the cities to which they belong.

**Table 2.** Descriptive statistics of the dependent and explanatory variables for 2015 years.

	N		Mean	Std. Deviation	Variance	Min.	Max.
	Valid	Missing					
AQI	81	0	175.447	95.828	9183.022	64	608.96
Wind Speed	81	0	1.777	0.676	0.457	0.6	3.786
Average Actual Pressure	81	0	938.401	60.874	3705.654	819.199	1017.386
Average Humidity	81	0	62.634	9.312	86.708	43.088	87.86
Google Altitude(M)	81	0	691.469	554.694	307684.927	4	1923
Average Sunshine Duration	64	17	6.204	1.286	1.654	1.596	8.378
Total Precipitation	76	5	673.499	401.505	161206.232	110.7	2390
Average Temperature	81	0	13.933	3.199	10.236	4.989	19.98
Number of Automobiles Per Capita	81	0	0.11	0.052	0.003	0.007	0.232
Number of People Per Car	81	0	16.455	22.437	503.431	4.311	136.654
Secon-Ind	81	0	24.374	9.350	87.416	8.17	50.458
GDP	81	0	28872191.272	84018762.234	7059152407365370	1428560	722567040
Percapita GDP	81	0	22668.494	7741.654	59933202.453	9657	49773
Number of Vehicles	81	0	246845.333	466433.285	217560009188.4	7851	3624403
Total Population	81	0	972111.765	1766432	3120282010079.6	78550	14657434
Population Density	81	0	124.682	314.226	98738.216	11.582	2820.907
Urbanization Rate	81	0	0.012	0.022	0.001	0.001	0.186

**Table 3.** Pollutant concentrations for each AQI category of according to Turkish-AQI [28].

Index Values	Category	SO <sub>2</sub> (1-hr) (µg/m <sup>3</sup> )	NO <sub>2</sub> (1-hr) (µg/m <sup>3</sup> )	CO (8-hr) (mg/m <sup>3</sup> )	O <sub>3</sub> (8-hr) (µg/m <sup>3</sup> )	PM <sub>10</sub> (24-hr) (µg/m <sup>3</sup> )
0-50	Good	0-100	0-100	0-5.5	0-120	0-50
51-100	Moderate	101-250	101-200	5.5-10	121-160	51-100
101-150	Unhealthy for sensitive groups	251-500	201-500	10-16	161-180	101-260
151-200	Unhealthy	501-850	501-1000	16-24	181-240	261-400
201-300	Very unhealthy	851-1100	1001-2000	24-32	241-700	401-520
300-500	Severe	>1101	>2001	>32	>701	>521

### 2.4. Exploratory Spatial Data Analysis (ESDA)

Exploratory spatial data analysis (ESDA) is frequently used in many fields of basic and social sciences. The first studies were generally on biology and ecology, but especially the map studies by Jhon Snow on a cholera epidemic in London in 1854 contributed to this method [29]. ESDA studies on air quality have been widely seen in the literature in recent years [10], [30-33]. The phrase "everything is related to everything else, but close things are more related to distant things", known as Waldo Tobler's basic law of geography, is known as the leading sentence for spatial studies [34]. Based on this idea, we wanted to examine whether the AQI index values are affected by neighboring cities. The concept of spatial dependence is similar to the autocorrelation that was encountered in time series [35]. Therefore, spatial dependence can be called spatial autocorrelation. Spatial autocorrelation can offer versatile dependence, unlike the one-way dependency in time series. Spatial dependence shows the degree of spatial relationship between similar units in a geographical region and error terms [36]. In this context, there are different indices that measure spatial dependence. The most frequently used ones can be listed as "Moran's I", "Geary's C" and "General G" [37-41], [10]. Spatial autocorrelation can be examined in two ways, local and global. Local spatial autocorrelation (Local Indicators of Spatial Association-LISA) has been defined to determine the "relationship between close neighbors". Global spatial autocorrelation is defined to determine the "spatial relationship of the entire region" [42-45]. In this study, Moran's I indices, which are frequently used in the literature, are used.

LISA, one of the spatial statistical analysis methods, was developed with an index determined by Moran in 1948 [46]. This study was extended by Anselin in 1995 [47]. It is used to examine the relationship between neighboring regions. A weight matrix is created depending on the

geographical or political proximity of the neighbors.  $W = (w_{ij}; i, j = 1, \dots, n)$  is the  $n \times n$  positive matrix as Eq. (2) [47]

$$\begin{bmatrix} w_{11} & w_{12} & \dots & w_{1n} \\ w_{21} & w_{22} & \dots & w_{2n} \\ \vdots & \vdots & \ddots & \vdots \\ w_{n1} & w_{n2} & \dots & w_{nn} \end{bmatrix} \quad (2)$$

The weight matrix, which is used to determine the neighborhood, can be defined as; if  $i$  and  $j$  "neighbors", then  $W_{ij} = 1$ , else  $W_{ij} = 0$  [48]. The spatial autocorrelation value for each region is calculated with LISA. The GeoDa program is frequently used for the creation of maps and for the calculation of Local Moran's I [47].

The local Moran's I (LISA) used to determine local spatial autocorrelation is as Eqs. (3-5).

$$I_i = \frac{Z_i}{k_2} \sum_j w_{ij} Z_j \quad (3)$$

$$k_2 = \frac{\sum_i Z_i^2}{N} \quad (4)$$

$$I = \sum_i \frac{I_i}{N} \quad (5)$$

where,  $I_i$  is the local spatial autocorrelation;  $N$ , number of observations;  $Z_i$  is the deviation from the average. In other words, Moran calculates autocorrelation by looking at the correlation between the variable of interest and the spatial average of that variable. Spatial average of a variable is calculated by taking the average of that variable value in the neighbors. The results are described in four categories; high-high, low-low, high-low and low-high. For example, a low-high relation indicates that once the AQI in province A is low, the average AQI of the neighboring provinces of province A is high. If there is also province B which shows similar pattern around province A, than province A and B are grouped. This indicates that these two provinces are under the influence of same regional source or process.

Global spatial autocorrelation for Global Moran's I is calculated as Eqs. (6-7):

$$I = \frac{n}{S_0} \frac{\sum_{i=1}^n \sum_{j=1}^n w_{ij} (x_i - \bar{x})(x_j - \bar{x})}{\sum_{i=1}^n (x_i - \bar{x})^2} \quad (6)$$

$$S_0 = \sum_{i=1}^n \sum_{j=1}^n w_{ij} \quad (7)$$

where,  $n$  is the number of cities;  $x_i$  and  $x_j$  is the AQI of a spatial location  $i, j$  [49]. Global Moran indices take values between -1 and +1.

### 2.5. Spatial Models

In many similar scientific studies, the standard approach was started by developing the non-spatial linear regression model and then, by developing the model by examining the spatial interaction effects of the model [50-52]. Linear regression models are often estimated by Ordinary Least Square (OLS). Spatial regression models, on the other hand, are assumed to be in correlation between each other, as opposed to traditional regression analysis [35].

In this study, it was started with the idea that neighboring provinces may have affected AQI values. It was studied with the idea that independent variables may also be affected by the neighborhood between provinces. SLM and SEM models were used to determine these interactions [53-54]). SEM model:

$$Y = \alpha t_n + X\beta + \lambda W u + \varepsilon \quad (8)$$

$$\varepsilon \sim N(0, \sigma^2 I_n)$$

where  $Y$  denotes an  $N \times 1$  vector the dependent variable for every unit in the sample ( $i = 1, \dots, N$ );  $t_N$  is an  $N \times 1$  vector of ones associated with the constant term parameter  $\alpha$ ;  $X$  denotes an  $N \times K$  matrix of exogenous explanatory variables;  $\beta$  is a  $K \times 1$  vector of parameters;  $\lambda$  is the spatial autocorrelation parameter;  $W$  denotes an  $N \times N$  spatial weight matrix;  $u$  is an  $N \times 1$  vector of residual and  $\varepsilon$  is a vector of normally distributed errors.

SLM model:

$$Y = \alpha t_n + X\beta + \rho W Y + \varepsilon \quad (9)$$

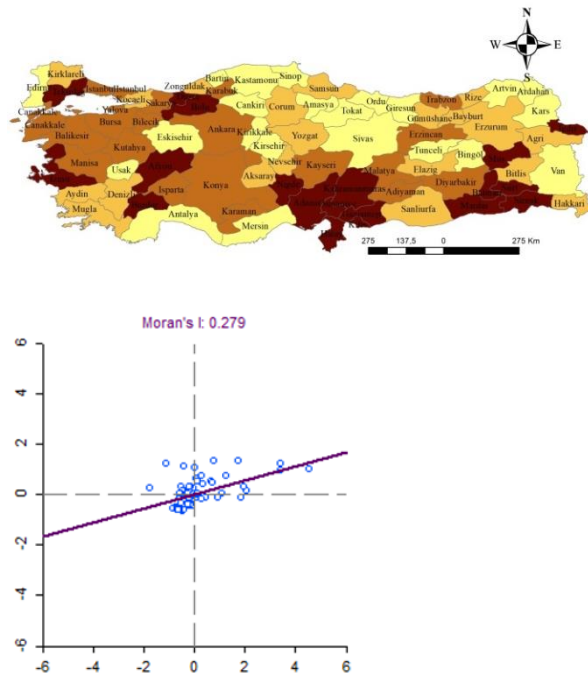
$$\varepsilon \sim N(0, \sigma^2 I_n)$$

where  $\rho$  is the auto-regressive parameter [53-54],[10]. In this study, parameter estimates were obtained by ordinary least squares Estimation (OLS) method. All spatial regression modeling was conducted using Anselin's Geoda Space and Geoda software. We used ArcGIS 10.6 and Geoda to generate maps.

## 3. Results and Discussion

### 3.1. Spatial Relationship Results for AQI

In the literature, there are studies that take the AQI as the dependent variable (i.e. the variable described). In this study, we examined which independent variables we can explain the AQI. We also examined whether there is a spatial relationship in the global and local sense. Based on this relationship, we wanted to suggest a model. Both cluster maps and Moran I index calculations proved that the air quality index and other variables show a spatial distribution. The spatial distribution maps for AQI (Figure 2) showed that all the variables determined were affected positively from neighboring provinces (i.e., the increase in the value of one province also increased in the neighboring province) Moran's I value was obtained as 0.279.



**Figure 2.** Spatial distribution of the AQI and Moran's I value for 2015 years.

In this study, spatial regression models were applied instead of the traditional regression model to investigate the relationship between the air quality index and meteorological and anthropogenic factors. The results of the variables showed that the independent variables determined for the spatial regression model are in a strong spatial relationship. These results show that AQI values are positively affected by neighboring provinces. These results are consistent with study in China [55].



### 3.2. Spatial Model Selection for AQI

For the error estimation of AQI, the ordinary least squares (OLS) method and classical regression model followed by the Spatial Error Model (SEM) was studied using MATLAB and Stata14 programs.

While choosing the spatial model, it was examined whether the spatial effect was caused by the error term or by delay. Yalcin et al. [25] worked with the data of the year 2014 and found out that the coefficient of determination (R2) of the OLS model was 0.2102, while R2 for the SEM was 0.2478. This result showed that a SEM is a better model than the OLS model. Also, the value of  $\rho$  in the model is 0.680 which is statistically significant.

Similarly, spatial analysis was made for data of the year 2015. It was concluded that the spatial effect occurred without spatial delay (probability values  $0.070 < 0.079$ ). For this reason, SLM model has been proposed. For the year 2015, the model's R2 with OLS was 0.238, whereas for SLM, the R2 was 0.290. This result showed that a SLM

was a better model than the OLS regression model. At the same time, the  $\rho$  value in the model was 0.320 and was statistically significant (Table 4). This value indicates that a 1% increase in the AQI value in one province causes a 3.2% increase in the AQI value in the neighboring provinces.

Results indicates that both OLS and SLM models showed statistically significant negative correlation with wind speed. It is well known that as the wind speed increases fresh air dilutes the polluted air in the cities and hence, AQI decreases. The GDP, on the other hand, showed statistically significant ( $p < 0.05$ ) positive correlation. This fact indicated that, although the coefficients were low, as the GDP of the cities increases, people tend to release more pollution to air. Finally, number of people per car data had a positive correlation in SLM model. The other parameters such as humidity, altitude, total precipitation, total population also showed correlation but their significance were between 0.10 and 0.05.

**Table 4.** OLS and SLM Model Coefficients for 2015.

Variables	OLS	SLM	Spatial Relationship	Value	Probability value
CONSTANT	1.8997**	2.365**			
Wind speed	-18.3913**	-16.5763**	Moran's I(error)	2.9484	0.003
Average Actual Pressure	-0.5737*	-0.4613	Log-Likelihood	-471.384	
Average Humidity	5.4329*	4.8364*	LM (lag)	3.2805	0.070
Google Altitude(M)	0.05644*	0.0525*	Robust LM (lag)	0.2239	0.636
Average Sunshine Duration	9.2518	10.1284	LM (error)	3.0793	0.079
Total Precipitation	-0.009303*	-0.011*	Robust LM (error)	0.0227	0.636
Average Temperature	20.1848	17.5375	LM (SARMA)	3.3032	0.191
Number of people per car	0.1878	0.056**			
GDP	0.002***	0.0003**			
Per capita GDP	-0.00002*	-0.003			
Total Population	-0.731*	-0.7338*			
Population Density	0.2760*	0.2338			
W= $\rho$		<b>0.320***</b>			
AIC	980.664				
SIC	1021.370				
R-squared	0.238				
Pseudo R-squared		0.290			

\*: %10 significant; \*\*: %5 significant; \*\*\*: %1 significant

### 3.3. LISA Map Results

For local spatial autocorrelation a result, local Moran's I indices of each city's AQI were calculated and were showed in Figure 3 and Figure 4 for the years 2014 and 2015, respectively.

The local Moran's I index results are between 0 and 1. There is said to be a correlation when the index value is greater than 0. The correlation is stronger as the index

value approaches to 1. The local Moran's I index for AQI values were calculated as 0.239 and 0.300 for the years 2014 and 2015, respectively. This result shows that according to AQI values more cities were correlated by each other in 2015.

LISA maps the year 2014 showed that 7 cities in two regions were categorized as high-high, 5 cities in two regions classified as low-low. In addition, the neighboring relationship was not statistically significant for 69



provinces. High-high relations were observed in Zonguldak, Bolu and Düzce provinces on Black Sea region and Mardin, Diyarbakır, Batman and Siirt provinces in Southeastern Anatolia. AQI values for the year 2014 of Zonguldak, Bolu and Düzce provinces, showed statistically significant correlation ( $p < 0.01$ ) with Pearson correlation coefficient varying between 0.602 (Zonguldak-Bolu) and 0.735 (Zonguldak-Düzce). The AQI of these provinces were statistically higher than the surrounding provinces. There are no strong natural source affecting this region. Therefore, anthropogenic emissions, especially coal combustion for household heating, seems to be the major source of pollution. Similar meteorological activity in the area could have a negative effect on accumulation of air pollutants in the atmosphere resulting in higher AQI. In the Southeastern Anatolia region, AQI for the year 2014 of the four provinces (Mardin, Diyarbakır, Batman and Siirt) also showed statistically significant correlation ( $p < 0.01$ ) with Pearson correlation coefficient varying between 0.330 (Batman-Mardin) and 0.728 (Diyarbakır-Mardin). Winter season household heating in the area is expected to be the major local source. However, there is a very strong natural source in the region: desert dust transport from Arabian Peninsula [56]. The dust transport from Arabian Peninsula seems to increase AQI values in the region.

For the both of the low-low zones observed in 2014, the AQI values were observed lower than the surrounding provinces. The reason of low AQI from the surrounding provinces could be due to lower pollutant emissions than the surrounding provinces or have a different meteorological condition that increases the air quality of the regions. In general, we do not expect to see lower emissions from the surrounding provinces under same meteorological activities, but location of the downtown area might have an effect on such observation.

LISA maps of AQI values for 2015 showed us that. Eight provinces in two regions were categorized as high-high, eight provinces were grouped as low-low in one region and two provinces were clustered as low-high. In addition, the neighboring relationship was not statistically significant for 63 cities. The low-low zone for the year 2015 in the Central Black Sea coast and composed of Kırıkkale, Çorum, Kastamonu, Sinop, Samsun, Ordu, Tokat and Amasya provinces. On the east of the low-low region, there was a low-high region consist of Bartın and Zonguldak provinces. AQI values for the year 2015 of

these low-low and low-high classified nine provinces, showed statistically significant correlation ( $p < 0.01$ ) with Pearson correlation coefficient varying between 0.265 (Kırıkkale-Sinop) and 0.845 (Çorum-Tokat). The results indicate that the meteorological conditions on the Central Black Sea coast together with some central Anatolia region decreases the AQI of the area. On the south of low-high region, there was a high-high cluster. This cluster was composed of Sakarya, Düzce and Bolu provinces. Daily AQI values for the year 2015 of these three provinces showed statistically significant correlation ( $p < 0.01$ ) with Pearson correlation coefficient varying between 0.320 (Sakarya-Bolu) and 0.749 (Düzce-Bolu). These three cities AQI values also showed statistically significant correlation with low-low and low-high provinces located on the Black Sea coast and Central Anatolia region ( $p < 0.05$ ). This indicates that AQI show similar pattern for this group of provinces. As indicated previously, there is not any regional natural source in the region. The only regional parameter is the meteorological events (precipitation and wind speed). These parameters could vary from province to province due to the topography of the downtown area. Therefore, this high-high relation could be a result of local anthropogenic emissions and similar negative effect of meteorological events. The second high-high cluster was on the south Anatolia and composed of Niğde, Adana, Kilis and Osmaniye and Antakya provinces. Daily AQI values for the year 2015 of these three provinces showed statistically significant correlation ( $p < 0.01$ ) with Pearson correlation coefficient varying between 0.439 (Niğde-Antakya) and 0.845 (Antakya-Osmaniye). In Adana, agriculture and agriculture related industry is dominant. In between Adana, Antakya and Osmaniye provinces, İskenderun Heavy Industry Zone is located. However, in the downtown area of the other provinces, there is not any important industrial area. Therefore, this high-high trend in the region could not be due to local or regional anthropogenic emissions. As indicated earlier, the South Eastern part of Anatolia region is under influence of desert dust transport from Arabian Peninsula. Also, studies conducted in this region showed that desert dust transport from Northern Africa increases the particulate matter concentrations in the region [57-58]. Therefore, the regional dust transport has a negative effect on AQI of these cities.

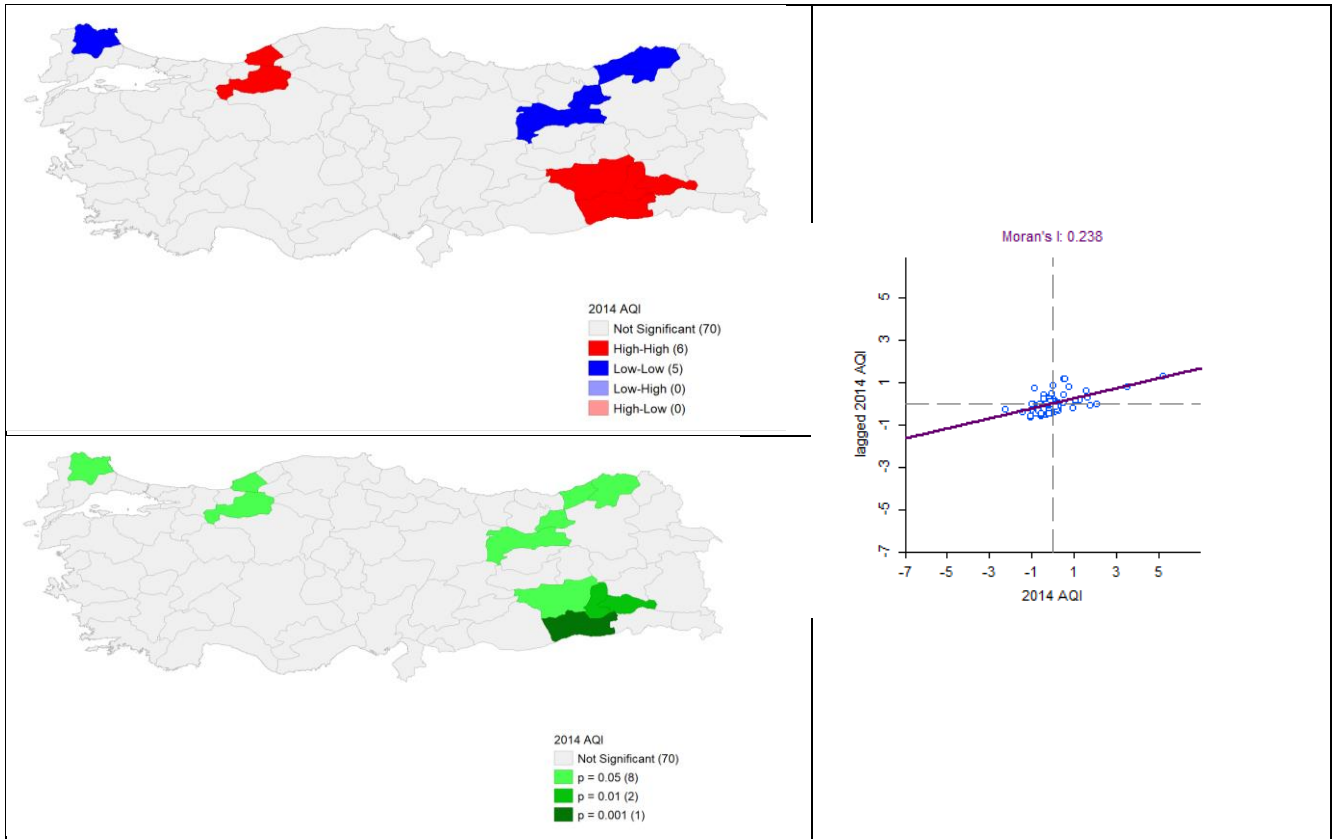


Figure 3. AQI Local Moran's I Graph and LISA Map for 2014.

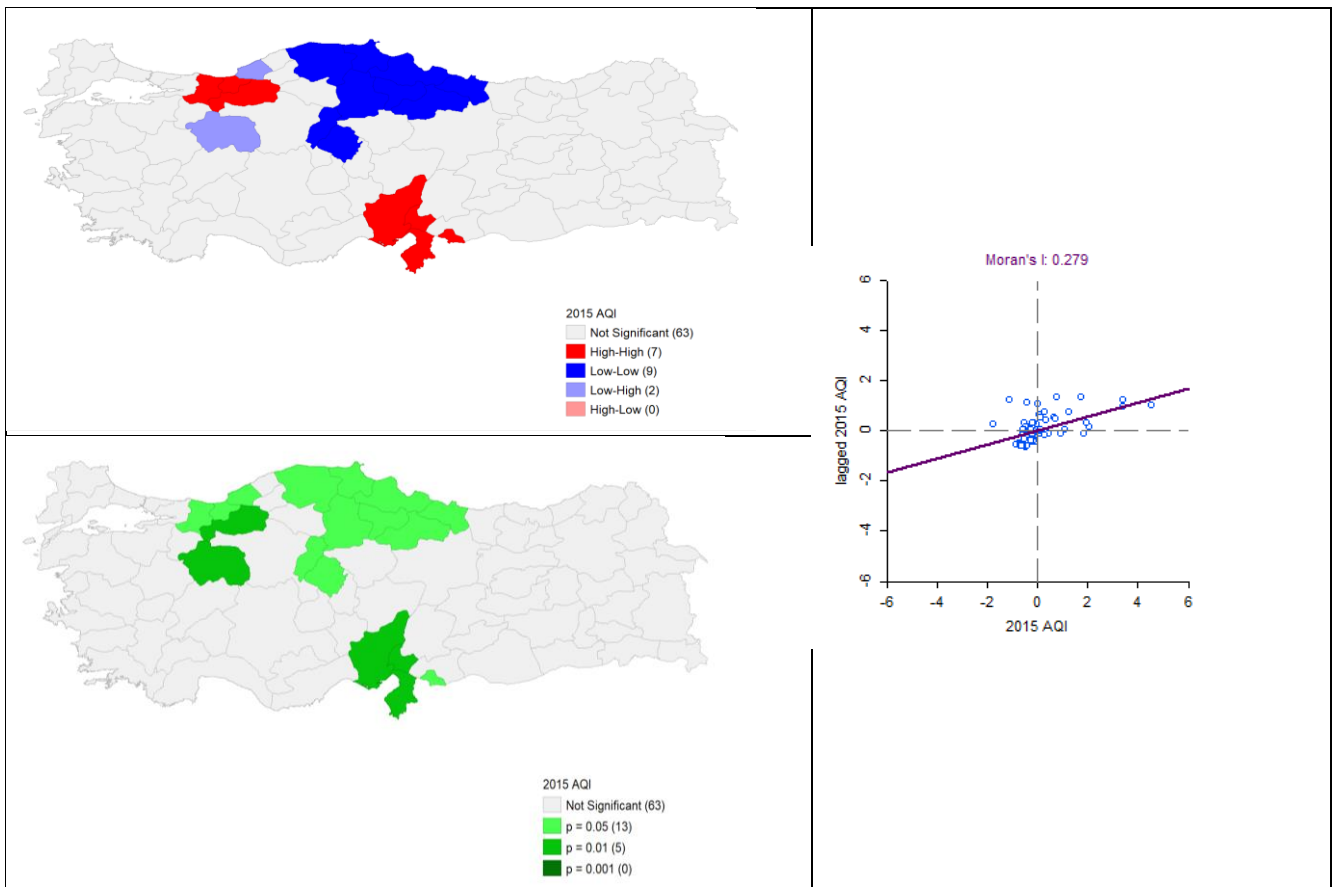


Figure 4. AQI Local Moran's I Graph and LISA Map for 2015.

### 3.3. Comparison of the AQI values of the years 2014 and 2015

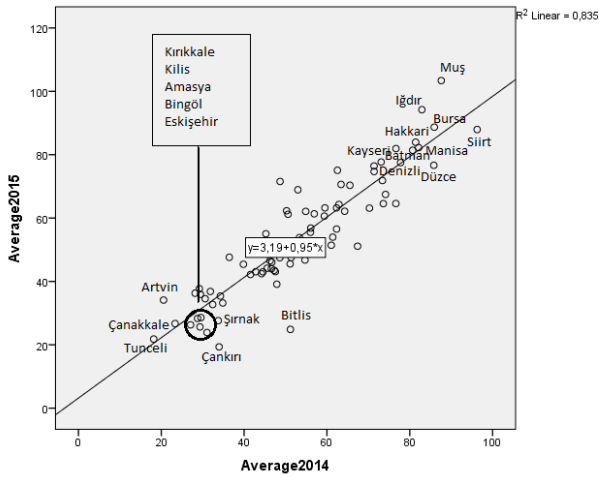
Before the comparison of the averages of 2014 and 2015 AQI values of provinces basis, normality test was conducted. The average values of the provinces were analyzed with the Kolmogorov-Smirnov Test and Shapiro-Wilk test provided by the normality assumption (Table 5). Accordingly, it was determined that the data is normally distributed for both years.

**Table 5.** Tests of Normality of Annual Average AQI of Cities for the years 2014 and 2015.

Tests of Normality						
	Kolmogorov-Smirnov			Shapiro-Wilk		
	Statistic	df	Sig.	Statistic	df	Sig.
Average 2014	0.075	80	0.200*	0.977	80	0.170
Average 2015	0.077	80	0.200*	0.981	80	0.275

\*. This is a lower bound of the true significance.

The mean of the cities average AQI values were not statistically different than each other with 95% confidence interval. This expected since most of the time, PM<sub>10</sub> values are lower than the 100 µg/m<sup>3</sup> and below this level, AQI and PM<sub>10</sub> levels show correlation with a line  $y = x$ . The correlation between average AQI of the years 2014 and 2015 are shown in Figure 5.



**Figure 5.** Correlation of average AQI of the provinces in Turkey for the years 2014 and 2015.

Only Muş for the year 2015 exceeded average AQI level of 100. This indicates that the air quality in Muş province was unhealthy for sensitive groups for the year 2015. In both years, 39 provinces had an average AQI less than 50 (Good) and rest of provinces had an average AQI between 51 and 100 (Moderate).

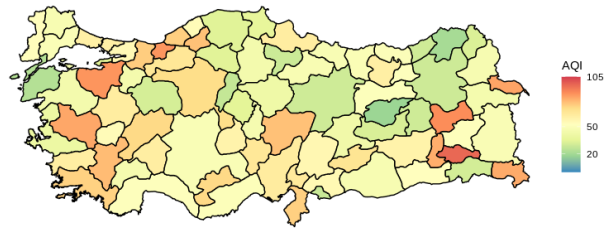
**Table 6.** Pearson Correlation Result of Annual Average AQI of Cities for the years 2014 and 2015.

Correlations			
		Average2014	Average2015
Average 2014	Pearson Correlation	1	0.914**
	Sig. (2-tailed)		0.000

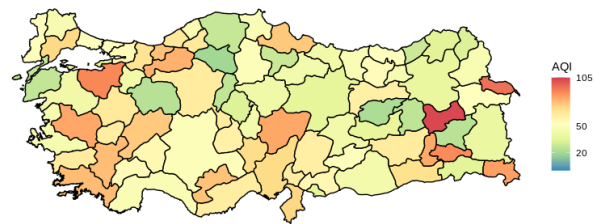
\*\* . Correlation is significant at the 0.01 level (2-tailed).

Since the data is normally distributed, the Pearson Correlation coefficient is examined and the coefficient was found to be 0.914, which is statistically significant in the 99% confidence interval. This result shows us that there is a strong relationship between the averages of 2014 and 2015 AQI values (Table 6).

The AQI values of the provinces for the years 2014 and 2015 are given in Figure 6 and Figure 7, respectively. The average AQI values of all cities were 53.1±18.2 and 53.7±18.9 for the years 2014 and 2015, respectively. The highest average AQI was calculated as 103 for Muş for the year 2015. The lowest average AQI was calculated as 18 for Tunceli for the year 2014.



**Figure 6.** Average AQI values of the provinces in Turkey for the year 2014.



**Figure 7.** Average AQI values of the provinces in Turkey for the year 2015.

It was determined that 9 out of 10 provinces with the highest AQI values were the same in both years. These nine provinces were Muş, Iğdır, Bursa, Siirt, Hakkâri, Manisa, Kayseri, Batman, Muğla and Denizli.

Muş, Iğdır, Siirt, Hakkâri and Batman provinces were located on the East Anatolia. There were almost no industrial activities on downtown area of the provinces. The main reason of the high AQI on these cities was

probably due to household heating and traffic emissions. Bursa and Kayseri were located on Marmara region and central Anatolia, respectively and Manisa and Denizli were on western Anatolia. These four cities host industrial production. Therefore, aside from household heating and traffic, industrial emissions could also contribute to high AQI. Muğla, on the other hand, was located on the Aegean Sea. Downtown Muğla was located 15 km from the sea and there were almost no industrial activities in downtown area of the province. Hence, household heating together with traffic emissions were the main sources of pollution in Muğla.

Six of the ten lowest AQI cities of the years 2014 and 2015 were the same. These were Tunceli, Çanakkale, Kırıkkale, Bingöl, Amasya and Rize. These six cities are located on different parts of the Anatolia (Tunceli and Bingöl are in Eastern Anatolia, Çanakkale is between Marmara and Aegean seas, Kırıkkale and Amasya are in central Anatolia and Rize is in Eastern Black Sea) is in and there were no important industrial settlements in the downtown areas of the cities.

#### 4. Conclusions

Understanding the need for regional air quality is going to help us to recognize the driving forces underneath. This study brings a different perspective to reveal the effects of natural and anthropogenic factors that are thought to affect the air quality index, which helps to understand air pollution. Considering the distribution of air pollution, the focus is on spatial autocorrelation. In this context, we tried to estimate the parameters of natural and anthropogenic effects through spatial regression models. It has been observed that there is a spatial distribution map of AQI values and Global Moran's I value (0.279). This information shows us that the AQI values in one province are affected by the AQI values in the neighboring province. Priority OLS method was used for parameter estimation of 12 independent variables which are thought to have an effect on AQI value and R2 value is 0.223. Spatial error and spatial lag models were created in this investigation with ESDA. It was concluded that the spatial effect resulted from spatial delay (probability values 0.070 <0.079). For the SLM model, R2 was obtained as 0.290. The model obtained with SLM was determined to be a better model compared to the model obtained according to the OLS method. In the model, the value of  $\rho$  expressing the presence of spatial effect was statistically significant and was found to be 0.320. This value indicates that a 1% increase in the AQI value in one province causes a 3.2% increase in the AQI value in the neighboring provinces. While wind speed causes a decrease in AQI value, increase

in GDP increases AQI.

The average AQI values for 2014 and 2015 were compared. The Pearson correlation coefficient of between the cities for the consecutive years was found to be 0.914, a value very close to 1. This result showed that the average AQI values of 2014 and 2015 are in a strong correlation relationship. In both years, just 39 provinces had average AQI value below 50; indicating most of the cities were not in the good air quality category.

In this study, though average air quality of the provinces did not change significantly from one year to other, responses of cities to meteorological factors and regional dust transport plays an important role to change air qualities of the regions. Desert dust transport seems to increase AQI index of cities located on the Southern Anatolia whereas, meteorological factors either decreases or increases AQI of regions located on the Black Sea coast.

#### Conflict of Interests

No conflict of interest was stated by the authors.

#### Acknowledgements

This study was supported by Akdeniz University the Scientific Research Projects Coordination Unit with Project No: FBA-2018-3410.

#### Declaration of Ethical Standards

The authors of this article declares that the materials and methods used in this study do not require ethical committee permission and legal-special permission.

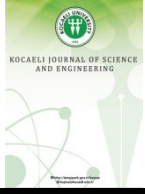
#### References

- [1] World Health Organization. (2006). WHO Air Quality Guidelines for Particulate Matter, Ozone, Nitrogen Dioxide and Sulfur Dioxide: Global Update 2005: Summary of Risk Assessment (No. WHO/SDE/PHE/OEH/06.02). World Health Organization.
- [2] Avnery S., Mauzerall D., Liu J., Horowitz L., 2011. Global Crop Yield Reductions Due to Surface Ozone Exposure: 1. Year 2000 Crop Production Losses and Economic Damage. *Atmospheric Environment*, **45**(13), pp. 2284–2296.
- [3] Nzotungicimpaye C. M., Abiodun B. J., Steyn D. G., 2014. Tropospheric Ozone and its Regional Transport Over Cape Town. *Atmospheric Environment*, **87**, pp. 228–238.

- [4] Dimitriou K., Kassomenos P., 2015. Three Year Study of Tropospheric Ozone with Back Trajectories at A Metropolitan and A Medium Scale Urban Area in Greece. *Science of the Total Environment*, **502**, pp. 493–501.
- [5] Cape J.N., Fowler D., Davison A., 2003. Ecological Effects of Sulfur Dioxide, Fluorides, and Minor Air Pollutants: Recent Trends and Research Needs. *Environment International*, **29**(2), pp. 201–211.
- [6] EPA, 2014. *Air Quality Index: A Guide to Air Quality and Your Health*. NC, USA.
- [7] Lee E., Chan C.K., Paatero P., 1999. Application of Positive Matrix Factorization in Source Apportionment of Particulate Pollutants in Hong Kong. *Atmospheric Environment*, **33**(19). pp. 3201–3212.
- [8] Querol X., Alastuey A., Rodriguez S., Plana F., Ruiz C.R., Cots N., Massagué G., Puig O., 2001. PM<sub>10</sub> and PM<sub>2.5</sub> Source Apportionment in the Barcelona Metropolitan Area, Catalonia, Spain. *Atmospheric Environment*, **35**(36), pp. 6407-6419.
- [9] Mansha M., Ghauri B., Rahman S. Amman A. 2012. Characterization and Source Apportionment of Ambient Air Particulate Matter (PM<sub>2.5</sub>) in Karachi. *Science Of The Total Environment*, **425**, pp. 176-183.
- [10] Liu H., Fang C., Zhang X., Wang Z., Bao C., Li F., 2017. The Effect of Natural and Anthropogenic Factors on Haze Pollution in Chinese Cities: A Spatial Econometrics Approach. *Journal of Cleaner Prod.*, **165**, pp. 323-333.
- [11] Xu W., Tian Y., Liu Y., Zhao B., Liu Y., Zhang X. 2019. Understanding the Spatial-Temporal Patterns and Influential Factors on Air Quality Index: The Case of North China. *International Journal of Environmental Research and Public Health*, **16**(16), pp. 2820.
- [12] Gaga E. O., Döğeroğlu T., Özden Ö., Ari A., Yay O. D., Altuğ H., Van Doorn, W., 2012. Evaluation of Air Quality by Passive and Active Sampling in An Urban City in Turkey: Current Status and Spatial Analysis of Air Pollution Exposure. *Environmental Science and Pollution Research*, **19**(8), pp. 3579-3596.
- [13] Demir M., Dindaroğlu T., Yılmaz S., 2014. Effects of Forest Areas on air Quality; Aras Basin and its Environment. *Journal of Environmental Health Science and Engineering*, **12**(1), pp. 60.
- [14] Tecer L. H., Tagil S., 2014. Impact of Urbanization on Local Air Quality: Differences in Urban and Rural Areas of Balıkesir, Turkey. *CLEAN–Soil, Air, Water*, **42**(11), pp.1489-1499.
- [15] Dursun S., Alqaysi N. H. H., 2016. Estimating Air Pollution Quality In Istanbul City Centre By Geographic Information System. *International Journal Of Ecosystems And Ecology Science-IjeeS*, **6**(3), pp. 329-340.
- [16] Kurnaz K., Cobanoğlu G., 2017. Biomonitoring of Air Quality in Istanbul Metropolitan Territory with Epiphytic Lichen *Physcia Adscendens* (Fr.) Olivier. *Fresen. Environ. Bull*, **26**, pp. 7296.
- [17] Baykara M., Im U., Unal A., 2019. Evaluation of Impact of Residential Heating on Air Quality of Megacity Istanbul by CMAQ. *Science of the Total Environment*, **651**, pp.1688-1697.
- [18] Güçlü Y. S., Dabanlı İ., Şişman E., Şen, Z., 2019. Air Quality (AQ) Identification by Innovative Trend Diagram and AQ Index Combinations in Istanbul Megacity. *Atmospheric Pollution Research*, **10**(1), pp. 88-96.
- [19] Gokce H. B., Arıoğlu E., Copty N. K., Onay T. T., Gun B., 2020. Exterior Air Quality Monitoring for The Eurasia Tunnel in Istanbul, Turkey. *Science of The Total Environment*, **699**, pp. 134312.
- [20] Dagsuyu C., 2020. Process Capability and Risk Assessment for Air Quality: an Integrated Approach. *Human and Ecological Risk Assessment: An International Journal*, **26**(2), pp. 394-405.
- [21] Yalcin F., 2016, “Spatial Analysis of The Factors Affecting The Room Price Offered by The Hotels in Antalya City” (in Turkish), Unpublished Doctorate Thesis, Akdeniz University, Graduate School of Social Sciences, Antalya, Turkey.
- [22] Yalcin F., Mert M., 2018. Determinación de Precios Hedónicos de Habitación de Hotel con Efecto Espacial en Antalya. *Economía, Sociedad y territorio*, **18**(58), pp.697-734.
- [23] Kowe P., Mutanga O., Odindi J., Dube T., 2019. Exploring the Spatial Patterns of Vegetation Fragmentation Using Local Spatial Autocorrelation Indices. *Journal of Applied Remote Sensing*, **13**(2), pp. 1-14.
- [24] Lutz S.U., 2019. The European Digital Single Market Strategy: Local Indicators of Spatial Association 2011–2016. *Telecommunications Policy*, **43**(5), pp. 393-410.
- [25] Yalcin F., Tepe A., Dogan G., Cizmeci N., 2019. Investigation of Air Quality Index by Spatial Data Analysis: a Case Study on Turkey. *Proceedings Book of the 2nd Mediterranean*, **23**.

- [26] Sensoy S., Demircan M., Ulupinar Y., Balta I., 2008. Climate of Turkey. Turkish State Meteorological Service, **401**.
- [27] Yalcin F., Tepe A. M., Doğan G., Cizmeci N. 2019. Regression Analysis of The Effect of Meteorological Parameters on Air Quality in Three Neighboring Cities Located on The Mediterranean Coast of Turkey. In AIP Conference Proceedings, July, Vol. 2116, No. 1, p. 100015. AIP Publishing LLC.
- [28] CSB. 2020. SIM Veri Bankasi. (Web page: <https://sim.csb.gov.tr>) (Date accessed: 01.04.2020).
- [29] Snow J., 1855. On the Mode of Communication of Cholera (2nd ed.). London: John Churchill.
- [30] Fang C., Liu H., Li G., Sun D., Miao Z., 2015. Estimating the Impact of Urbanization on Air Quality in China Using Spatial Regression Models. *Sustainability*, **7**(11), pp. 15570-15592.
- [31] Mahara G., Wang C., Yang K., Chen S., Guo J., Gao Q., Guo, X., 2016. The Association Between Environmental Factors and Scarlet Fever Incidence in Beijing Region: Using GIS and Spatial Regression Models. *International Journal of Environmental Research and Public Health*, **13**(11), pp.1083.
- [32] Guo Y., Tang Q., Gong D. Y., Zhang Z., 2017. Estimating Ground-Level PM<sub>2.5</sub> Concentrations in Beijing Using a Satellite-Based Geographically and Temporally Weighted Regression Model. *Remote Sensing of Environment*, **198**, pp. 140-149.
- [33] Li H., You S., Zhang H., Zheng W., Zheng X., Jia J., Zou L., 2017. Modelling of AQI Related to Building Space Heating Energy Demand Based on Big Data Analytics. *Applied Energy*, **203**, pp. 57-71.
- [34] Tobler W. R., 1970. A Computer Movie Simulating Urban Growth in The Detroit Region. *Economic Geography*, **46**(sup1), pp. 234-240.
- [35] Anselin L., 1988. *Spatial Econometrics: Methods And Models*, Kluwer Academic Publishers, Dordrecht.
- [36] Cliff A. D., Ord J. K., Haggett P., Versey G. R., 1981. *Spatial Diffusion: An Historical Geography of Epidemics in an island community* (Vol. 14). CUP Archive.
- [37] Moran P.A.P., 1950a. Notes on Continuous Stochastic Phenomena. *Biometrika*, **37**, pp.17-23.
- [38] Moran P.A.P., 1950b. A Test for The Serial Independence of Residuals. *Biometrika*, **37**, pp. 178-181.
- [39] Geary R. C., 1954. The Contiguity Ratio and Statistical Mapping. *The Incorporated Statistician*, **5**(3), pp. 115-146.
- [40] Getis A., 2008. A History of The Concept of Spatial Autocorrelation: A Geographer's Perspective. *Geographical Analysis*, **40**(3), pp. 297-309.
- [41] Wheeler D.C., Tiefelsdorf M., 2005. Multicollinearity and Correlation Among Local Regression Coefficients in Geographically Weighted Regression. *Journal of Geographical Systems* **7**, pp. 161–87.
- [42] Ord J. K., Getis A., 1995. Local Spatial Autocorrelation Statistics: Distributional Issues and an Application. *Geographical Analysis*, **27**(4), pp. 286-306.
- [43] Anselin L., Bera A. K., Florax R., Yoon M. J., 1996. Simple Diagnostic Tests for Spatial Dependence. *Regional Science and Urban Economics*, **26**(1), pp. 77-104.
- [44] Getis A., Ord J. K., 1996. Spatial Analysis and Modeling in A GIS Environment. *A research Agenda for Geographic Information Science*, pp.157-196.
- [45] Boots B., Tiefelsdorf M., 2000. Global and Local Spatial Autocorrelation in Bounded Regular Tessellations. *Journal of Geographical Systems*, **2**(4), pp. 319-348.
- [46] Moran P.A.P., 1948. The Interpretation of Statistical Maps. *Journal of the Royal Statistical Society B.*, **10**, pp. 243-251
- [47] Anselin L., 1995. Local Indicators of Spatial Association-LISA, *Geographical Analysis*, **27**, pp. 93-115.
- [48] Anselin L., Florax, R.J.G.M., Rey, S.J. (ed.). 2004. *Advances in Spatial Econometrics, Methodology, Tools and Applications*. Springer-Verlag Berlin Heidelberg, Berlin.
- [49] Anselin L., Hudak S., 1992. Spatial Econometrics in Practice: A Review of Software Options. *Regional Science and Urban Economics*, **22**(3), pp.509-536.
- [50] Li X. X., Wang L. X., Zhang J., Liu Y. X., Zhang H., Jiang S. W., Zhou X. N., 2014. Exploration of Ecological Factors Related to The Spatial Heterogeneity of Tuberculosis Prevalence in PR China. *Global Health Action*, **7**(1), pp.23620.
- [51] Jung M. C., Park J., & Kim S., 2019. Spatial Relationships Between Urban Structures and Air Pollution in Korea. *Sustainability*, **11**(2), p. 476.

- [52] Wang M., Wang H., 2020. Spatial Distribution Patterns and Influencing Factors of PM 2.5 Pollution in the Yangtze River Delta: Empirical Analysis Based on a GWR Model. *Asia-Pacific Journal of Atmospheric Sciences*, pp.1-13.
- [53] Anselin L., 2013. *Spatial Econometrics: Methods and Models (Vol. 4)*. Springer Science & Business Media.
- [54] Elhorst J. P., 2010. Applied Spatial Econometrics: Raising the Bar. *Spatial Economic Analysis*, **5**(1), pp. 9-28.
- [55] Liu, H., Fang, C., Zhang, X., Wang, Z., Bao, C., Li F., 2017. The Effect of Natural and Anthropogenic Factors on Haze Pollution in Chinese Cities: A Spatial Econometrics Approach. *Journal of Cleaner Prod.*, **165**, pp. 323-333
- [56] Ecer A., Sarikaya B., Tepe A. M., Doğan, G., 2017. Mardin İli Hava Kalitesinin Değerlendirilmesi. Paper Presented at the 7. Ulusal Hava Kirliliği ve Kontrolü Sempozyumu, Antalya, Turkey.
- [57] Tepe A. M., Doğan G., 2016. Comparison of Effect of Saharan Dust Transport to Cities Located on Black Sea and Mediterranean Coasts of Turkey. Paper Presented at the 1st International Black Sea Congress on Environmental Sciences, Giresun, Turkey.
- [58] Tepe A. M., Doğan G., 2019. Türkiye'nin Güney Sahilinde Yer Alan Dört Şehrin Hava Kalitelerinin İncelenmesi. *Mühendislik Bilimleri ve Tasarım Dergisi*, **7**(3) , pp. 585-595.



Kocaeli University

Kocaeli Journal of Science and Engineering

<http://dergipark.org.tr/kojose>

## Model Updating of a Euler-Bernoulli Beam Using the Response Method

Cevher Yusuf İNAN Akın OKTAV<sup>2</sup> <sup>1</sup>Abdullah Gul University, Mechanical Engineering Departmen, Kayseri, Turkey, **ORCID:** 0000-0002-8818-4750<sup>2</sup>Abdullah Gul University, Mechanical Engineering Departmen, Kayseri, Turkey, **ORCID:** 0000-0001-5983-3953

### Article Info

#### Research paper

Received : July 11, 2020

Accepted : December 24, 2020

#### Keywords

Frequency Response Function,  
Model Updating,  
Structural Damping,  
Viscous Damping

### Abstract

In this study, the computational model is updated using an analytical model instead of an experimental one. Continuous and discrete parameter models of a Euler–Bernoulli beam are constructed analytically and computationally. To construct the computational models, Ansys™ software is employed, and 1-D beam elements are chosen to get the finite element model of a cantilever beam. To get analytical solutions for the continuous and discrete parameter models, a state-space representation is employed. In the first step, only mass and stiffness matrices are considered to model the beam. Eigenfrequencies and eigenvectors of the beam are calculated. The analytical and computational eigenfrequencies of continuous and discrete parameter models are compared. In the seconds step, non-proportional viscous damping and non-proportional structural damping matrices are introduced into the analytical discrete parameter model. Then, the frequency response functions of the model are generated. The damping matrices are identified using the generated frequency response functions. The damping matrices used in the analytical model, and the damping matrices identified using the frequency response functions are compared. It is observed that the assigned damping matrices and the identified damping matrices are identical, which shows that the computational model can be accurately updated provided the FRFs are available.

## 1. Introduction

Deterministic element-based methods are widely used for modeling in structural dynamics; the most common one is the finite element method (FEM). Dynamic systems are mathematically expressed by mass, stiffness, and damping matrices. Finite element packages can populate mass and stiffness matrices using the data given in the preprocessing step such as, geometry and material properties of the structure. At this step, the model does not have a damping property, yet. Based on the Rayleigh damping model, a proportional damping matrix can be created using mass and stiffness matrices. This damping matrix does not reflect the actual physical behavior. For this reason, errors may occur in the final updated model. The error rate increases as the degrees of freedom (dof) of the dynamic model increase.

Model updating has been developed with many different methods proposed since 1980s. Mottershead and Friswell systematically summarized the classical model update theory [1]. There are different approaches to model updating in the literature. The relevant methods are based on a direct algorithm or an iteration algorithm. System parameter-based methods have a more apparent physical meaning and better computing performance than matrix-based methods. Response data-based methods are becoming more common as there is an advantage to avoid errors arising from mode identification. Due to the difficulty of modeling damping and measuring the dynamic properties, there is incompleteness in updating the damping values in existing model update methods.

The mass matrix of a structure can accurately be estimated by finite element model, but there may be errors in the stiffness matrix. For this reason, it is stated that the stiffness matrix should be updated using an appropriate method [2]. A method that reduces the norm of the difference between the computational and the experimental modes is proposed [3]. It states that the mass and the

\* Corresponding Author: [akin.oktav@agu.edu.tr](mailto:akin.oktav@agu.edu.tr)





stiffness matrices should be evaluated simultaneously, when updating a model. The model update process would be more successful, if performed with the experimental model [4]. In another study, it is stated that mass, stiffness, and damping matrices should be updated simultaneously with the experimental data [5]. In a study held in 2012, uncertainties in experimental data were evaluated [6]. These studies mentioned in the literature are direct methods.

Iteration methods are another topic in model update. It is the method of matching the modal matrices obtained with computational models using experimental data and constructing the updated model. In the literature, iteration is performed using frequency response functions (FRFs) measured experimentally, which is known as the response function method [7]. The response function method is expanded to update the proportional viscous and the proportional structural damping matrices [8]. In another study, the differences between the computational data and the experimental data are minimized by the so-called Taguchi method [9]. Sippl and Sanayei proposed a new approach to solve the inverse problem [10]. They used a new frequency response function-based model update method by employing numerical sensitivity, instead of analytical sensitivity [10]. It is proposed that the model update should be performed with undamped frequency response functions [11]. Researchers developed a new method to define the structural damping matrix which can be used in simple structures as the procedure requires exact measurements [12]. The error margin in the model update approach is computed by Matta and Stefano [13] using the experimental data of a large building. Damping is a crucial parameter in model updating studies. There are studies which compare different damping models in the literature [14][15].

In the response method, frequency response functions are used to quantify the dynamic characteristics of the model [16-18]. Natke has summarized the model updating methods based on the transfer character [19]. In another study, residues in resonance and anti-resonance are taken as a reference to update a damped model. Lu and Zhenguo evaluated the structural parameters and the damping parameters at different network levels [20]. However, when Rayleigh damping is employed, the physical meaning of the modes is in question. To increase the accuracy of the lightweight structure tests, the stiffness and the damping matrices are updated using an experimental setup [21]. The damping identification in Ref [22] can provide a non-proportional structural damping matrix, which can be used directly in calculations.

In this study, the computational model is updated using an analytical model, instead of an experimental one. Non-proportional structural damping and non-proportional

viscous damping matrices are obtained using the response method. First, a computational and an analytical model of a 600-mm length Euler-Bernoulli aluminum beam with a rectangular cross-section of 19 mm × 3 mm is constructed. The boundary conditions are fixed-free, i.e., a cantilever beam. The material properties are as follows: Young's modulus,  $E = 71$  GPa and density,  $\rho = 2,770$  kg/m<sup>3</sup>. Computational and analytical models are considered as continuous and discrete parameter systems. The percentage error between the computational and the analytical model is computed. In finite element modeling, as the number of elements increase, the convergence rate increases. Computational models are formed using Ansys<sup>TM</sup> where, a 1-D beam element is chosen to obtain a finite element model of the structure. Continuous and discrete parameter analytical models are constructed using Matlab<sup>TM</sup>. In the first step, the eigenfrequencies and the eigenvectors of the beams are calculated by considering mass and stiffness matrices only. Computational and analytical results of the continuous and the discrete parameter models are compared for the transverse vibration case. In the second step, non-proportional structural damping and non-proportional viscous damping matrices are introduced to the analytical models. Frequency response functions of the analytical models are obtained through a state-space representation. The damping matrices are identified using the frequency response functions. The damping matrices that are used in the analytical model, and the damping matrices identified using frequency response functions are compared.

## 2. Continuous Beam Model

The continuous beam model is analyzed computationally and analytically. Transverse vibration results of the two analyses are compared. In both models, the first six eigenfrequencies are considered, and a cantilever Euler-Bernoulli aluminum beam is used. The dimensions of the beam are as follows:  $L \times W \times H = 600 \times 19 \times 3$  in millimeters.

### 2.1. Computational Continuous Beam Model

Ansys Workbench is employed for the computational modeling of the continuous model. A 1-D beam element is used for the modeling procedure. In the first step, an undamped model is constructed. The beam is modeled in different element numbers to observe the convergence in the results. Convergence in the results is tabulated in Table 1, where the number of elements is increased systematically.

### 2.2. Analytical Continuous Beam Model

The analytical solution of the continuous beam model is obtained using Matlab 2019b. The equation of motion for a continuous Euler-Bernoulli beam is given as follows:

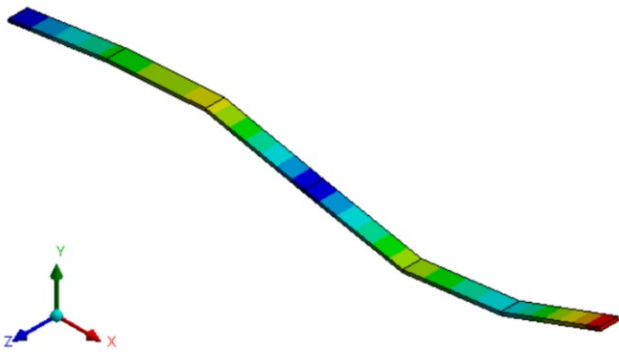
$$\frac{d^2}{dx^2} \left\{ EI(x) \frac{d^2 Y(x)}{dx^2} \right\} = \omega^2 m(x) Y(x) \tag{1}$$

**Table 1** The comparison of first six eigenfrequencies of computational continuous model and analytical continuous model

#	Analytical continuous mode frequencies (Hz)	Computational continuous mode frequencies (Hz)							
		6 Elements	Error (%)	8 Elements	Error (%)	10 Elements	Error (%)	100 Elements	Error (%)
1	6,815	6,815	0,0	6,815	0,0	6,815	0,0	6,815	0,0
2	42,711	42,738	0,06	42,715	0,01	42,709	0,005	42,705	0,01
3	119,592	120,24	0,54	119,77	0,15	119,64	0,04	119,55	0,04
4	234,353	239,13	2,04	235,82	0,63	234,89	0,23	234,21	0,06
5	387,402	408,46	5,44	394,04	1,71	389,99	0,67	387,02	0,1
6	578,712	655,05	13,20	600,48	3,76	587,47	1,51	577,88	0,14

In Eq. (1),  $E$  is the modulus of elasticity,  $I$  is the moment of inertia of the beam’s cross section,  $Y(x)$  is transverse displacement,  $\omega$  is natural frequency,  $m$  is mass per unit length, and  $x$  is the distance from the fixed point of the beam (See A.1 for a closed form solution).

Computationally and analytically calculated eigenfrequencies are tabulated in Table 1, and the percentage error is calculated over the analytical results. The third mode shape of the continuous six dof beam model is shown in Figure 1.



**Figure 1.** Third mode shape of the computational continuous model

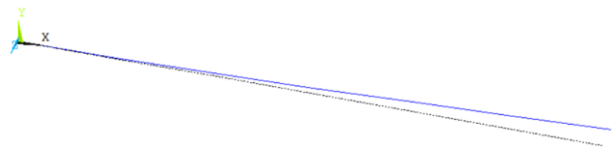
### 3. Discrete Beam Model

For discrete parameter modeling, the identical beam is analyzed computationally and analytically. Computational discrete beam model analysis results are obtained using Ansys APDL Mechanical, and Matlab is employed to construct the analytical discrete parameter model. Eigenfrequencies of the 6-element beam are calculated. In the first step, the results of an undamped

model are compared. Then, the frequency response functions are generated by assigning non-proportional damping values to the analytical discrete parameter model. The damping matrices are identified through the generated frequency response functions. (See Section 5)

#### 3.1. Computational Discrete Beam Model

A 6-element beam model is constructed in Ansys APDL Mechanical, and the eigenfrequencies are computed. The computed eigenfrequencies are tabulated in Table 2. First mode shape of the computational discrete parameter model is shown in Figure 2.



**Figure 2.** First mode shape of the computational discrete parameter model

#### 3.2. Analytical Discrete Beam Model

The 6-dof discrete parameter model is built in Matlab using a state-space representation (See A.2). The 6-dof analytical discrete parameter model is shown in Figure 3, where  $m$ ,  $k$ ,  $c$  and  $d$  stand for mass, stiffness, viscous damping, and structural damping, respectively. Eigenfrequencies and frequency response functions can be calculated by introducing mass, stiffness, and damping matrices to the system. The mass and stiffness matrices are

derived from Ansys APDL Mechanical using the “DMAT” command. The mass matrix and the stiffness matrix are given in Table 3 and Table 4, respectively. The undamped eigenfrequencies and the percentage error values are tabulated in Table 2. Then, viscous, and structural damping matrices, where introduced in Section 5 are assigned.

**Table 2.** Comparison of eigenfrequencies of computational discrete beam model and analytical discrete beam model.

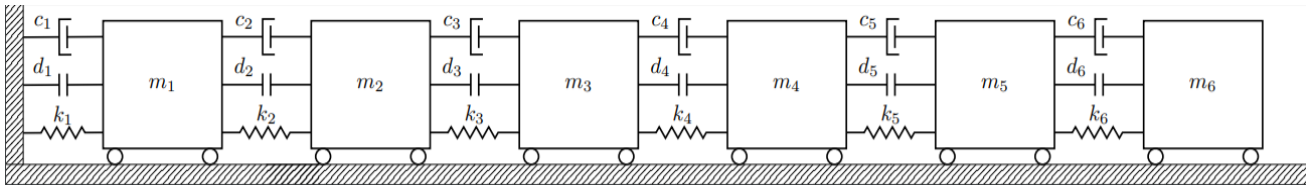
Mode	Computational-discrete (rad/s)	Analytical-discrete (rad/s)	Error (%)
1	891,08	891,23	0,02
2	2734,57	2735	0,02
3	4762,15	4762,96	0,02
4	7068,58	7069,94	0,02
5	9552,95	9554,43	0,02
6	11463,04	11464,73	0,02

**Table 3.** The mass matrix of analytical discrete beam model

1.053e-2	2.631e-3	0	0	0	0
2.631e-3	1.053e-2	2.631e-3	0	0	0
0	2.631e-3	1.053e-2	2.631e-3	0	0
0	0	2.631e-3	1.053e-2	2.631e-3	0
0	0	0	2.631e-3	1.053e-2	2.631e-3
0	0	0	0	2.631e-3	5.263e-3

**Table 4.** The stiffness matrix of analytical discrete beam model

3.637e5	-1.819e5	0	0	0	0
-1.819e5	3.637e5	-1.819e5	0	0	0
0	-1.819e5	3.637e5	-1.819e5	0	0
0	0	-1.819e5	3.637e5	-1.819e5	0
0	0	0	-1.819e5	3.637e5	-1.819e5
0	0	0	0	-1.819e5	1.819e5



**Figure 3** Discrete parameter system of six degrees of freedom analytical model (m: mass; k: stiffness, c: viscous damping; d: structural damping)

### 4. Damping Identification

Equation of motion of a damped system in time domain is given as follows:

$$\mathbf{M}\ddot{\mathbf{x}}(t) + \mathbf{C}\dot{\mathbf{x}}(t) + (\mathbf{iD} + \mathbf{K})\mathbf{x}(t) = \mathbf{f}(t) \quad (2)$$

Here  $\mathbf{M}$ ,  $\mathbf{K}$ ,  $\mathbf{C}$  and  $\mathbf{D}$  represent  $n \times n$  mass, stiffness, viscous damping, and structural damping matrices, respectively.  $\mathbf{f}$  and  $\mathbf{x}$  are  $n \times 1$  force and displacement vectors. If the excitation is harmonic,  $\mathbf{f}(t) = \mathbf{F}(\omega)e^{i\omega t}$  and  $\mathbf{x}(t) = \mathbf{X}(\omega)e^{i\omega t}$ . Hence, Eq. (2) can be written in frequency domain as follows:

$$[-\omega^2\mathbf{M} + \mathbf{iC}\omega + \mathbf{iD} + \mathbf{K}]\mathbf{X}(\omega) = \mathbf{F}(\omega) \quad (3)$$

The term in square brackets is the dynamic stiffness matrix, and the inverse of this matrix is the complex receptance matrix ( $\mathbf{R}^c(\omega)$ ):

$$[(\mathbf{K} - \omega^2\mathbf{M}) + \mathbf{i}(\mathbf{C}\omega + \mathbf{D})] = [\mathbf{R}^c(\omega)]^{-1} \quad (4)$$

The receptance matrix can be populated using the receptance functions estimated through experimentation,

where the displacement vector  $\mathbf{X}(\omega)$  is measured. The relation is given by:

$$\mathbf{X}(\omega) = \mathbf{R}^c(\omega)\mathbf{F}(\omega) \quad (5)$$

The complex receptance matrix consists of real and imaginary parts, which can be expressed:

$$\mathbf{R}^c(\omega) = \mathbf{R}_R^c(\omega) + \mathbf{iR}_I^c(\omega) \quad (6)$$

where the subscripts  $R$  and  $I$  stand for the real and imaginary values of the matrix, respectively. The undamped or normal receptance matrix can be expressed as follows:

$$\mathbf{R}^N(\omega) = [\mathbf{K} - \omega^2\mathbf{M}]^{-1} \quad (7)$$

which is the receptance type frequency response function matrix generated from the normal modes. Pre-multiplying Eq. (2) by the normal receptance matrix yield

$$\mathbf{X}(\omega) + \mathbf{iR}^N(\omega)(\omega\mathbf{C} + \mathbf{D})\mathbf{X}(\omega) = \mathbf{R}^N(\omega)\mathbf{F}(\omega) \quad (8)$$

Transformation matrix can be expressed by

$$\mathbf{T}(\omega) = \mathbf{R}^N(\omega)(\omega\mathbf{C} + \mathbf{D}) \quad (9)$$

Substituting the transformation matrix into Eq. (8), yields

$$[\mathbf{I} + i\mathbf{T}(\omega)]\mathbf{X}(\omega) = \mathbf{R}^N(\omega)\mathbf{F}(\omega) \quad (10)$$

where  $\mathbf{I}$  denote identity matrix. Using the relation given by Eq. (6), Eq. (10) can be rewritten as

$$[\mathbf{I} + i\mathbf{T}(\omega)]\mathbf{R}^c(\omega) = \mathbf{R}^N(\omega) \quad (11)$$

so as to eliminate the displacement vector  $\mathbf{X}(\omega)$ . Substituting Eq. (6) into Eq. (11) yields

$$[\mathbf{I} + i\mathbf{T}(\omega)][\mathbf{R}_R^c(\omega) + i\mathbf{R}_I^c(\omega)] = \mathbf{R}^N(\omega) \quad (12)$$

which can be rearranged as

$$\begin{aligned} [\mathbf{R}_R^c(\omega) - \mathbf{T}(\omega)\mathbf{R}_I^c(\omega)] \\ + i[\mathbf{R}_I^c(\omega) \\ + \mathbf{T}(\omega)\mathbf{R}_R^c(\omega)] = \mathbf{R}^N(\omega) \end{aligned} \quad (13)$$

where the left-hand side has real and imaginary components. Since the right-hand side of Eq. (13) has only real components, the following statements are true for all frequencies:

$$[\mathbf{R}_I^c(\omega) + \mathbf{T}(\omega)\mathbf{R}_R^c(\omega)] = 0 \rightarrow \quad (14)$$

$$\mathbf{T}(\omega) = -\mathbf{R}_I^c(\omega)[\mathbf{R}_R^c(\omega)]^{-1}$$

$$\mathbf{R}_R^c(\omega) - \mathbf{T}(\omega)\mathbf{R}_I^c(\omega) = \mathbf{R}^N(\omega) \quad (15)$$

Viscous and structural damping can be identified by substituting Eq. (9) into Eq. (14), which yields:

$$(\omega\mathbf{C} + \mathbf{D}) = -[\mathbf{R}^N(\omega)]^{-1}\mathbf{R}_I^c(\omega)[\mathbf{R}_R^c(\omega)]^{-1} \quad (16)$$

If the complex receptance matrix has been measured experimentally, the normal receptance matrix can be calculated, and if the normal receptance matrices are known, damping matrix can be calculated. Note that, Eq. (16) can be solved in a least-squares approach. It is recommended to use the pseudo inverse operator  $([\cdot]^+)$  for the matrix inversion, which returns a least-squares solution. Hence,

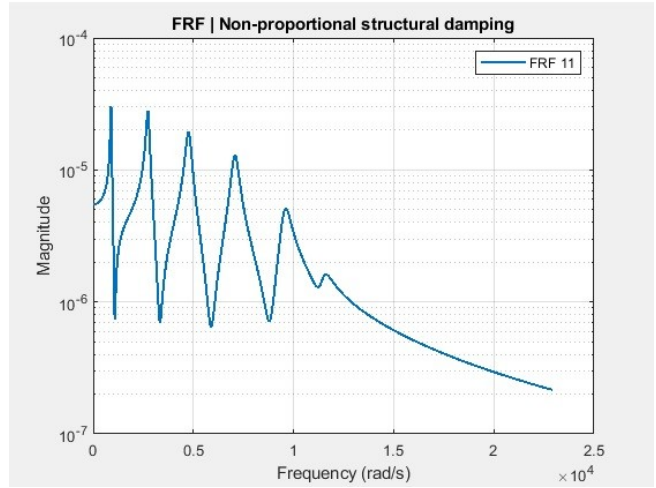
$$\begin{bmatrix} \mathbf{D} \\ \mathbf{C} \end{bmatrix} = - \begin{bmatrix} \mathbf{R}^N & \omega_1 \mathbf{R}^N \\ \vdots & \vdots \\ \mathbf{R}^N & \omega_n \mathbf{R}^N \end{bmatrix}^+ \begin{bmatrix} \mathbf{R}_I^c(\omega_1) \\ \vdots \\ \mathbf{R}_I^c(\omega_n) \end{bmatrix} \begin{bmatrix} (\mathbf{R}_R^c(\omega_1))^+ \\ \vdots \\ (\mathbf{R}_R^c(\omega_n))^+ \end{bmatrix} \quad (17)$$

## 5. Frequency Response Functions

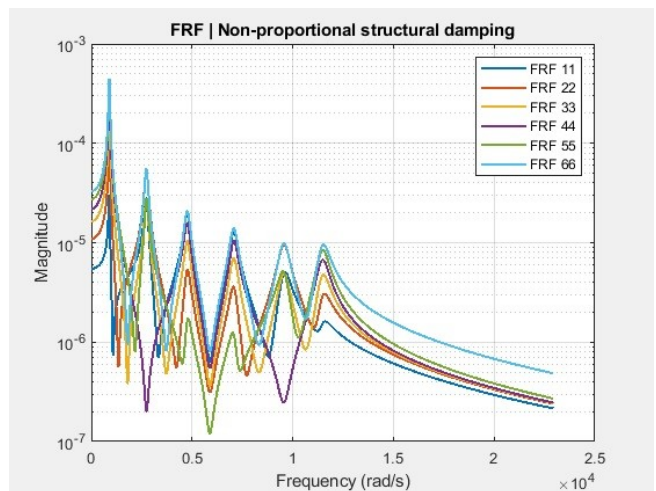
In this section, non-proportional damping matrices are assigned to the analytical discrete parameter model, and the complex frequency response functions are

generated. The assigned viscous and structural damping matrices are identified through the complex frequency response functions.

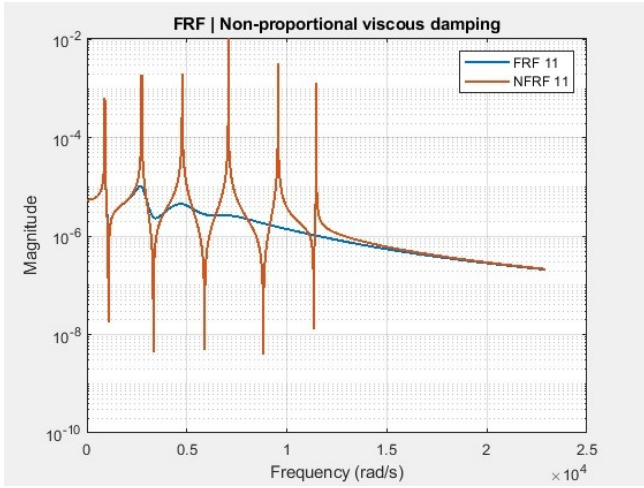
One of the frequency response functions of the non-proportional structural damped six degrees of freedom discrete parameter model, namely FRF11 is shown in Figure 4. In Figure 5, all the diagonal terms of the frequency response function matrix of the discrete parameter model are given. To yield the effect of damping on the model, the undamped aka normal frequency response functions (NFRFs) of the model are compared with the damped frequency response function. The comparisons are made for viscously damped and structurally damped models in Figures 6 and 7, respectively.



**Figure 4.** Frequency response function of the non-proportional structural damped six degrees of freedom discrete parameter model (FRF 11)



**Figure 5.** Frequency response functions of non-proportional structural damped six degrees of freedom discrete parameter model (FRFs)



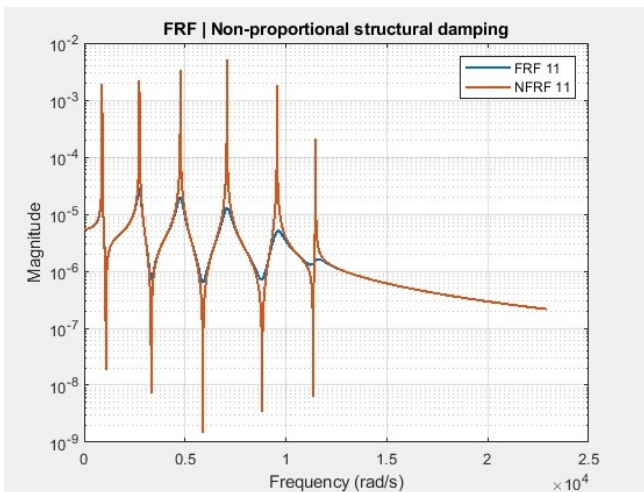
**Figure 6.** Frequency response function and normal frequency response function of the non-proportional viscous damped six degrees of freedom discrete parameter model (FRF 11 and NFRF 11)

The non-proportional viscous damping matrix assigned to the analytical discrete parameter model is as follows:

$$C = \begin{bmatrix} 18 & -10 & 0 & 0 & 0 & 0 \\ -10 & 25 & -15 & 0 & 0 & 0 \\ 0 & -15 & 27 & -12 & 0 & 0 \\ 0 & 0 & -12 & 26 & -14 & 0 \\ 0 & 0 & 0 & -14 & 27 & -13 \\ 0 & 0 & 0 & 0 & -13 & 13 \end{bmatrix}$$

The identified viscous damping matrix through the complex frequency response functions is as follows:

$$C_{\text{identified}} = \begin{bmatrix} 18 & -10 & 0 & 0 & 0 & 0 \\ -10 & 25 & -15 & 0 & 0 & 0 \\ 0 & -15 & 27 & -12 & 0 & 0 \\ 0 & 0 & -12 & 26 & -14 & 0 \\ 0 & 0 & 0 & -14 & 27 & -13 \\ 0 & 0 & 0 & 0 & -13 & 13 \end{bmatrix}$$



**Figure 7.** Frequency response function and normal frequency response function of the non-proportional structural damped six degrees of freedom discrete parameter model (FRF 11 and NFRF 11)

The non-proportional structural damping matrix assigned to the analytical discrete parameter model is as follows:

$$D = \begin{bmatrix} 2382,9 & -11095,9 & 0 & 0 & 0 & 0 \\ -11095,9 & 21646,1 & -10550,2 & 0 & 0 & 0 \\ 0 & -10550,2 & 17989,91 & -7439,71 & 0 & 0 \\ 0 & 0 & -7439,71 & 18353,71 & -10914 & 0 \\ 0 & 0 & 0 & -10914 & 20009 & -9095 \\ 0 & 0 & 0 & 0 & -9095 & 9095 \end{bmatrix}$$

The identified structural damping matrix through the complex frequency response functions is as follows:

$$D_{\text{identified}} = \begin{bmatrix} 2382,9 & -11095,9 & 0 & 0 & 0 & 0 \\ -11095,9 & 21646,1 & -10550,2 & 0 & 0 & 0 \\ 0 & -10550,2 & 17989,91 & -7439,71 & 0 & 0 \\ 0 & 0 & -7439,71 & 18353,71 & -10914 & 0 \\ 0 & 0 & 0 & -10914 & 20009 & -9095 \\ 0 & 0 & 0 & 0 & -9095 & 9095 \end{bmatrix}$$

It is shown that the assigned and the identified damping matrices are identical.

## 6. Conclusions

- It is shown that the damping matrix values assigned to the model can be identified identically through the complex frequency response functions of the model.
- Once the frequency response functions of a structure are known by measurement, the structural and viscous damping matrices can be identified.
- If the computational model is updated using the identified damping matrices, the results will be more accurate for engineering structures.

## Conflict of Interests

No conflict of interest was stated by the authors.

## Declaration of Ethical Standards

The authors of this article declares that the materials and methods used in this study do not require ethical committee permission and legal-special permission.

## References

- [1] Mottershead J.E., Friswell M.I., 1993. Model updating in structural dynamics: a survey. *Journal of Sound and Vibration*, **167**, 347-375.

- [2] Baruch M., 1978. Optimization procedure to correct stiffness and flexibility matrices using vibration tests. *AIAA Journal*, **16**, 1208-1210.
- [3] Berman A., Nagy E.J., 1983. Improvement of a large analytical model using test data. *AIAA Journal*, **21**, 1168-1173.
- [4] Wei F-S., 1990. Analytical dynamic model improvement using vibration test data. *AIAA Journal*, **28**, 175-177.
- [5] Friswell M.I., Inman D., Pilkey D., 1998. Direct updating of damping and stiffness matrices. *AIAA Journal*, **36**, 491-493.
- [6] Imregun M., Visser W.J., Ewins D.J., 1995. Finite element model updating using frequency response function data – 1: Theory and initial investigation. *Journal of Mechanical Science and Technology*, **9**, 187–202.
- [7] Lin R-M., Ewins D., 1990. Model updating using FR data. Paper presented at the 15<sup>th</sup> International Seminar on Modal Analysis, pp.141-162.
- [8] Kwon K.S., Lin R.M., 2005. Robust finite element model updating Taguchi method. *Journal of Sound and Vibration*, **280**, 77-99.
- [9] Jacquelin E., Adhikari S., Fiswell M.I., 2012. A second-moment approach for direct probabilistic model updating in structural dynamics. *Mechanical Systems and Signal Processing*, **29**, 262-283.
- [10] Sipple J.D., Sanayei M., 2014. Finite element model updating using frequency response functions and numerical sensitivities. *Structural Control and Health Monitoring*, **21**, 784–802.
- [11] Pradhan S., Modak S., 2012. Normal response function method for mass and stiffness matrix updating using complex FRFs. *Mechanical Systems and Signal Processing*, **32**, 232-250.
- [12] Arora V., 2014. FE model updating method incorporating damping matrices for structural dynamic modifications. *Structural Engineering and Mechanics*, **52**, 261-274.
- [13] Matta E., Stefano A., 2012. Robust finite element model updating of a large-scale benchmark building structure. *Structural Engineering and Mechanics*, **43**, 371-394.
- [14] Adhikari S., 2001. Damping models for structural vibration. Doctoral dissertation, University of Cambridge, Cambridge, England.
- [15] Salamon R., Kamiński H., Fritzkowski P., 2020. Estimation of parameters of various damping models in planar motion of a pendulum. *Meccanica*, 1-23.
- [16] Shadan F., Khoshnoudian F., Inman D.J., Esfandiari A., 2018. Experimental validation of a FRF-based model updating method. *Journal of Vibration and Control*, **24**, 1570–1583.
- [17] Shadan F., Khoshnoudian F., Esfandiari A., 2016. A frequency response- based structural damage identification using model updating method. *Structural Control and Health Monitoring*, **23**, 286-302.
- [18] Zin M.M., Rani M.A., Yunus M.A., Sani M.S.M., Wan Iskandar Mirza W.I.I., Mat Isa A.A. 2018. Frequency response function (FRF) based updating of a laser spot welded structure. In *AIP Conference Proceedings (Vol. 1952, No. 1, p. 020055)*. AIP Publishing LLC.
- [19] Natke H.G., 1988. Updating computational models in the frequency domain based on measured data: a survey. *Probabilistic Engineering Mechanics*, **3**, 28-35.
- [20] Lu Y., Zhenguo T., 2004. A two-level neural network approach for dynamic FE model updating including damping. *Journal of Sound and Vibration*, **275**, 931-952.
- [21] Lepoittevin G., Gerald K., 2011. Finite element model updating of vibrating structures under free–free boundary conditions for modal damping prediction., *Mechanical Systems and Signal Processing*, **25**, 2203-2218.
- [22] Oktav A., 2020. Identification of non-proportional structural damping using experimental modal analysis data. *Journal of Measurements in Engineering*, **8**, 34-45.

## Appendices

Using (Eq.1) and the boundary conditions for a cantilever beam, the closed form natural frequency can be written as follows:

$$\omega_i = \beta_i^2 \sqrt{\frac{EI}{mL^4}} \quad (\text{A.1})$$

$$\beta_i = 1.875, 4.694, 7.885, ..$$










The state-space representation used for the system is as follows:

$$A = \begin{bmatrix} \mathbf{0} & \mathbf{I} \\ -\mathbf{M}^{-1}(\mathbf{iD} + \mathbf{K}) & -\mathbf{M}^{-1}\mathbf{C} \end{bmatrix} \quad (\text{A.2})$$
$$B = \begin{bmatrix} \mathbf{0} \\ \mathbf{M}^{-1} \end{bmatrix}; \quad C = [\mathbf{I} \quad \mathbf{0}]; \quad D = \mathbf{0}$$





## Development of Personal Protective Respirator Based on Additive Manufacturing Technologies in Fighting Against Pandemic

Levent AYDIN <sup>1,\*</sup> , Sumeyya ILKIN <sup>2</sup> , Mehmet Onur ARICAN <sup>3</sup> , Ayfer Peker KARATOPRAK <sup>4</sup> ,  
Suhap SAHIN <sup>5</sup> , Guralp OZKOC <sup>6</sup> , Maksut Gorkem AKSU <sup>7</sup> , Serdar KUCUK <sup>8</sup> ,  
Ozcan GUNDOGDU <sup>9</sup> 

<sup>1</sup> Podology Program, Vocational School of Kocaeli Health Services, Kocaeli University, Kocaeli, 41001, Turkey, **ORCID:** 0000-0002-2372-1711

<sup>2</sup> Department of Computer Engineering, Kocaeli University, Kocaeli, 41001, Turkey, **ORCID:** 0000-0002-0570-2250

<sup>3</sup> Department of Polymer Science and Technology, Kocaeli University, Kocaeli, 41001, Turkey, **ORCID:** 0000-0003-3776-9174

<sup>4</sup> Podology Program, Vocational School of Kocaeli Health Services, Kocaeli University, Kocaeli, 41001, Turkey, **ORCID:** 0000-0003-1723-2038

<sup>5</sup> Department of Computer Engineering, Kocaeli University, Kocaeli, 41001, Turkey, **ORCID:** 0000-0003-1340-8972

<sup>6</sup> Department of Chemical Engineering and Polymer Science and Technology, Kocaeli University, Kocaeli, 41001, Turkey, **ORCID:** 0000-0002-3194-5256

<sup>7</sup> Department of Radiation Oncology, Kocaeli University, Kocaeli, 41001, Turkey, **ORCID:** 0000-0001-5532-2742

<sup>8</sup> Department of Biomedical Engineering, Kocaeli University, Kocaeli, 41001, Turkey, **ORCID:** 0000-0002-5543-7539

<sup>9</sup> Department of Biomedical Engineering, Kocaeli University, Kocaeli, 41001, Turkey, **ORCID:** 0000-0003-0171-3179

### Article Info

#### Research paper

Received : November 29, 2020

Accepted : January 27, 2021

#### Keywords

Covid-19

FDM

Mask

Respirator

N95

Pandemic

### Abstract

Flexible manufacturing systems have been widely used especially in the field of medicine to develop personal protective types of equipment such as ventilator components or sample collection apparatuses except the face visors and masks/respirators during the fight against the pandemic. In this study, an N95 derivative respirator was designed based on the FDM technology and then compared with similar known mask models in literature in terms of manufacturing costs and functionality. Optimization was carried out on printing parameters to improve the speed of manufacturing. Finally, all components of the mask were assembled and prepared to be used for medical needs during the pandemic. The cost of the mask and filter components were reduced to 7 ₺ for 2 hours and 32 minutes for each mask. Moreover, the durability of each mask was increased three times more than known protective types of equipment to offer longer usage without any fractures caused by daily activities and to have improved airtightness. Besides, the mask was designed to have multi-layered filters with the ability of replaceable membranes according to the epidemic agent, and the sterilization procedures were explained. Thus, a more economical and healthier protective equipment was created compared to the known respirators in the literature.

## 1. Introduction

The disease of Covid-19 (Coronavirus) was first detected in Wuhan in December 2019. It has turned into a pandemic in early 2020 that reached 26 million cases causing more than 864 thousand deaths in 188 countries [1-2]. While the most common symptoms of the disease are known as fever and dry cough, there are also less frequent symptoms such as pain and diarrhea. For patients with worsening conditions, respiratory distress and

shortness of breath occur and may require urgent medical assistance such as intubation or oxygen therapy. In addition, patients with diffuse pneumonia findings on chest radiography or tomography are isolated in intensive care units and need to be treated according to a specific algorithm [3]. With the onset of the pandemic, both patients and healthcare workers needed a lot of protective equipment, and it was not possible for every center to meet these requirements. Many different applications such as ventilator components or sample collection apparatus, protective equipment (i.e., visors and respirators), which can be easily produced via flexible manufacturing systems, were used to fight against the pandemic [4]. In particular, Fused Deposition Modelling (FDM) based additive

\* Corresponding Author: [levent.aydin@kocaeli.edu.tr](mailto:levent.aydin@kocaeli.edu.tr)





manufacturing systems were widely used in the production of such equipment and component due to their cost-effectiveness. At the beginning phase of the pandemic, rapid solutions were required to be addressed with regards to crisis management based on health priority [5]. Since these manufactured equipment types were used by many people in health centers and hospitals, where they both have high-risk factors, the protection and functionality were not known well leading to create significant risks [6]. For this reason, some definitions and standards for the development of protective equipment based on additive manufacturing technologies have been determined by the authorized organizations (i.e., FDA, CDC, NIH). The Food and Drug Administration (FDA) has recently stated that 3D printed personal protective equipment (PPE) cannot provide one-to-one protection compared to FDA-approved masks. On the other hand, guidelines on 3D printable devices for emergency use such as ventilator components have been published by FDA [7]. Likewise, the Centers for Disease Control and Prevention (CDC) did not approve homemade face protectors in the category of PPE [8]. However, the National Institutes of Health (NIH) together with the FDA created an online repository for developable PPE prototypes based on additive manufacturing technologies but reported safety limitations due to differences in 3D printing systems, production parameters, and polymer materials used in manufacturing [9]. Although its reliability is questionable, during the pandemic, additive manufacturing technologies-based visors, masks/respirators, goggles, breathing apparatus, and laryngoscope production have been beneficial because a huge equipment need has been met significantly [10-12]. In this scope, it is necessary to know the properties of the equipments used, to ensure the functionality and protection of the products developed and to establish more ergonomic equipment for long-term usage. In addition, it is important to minimize the manufacturing time and cost in order to provide widespread effective protection. Specifically for N95-derived respirators, filters, and filter membrane porosity are important not only for sterilization but also for effectiveness and reusability. Considering these factors, the development of PPE, based on additive manufacturing technologies, gains great importance during the pandemic. Hence, many additive manufacturing methods were utilized in PPE production such as Direct Metal Laser Sintering (DMLS), Selective Laser Sintering (SLS), Fused Deposition Modelling (FDM), and Stereolithography (SLA) methods. FDM method-based equipment manufacturing is more widely used than other additive manufacturing technologies due to its low cost and feasibility [13-15]. Mostly PLA (Polylactic Acid), ABS (Acrylonitrile Butadiene Styrene), PC (Polycarbonate), PETG (Polyethylene Terephthalate Glycol), and various

composite polymers are used during the manufacturing [16-17].

In the FDM method, the printing process is carried out by melting and extruding a thermoplastic polymer to form the target object on a printing table. In this scope, the target three-dimensional (3D) model is first divided into transverse 2D (two-dimensional) sections with a slicing software, and then derived G-Codes (machine codes) determine the system behavior until manufacturing is complete. Instant solidification of the molten thermoplastic polymer is provided by a fan during this printing process. However, the nozzle can be clogged due to the burnt polymer residues during printing [18]. Excessive application of the airflow that provides solidification may cause instant solidification of the molten polymer in the nozzle. For these significant and inevitable reasons, these systems must be well calibrated before printing.

Today, there are various defined standards for respirators and filter membranes. Although these standards are named differently according to the countries, they specify the same functionality and mostly express particle permeability efficiency with a minimum size of  $0.3 \mu$  [19]. The respirators are named as N95, N99, and N100 in the United States, and as KN90, KN95, and KN100 in China, the numbers defined next to the letters together express the percentage efficiency at a particle permeability of  $0.3 \mu$  [20]. Consequently, N95 and KN95 have the same functionality and have particle retention of  $0.3 \mu$  at 95%. In Europe, particle permeability has been determined as FFP1 (P1), FFP2 (P2), and FFP3 (P3), and it means filtering efficiency at 80%, 94%, and 99.95%, respectively [21]. In addition, the MERV (Minimum Efficiency Rating Value) standard was developed to define the filter efficiency and graded between 1 and 17 as shown in Table 1. MERV standard is based on particle permeability in three different size that range between ( $3.0 - 10.0 \mu$ ,  $1.0 - 3, 0 \mu$ , and  $0.3 - 1.0 \mu$ ) are also categorized in Table 1 [22-23].

In Table 1, it is observed that MERV 17 filter group has 99% retention in the  $0.3 - 1.0 \mu$  particle size band, while the MERV 13-16 filter group has less than 95% retention in the same particle size band. Accordingly, it is understood that the HEPA (High-Efficiency Particulate Arresting) filter group provides better protection than the Superior MERV filter group. Therefore, considering the spread rate of the virus during the pandemic, the use of HEPA Group filters in PPE development becomes even more important. It has not been possible in all cases to supply these filter membranes, which are used especially in the production of N95-derived respirators, at the beginning of the pandemic. Hence, a need was raised to prefer or develop alternative membranes. In line with this requirement, researchers have developed filter membranes with a certain porosity by means of electrospinning

methods [24-26]. On the other hand, vacuum cleaner filters were determined as suitable owing to the standard manufacturing and procurable especially at the beginning

of the pandemic. Table 2 contains statements regarding HEPA filter groups and their activities [27-28].

**Table 1.** MERV filter membrane standards [22-23].

Catalog No	0.3-1.0 micron	1-3 micron	3-10 micron	Filter Type	Controlled Particles
MERV 1	-	-	<20%	Pre-Filter/Aluminum mesh	Dust, dust mites, animal dander, pollen
MERV 2	-	-	<20%		
MERV 3	-	-	<20%		
MERV 4	-	-	<20%		
MERV 5	-	-	20-34%	Low Quality MERV Filter	Mildew, spores, baking soda, hair spray
MERV 6	-	-	35-49%		
MERV 7	-	-	50-69%		
MERV 8	-	<20%	<70%		
MERV 9	-	<35%	<35%	Standard MERV Filter	Lead dust, smaller mold, smaller pollen
MERV 10	-	50-64%	<75%		
MERV 11	<20%	65-79%	<80%		
MERV 12	<35%	80%	<85%		
MERV 13	<50%	<90%	<90%	Superior MERV Filter	Bacteria, virus, fine dust
MERV 14	75-84%	<90%	<90%		
MERV 15	85-94%	<90%	<90%		
MERV 16	<95%	<95%	< 95%		
MERV 17	99.97000%	<99%	< 99%	HEPA Group/ULPA Filter	Little bacteria and viruses, fumes

**Table 2.** HEPA filter membrane standards [27-28].

Usage	Class	Performance	Performance Test	100% Retained Particle Size	Test Standard
Coarse filters (preferred as a primary filter)	G1	65%	Average value	>5 µm	BS EN779
	G2	65-80%	Average value	>5 µm	BS EN779
	G3	80-90%	Average value	>5 µm	BS EN779
	G4	90%-	Average value	>5 µm	BS EN779
Fine filters (preferred as a secondary filter)	M5	40-60%	Average value	>5 µm	BS EN779
	M6	60-80%	Average value	>2 µm	BS EN779
	F7	80-90%	Average value	>2 µm	BS EN779
	F8	90-95%	Average value	>1 µm	BS EN779
Semi HEPA filters	F9	95%-	Average value	>1 µm	BS EN779
	E10	85%	Minimum value	>1 µm	BS EN1822
	E11	95%	Minimum value	>0.5 µm	BS EN1822
HEPA filters	E12	99.5%	Minimum value	>0.5 µm	BS EN1822
	H13	99.95%	Minimum value	>0.3 µm	BS EN1822
ULPA	H14	99.995%	Minimum value	>0.3 µm	BS EN1822
	U15	99.9995%	Minimum value	>0.3 µm	BS EN1822
	U16	99.99995%	Minimum value	>0.3 µm	BS EN1822
	U17	99.999995%	Minimum value	>0.3 µm	BS EN1822

According to Table 2, class, performance in percentage, performance test, particle size retained in percentage, and related test standard information are given for each filter. It can be observed that HEPA13 and HEPA14 filters are used as vacuum filter membranes in HEPA filter groups [29]. Especially HEPA13 filter membranes, which are more cost-effective and easily available, cannot hold 50 in 100.000 particles (99.95%

efficiency). This filtration ability can also be improved by increasing the existing filter membrane thickness or by using a second filter membrane [30,31]. Thus, the current filtration efficiency can be increased. In addition, during the fight against the pandemic, environment and equipment sterilization are of great importance as PPEs. For this purpose, mobile robots that carrying portable UV-C (Ultraviolet C) lamps with 254 nm wavelength have been





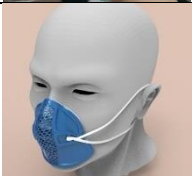
developed in some hospitals for equipment and environment sterilization [32]. Likewise, UV-C lighting is known to kill many bacteria and micro-organisms. This light source causes DNA degradation in structures such as Corona and Sars viruses [33]. Although it may cause permanent damage to the skin and eyes, it is recommended to be used as an ideal solution for unmanned environment isolation and equipment sterilization. Parameters such as lamp power and distance are important in the effectiveness of sterilization [33]. Therefore, a sterilization process that is developed as a result of an optimization or a suggested protocol is required to be applied in terms of efficiency. In this study, a respirator mask that can be used as an N95 derivative was designed and manufactured by means of an FDM based system. Before the design of the respirator, other similar models based on the FDM method in the literature, were determined and evaluated. In addition, the manufacturing time and cost of each model was calculated and compared with the developed prototype. Finally, optimization and revisions were applied to minimize

manufacturing costs and improve the custom fitting of the developed mask to increase protectiveness. Consequently, PPEs may be manufactured at minimal cost and quickly where material supply is difficult to distribute. Moreover, more effective protection can be ensured for healthcare personnel and all other employees, active in the field during the fight against the coronavirus.

## 2. FDM Method Based Personal Protective Masks, Properties, and Production Planning

Before the manufacturing of the developed N95 derived respirator prototype, existing FDM based models utilized in hospitals and health centers were evaluated in terms of time and cost. In this study, the developed face mask design criteria and components were determined using the obtained data. Commonly used masks during the fight against Covid-19 and their features were listed in Table 3.




**Table 3.** FDM-based face masks.

Ref.	Image	Designer	Time*	Cost*	Explanation
[34]		Copper3d (Open Source)	3 h 14 min	35 g	The model consists of 3 components. Printing time and cost are affordable.
[35]		LaFactoria3d (Open Source)	8 h 45 min	96 g	The model consists of 3 components. Although the printing time is quite long, the cost is also a bit high.
[36]		Cagriahiskali (10 €)	10 h 3 min	113 g	The model consists of 3 components. Although the printing time is quite long, the cost is also a bit high.
[37]		Harnelbe (2 €)	5 h 17.3 min	54.3 g	The model consists of 2 components. It is not possible to form the model properly without supporting structures on a flat table surface. The printing time is a little longer while the cost is normal.
[38]		Michaeledi (Open Source)	3 h 24 min	35.5 g	The model consists of 3 components. It is not possible to form the model properly without supporting structures on a flat table surface. Printing time and cost are affordable.

**Table 3.** (Cont.) FDM-based face masks.

[39]	Mask6		3d-mon (Open Source)	20 h 22 min	212 g	The model consists of 3 components. It is not possible to form the model properly without supporting structures on a flat table surface. The printing time is quite long, and the cost is very high.
[40]	Mask7		Aleexstudios_2019 (67 €)	9 h 23 min	83.5 g	The model consists of 5 components. The printing time is quite long, and the cost is also a bit high.
[41]	Mask8		Stan_x (Open Source)	4 h 39 min	47.5 g	The model consists of 2 components. Printing time and cost are normal.
[42]	Mask9		3dpicasso (5.517 €)	13 h 45 min	151 g	The model consists of 3 components. It is not possible to form the model properly without supporting structures on a flat table surface. The printing time is a bit longer, and the cost is also a bit high.
[43]	Mask10		Imalize (Open Source)	7 h 7 min	72 g	The model consists of 2 components. It is not possible to form the model properly without supporting structures on a flat table surface. The printing time is a bit longer, and the cost is also a bit high.
[44]	Mask11		Victorottati (53 €)	8 h 29 min	82 g	The model consists of 7 components. It is not possible to form the model properly without supporting structures on a flat table surface. The printing time is a bit longer, the cost is also a bit high.
[39]	Mask12		3d-mon (Open Source)	20 h 22 min	212 g	The model consists of 3 components. It is not possible to form the model properly without supporting structures on a flat table surface. The printing time is quite long, and the cost is very high.
[46]	Mask13		Copper3d (Open Source)	5 h 16 min	48 g	The model consists of 3 components. The printing time is a bit long, but the manufacturing cost is affordable.
[47]	Mask14		Raimbault_ Industrie (Open Source)	19 h 38 min	216 g	The model consists of 5 components. The printing time is quite long, and the manufacturing cost is also very high.
[48]	Mask15		Ndreu (Open Source)	3 h 34 min	37 g	The model consists of 3 components. It is not possible to form the model properly without supporting structures on a flat table surface. Print time and cost are normal.
[49]	Mask16		_Msa_ (10 €)	9 h 19 min	103 g	The model consists of 11 components. It is not possible to form the model properly without supporting structures on a flat table surface. The printing time is quite long, and the manufacturing cost is quite high.

**Table 3.** (Cont.) FDM-based face masks.

[50]	Mask17		Malamaker (Open Source)	8 h 5 min	81 g	The model consists of 8 components. The printing time is long, the manufacturing cost is also a bit high. Providing an elastic membrane between the mask and the face using a mold is the biggest advantage of the mask.
[51]	Mask18		Think3ddd (Open Source)	8 h 42 min	102 g	The model consists of 3 components. The printing time is long, and the manufacturing cost is also a bit high.
[52]	Mask19		Inhol (Open Source)	8 h 50 min	97 g	The model consists of 3 components. The printing time is long, and the manufacturing cost is also a bit high.

\* The time and cost calculations specified in the table are valid for only one of a mask manufacturing. In addition, it was determined that 50 grams of material consumption with an average time of 4 hours were normal or affordable in the manufacturing of one mask for an FDM-based system. The evaluations of manufacturing in the table were generated based on this reference.

Ultimaker Cura slicing software was used for the time and cost calculations in Table 3. Printing parameters of each mask model in this calculation step are listed in Table 4.

**Table 4.** Printing parameters for cost calculation.

Parameter	Value
Nozzle diameter	400 $\mu$
Layer height	200 $\mu$
Inner fill rate	100%
Inner fill pattern	Line
Default print temperature	200 °C
Default tray temperature	60 °C
Print speed	60 mm/sec
Inner filling print speed	60 mm/sec
Wall printing speed	30 mm/sec
Top/bottom layer printing speed	30 mm/sec
Cooling	Active
Support	Close
Tray adhesion function	Close

The duration of the printing process can be improved by parameters of layer height, internal fill rate, or printing speed. However, in order to clearly determine the cost differences between all models, the ideal manufacturing parameters, that can provide to obtain the target model into a correct geometry as fast as possible, should be taken as reference. Therefore, manufacturing parameters can also be optimized for all mask models. Thus, printing time can be

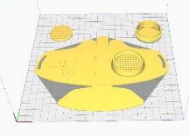
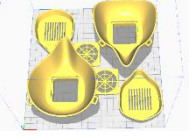
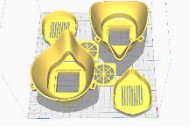
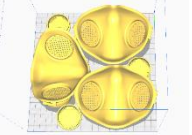
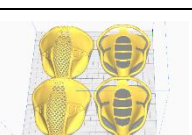
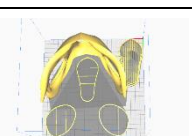
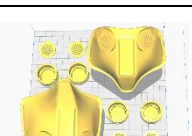
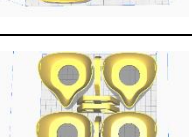
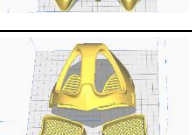
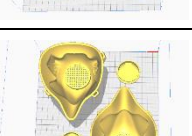
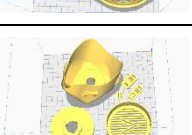
significantly reduced by utilizing the following changes as an example:

- Increasing the layer height from 200  $\mu$  to 350  $\mu$  depending on the nozzle diameter,
- Increasing the printing speed from 60 mm/sec to 120 mm/sec depending on the system mechanics,
- Reducing the inner fill rates from 100% to 30% in the target model for unnecessary solid regions,

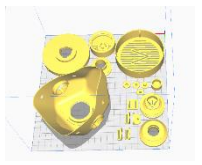
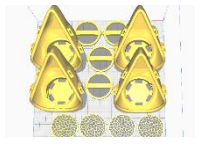
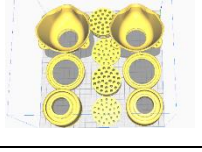

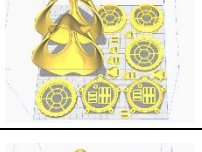
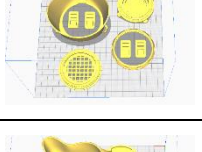
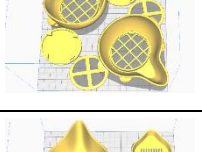
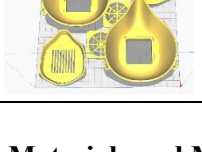
It should be noted that the output must be controlled after each revision in order to ensure the quality of the equipment. In addition, the cost calculations include only the 3D printed body parts and sub-components but not any filter membrane or fixing apparatuses such as rubber. Table 5 contains the ideal manufacturing plan of different types of equipment as listed in Table 3 (excluding filter membrane and rubber components). The mentioned costs were determined by utilizing the grams spent in manufacturing for ESUN PLA filament (1 kg = 100 ₺) and Ultimaker PLA filament (1 kg = 480 ₺). During this cost calculation build plate of the printer was identified as 220 mm/220 mm (X/Y). Each mask model was placed on the same build plate, and printing parameters were fixed for each model. Moreover, their functionalities were evaluated as listed in Table 5. Consequently, basic needs for mask manufacturing were determined according to the results of this evaluation. In this study, an N95 derivative face mask was designed based on the FDM technology and compared with similar known mask models in literature in terms of manufacturing costs and functionality. Furthermore, optimization was carried out on printing parameters to improve the speed of manufacturing. Finally, all components of the mask were assembled and prepared to be used for medical needs during a pandemic.



**Table 5.** Manufacturing plan of masks (manufacturing cost of each model was determined in term of Turkish Lira, ₺).

Image	Max.*	Cost*	Explanation
Mask1 	1 pc	Esun 3.5 ₺ Ultimaker 16.8 ₺	Only one mask can be obtained during manufacturing. In addition, the wall thickness of the model is very thin and it must be manufactured with a flexible thermoplastic elastomer polymer such as ESUN e-Lastic. Otherwise, it may break or crack. In addition, it may not fit every facial anatomy and may require additional rubber components.
Mask2 	2 pcs	Esun 9.6 ₺ Ultimaker 46.08 ₺	Two masks can be obtained during manufacturing. The apparatus used to fix the filter membrane on the main body of the mask may fall. In addition, it may not fit every facial anatomy and may require additional rubber components.
Mask3 	2 pcs	Esun 11.3 ₺ Ultimaker 54.24 ₺	Two masks can be obtained during manufacturing. The apparatus used to fix the filter membrane on the main body of the mask may fall. In addition, it may not fit every facial anatomy and may require additional rubber components.
Mask4 	3 pcs	Esun 5.43 ₺ Ultimaker 26.064 ₺	Three masks can be obtained during manufacturing. It offers a solid fixation opportunity with its screwed apparatus. With the dual filter membrane support, it allows to breathe more easily, but it may not fit every facial anatomy and may require additional rubber components. In addition, it is very difficult to manufacture with an FDM-based system without a support structure.
Mask5 	2 pcs	Esun 3.55 ₺ Ultimaker 17.04 ₺	Two masks can be obtained during manufacturing. The apparatus used to fix the filter membrane on the main body of the mask may fall. It may not fit every facial anatomy and may require additional rubber components. In addition, it is very difficult to manufacture with an FDM-based system without a support structure.
Mask6 	1 pc	Esun 21.2 ₺ Ultimaker 101.76 ₺	Only one mask can be obtained during manufacturing. The filter membrane fixing apparatus is relatively thin and It may not fit every facial anatomy and may require additional rubber components. In addition, it is very difficult to manufacture with an FDM-based system without a support structure.
Mask7 	2 pcs	Esun 8.35 ₺ Ultimaker 40.08 ₺	Two masks can be obtained during manufacturing. It offers a solid fixation opportunity with its screwed apparatus. With the dual filter membrane support, it allows to breathe more easily, but it may not fit every facial anatomy and may require additional rubber components. In addition, it is very difficult to manufacture with an FDM-based system without a support structure.
Mask8 	4 pcs	Esun 4.75 ₺ Ultimaker 22.8 ₺	Four masks can be obtained during manufacturing. The apparatus used to fix the filter membrane on the main body of the mask may fall. In addition, it may not fit every facial anatomy and may require additional rubber components.
Mask9 	1 pc	Esun 15.1 ₺ Ultimaker 72.48 ₺	Only one mask can be obtained during manufacturing. The apparatus used to fix the filter membrane on the main body of the mask may fall. It may not fit every facial anatomy and may require additional rubber components. In addition, it is very difficult to manufacture with an FDM-based system without a support structure.
Mask10 	2 pcs	Esun 7.2 ₺ Ultimaker 34.56 ₺	Two masks can be obtained during manufacturing. It may not fit every facial anatomy and may require additional rubber components. In addition, it is very difficult to manufacture with an FDM-based system without a support structure.
Mask11 	1 pc	Esun 8.2 ₺ Ultimaker 39.36 ₺	Only one mask can be obtained during manufacturing. The apparatus used to fix the filter membrane on the main body of the mask may fall. It may not fit every facial anatomy and may require additional rubber components. In addition, it is very difficult to manufacture with an FDM-based system without a support structure.

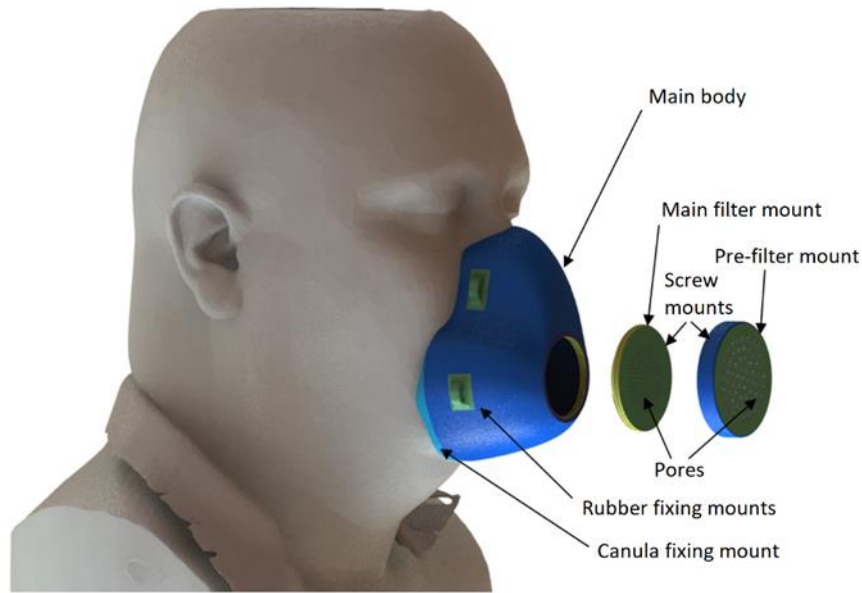
**Table 5.** (Cont.) Manufacturing plan of masks (manufacturing cost of each model was determined in term of Turkish Lira, ₺).

Image	Max.*	Cost*	Explanation
Mask12 	1 pc	Esun 11.8 ₺ Ultimaker 56.64 ₺	Only one mask can be obtained during manufacturing. The apparatus used to fix the filter membrane on the main body of the mask may fall. It may not fit every facial anatomy and may require additional rubber components. In addition, it is very difficult to manufacture with an FDM-based system without a support structure. The existing mask structure consists of too many components.
Mask13 	4 pcs	Esun 4.8 ₺ Ultimaker 23.04 ₺	Four masks can be obtained during manufacturing. It may not fit every facial anatomy and may require additional rubber components.
Mask14 	2 pcs	Esun 21.6 ₺ Ultimaker 103.68 ₺	Two masks can be obtained during manufacturing. The apparatus used to fix the filter membrane on the main body of the mask may fall. It may not fit every facial anatomy and may require additional rubber components. In addition, it is very difficult to manufacture with an FDM-based system without a support structure.
Mask15 	2 pcs	Esun 3.7 ₺ Ultimaker 17.76 ₺	Two masks can be obtained during manufacturing. It may not fit every facial anatomy and may require additional rubber components. In addition, it is very difficult to manufacture with an FDM-based system without a support structure.
Mask16 	2 pcs	Esun 10.3 ₺ Ultimaker 49.44 ₺	Two masks can be obtained during manufacturing. It may not fit every facial anatomy and may require additional rubber components. In addition, it is very difficult to manufacture with an FDM-based system without a support structure. The existing mask structure consists of too many components.
Mask17 	1 pc	Esun 8.1 ₺ Ultimaker 38.88 ₺	Only one mask can be obtained during manufacturing. It has a molded elastic membrane that allows a better custom fitting and prevents leakage. It is very difficult to manufacture with an FDM-based system without a support structure.
Mask18 	2 pcs	Esun 10.2 ₺ Ultimaker 48.96 ₺	Two masks can be obtained during manufacturing. It may not fit every facial anatomy and may require additional rubber components.
Mask19 	2 pcs	Esun 19.4 ₺ Ultimaker 93.12 ₺	Two masks can be obtained during manufacturing. It may not fit every facial anatomy and may require additional rubber components. In addition, it is very difficult to manufacture with an FDM-based system without a support structure.

### 3. Materials and Methods

Initially, additive manufactured masks in the literature were evaluated in terms of design, functionality, and manufacturing cost. Considering these features, a cost-effective mask model that can use any standard filter membrane and printed quickly without support structures was developed. The main body of the mask was designed in SolidWorks 2019 (Dassault Systemes) workspace.

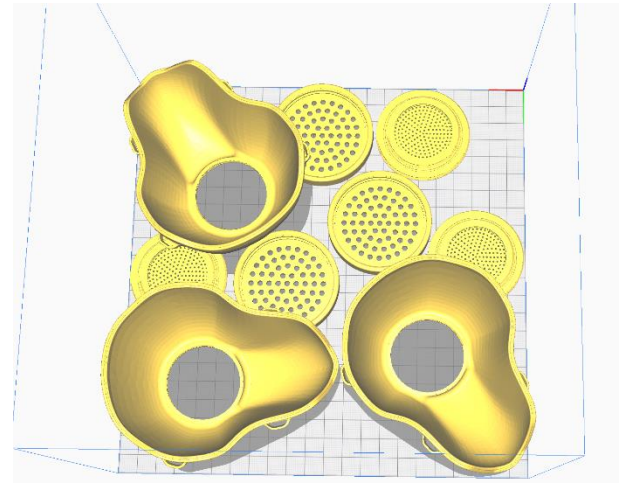
During the design step, the mask body was manufactured without support structures and developed at sufficient thickness to prevent any leakage. In addition, the filtering process was planned gradually in order to increase protection. Thus, it was possible to filter large particles directly with a pre-filter and smaller particles were collected by a second filter membrane. Figure 1 illustrates the 3D mask model and the sub-components.



**Figure 1.** Schematic drawing of the mask model and sub-components.

In the design step, a special filtering apparatus was created according to the gradual filtering process, which can be fixed via screw mounts to create a sealing between the filter apparatus and the main body of the mask. It was planned to provide airflow through 3 mm holes on the pre-filtering apparatus and 500  $\mu$  holes on the main filtering apparatus to create a gradual filtration. The circular membrane width to be placed on the filter apparatus was designed as 40 mm and all components had a thickness of 3 mm to prevent any cracking or leaking.

The manufacturing plan was made after the final design of the mask model was completed. It was possible to manufacture at least 3 masks at one time, according to the manufacturing scenario that was realized in Ultimaker Cura software, for any FDM-based system with 220 mm/220 mm build area. Figure 2 illustrates the maximum manufacturing plan of the developed mask model for the 22 cm<sup>2</sup> build table. Support structures were not included during this planning in order to save time. Likewise, too much manufacturing at one time by placing the components on top of each other was not included in order to ensure the product quality. Therefore, each component was planned to contact the surface of the build table. Hence, any production risk related to complex geometry, which may prevent the printing process, was avoided. The purpose of this planning with the mentioned criteria was to produce a high protective and healthy equipment in a short time and to deliver as fast as possible for mask users. Figure 2 illustrates the maximum production planning of the 3D mask model and its sub-components.



**Figure 2.** Production planning of the developed mask.

After the production plan, the mask model was manufactured by an FDM based 3D printer (Ender 3 Pro, Creality). Before manufacturing, GCodes were derived by utilizing the parameters given as reference in Table 4, and then the mask was manufactured with ESUN PLA filament. With the completion of the manufacturing process, other sub-components such as rubber and filter membrane were determined. In this context, the mesh density of an existing filter membrane in FFP2 standard and filter membrane in 2 different HEPA13 standards was observed via a microscope (Portable Digital USB microscope 1000X, Ultra-eye-Optics Ltd.) and measured with ImageJ (Fiji) software. It was observed that HEPA13 standard vacuum cleaner filters were cost-effective and can be obtained easier than other FFP3 and FFP2 standard filter membranes especially at the initial stage of the pandemic. For this reason, in this study, it was planned to use 2 layers of a 1000  $\mu$  thick HEPA13 standard vacuum



cleaner (Philips, Marathon) filter as a filter membrane. In addition, nasal cannula tubing was used as a silicone sealing apparatus on the main body of the mask that provides better fitting on any facial anatomy. A rubber, 5 mm wide, oval-shaped, tres knitted rope was preferred for long-term use. After the assembly step, improvements, as given in Table 6, were made to the existing manufacturing process to reduce the time and cost. Finally, ideal manufacturing parameters were determined to obtain the developed protective equipment at a minimal cost.

#### 4. Results and Discussion

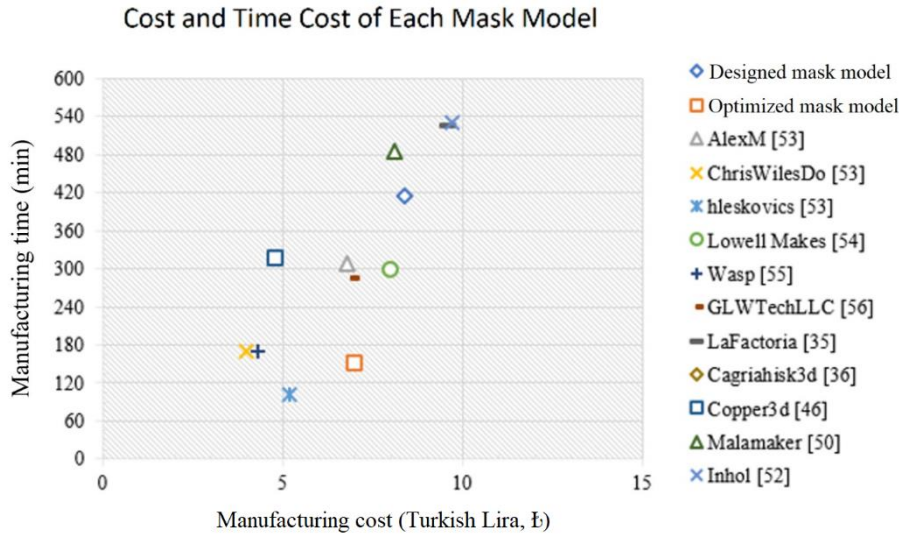
The manufacturing time of a mask and sub-components was calculated as 6 hours 55 minutes. The consumable material required for production was also determined as 84 grams. The internal fill rate was reduced to 30% for regions thicker than 3 mm on the main body of the mask. Likewise, other manufacturing parameters were revised and determined as ideal for the developed mask as shown in Table 6. The processing time was reduced to 2 hours 32 minutes and the amount of material to 70 grams by using the parameters given in Table 6. Thus, masks can

be manufactured with a desired thick wall to prevent any deformation during daily usage. As a result, the manufacturing cost of a mask was determined as 7 ₺ for ESUN PLA filament, excluding rubber, filter membrane, and sealing component.

**Table 6.** Optimized printing parameters for the slicer.

Parameter	Value
Layer height	300 $\mu$
Inner fill rate	30%
Print speed	120 mm/sec
Inner filling print speed	120 mm/sec
Wall printing speed	60 mm/sec
Top/bottom layer printing speed	60 mm/sec

Figure 3 illustrates the comparison of the time and costs required for the manufacturing of a mask body and sub-components only.



**Figure 3.** FDM-based production time and costs of N95-derived masks.

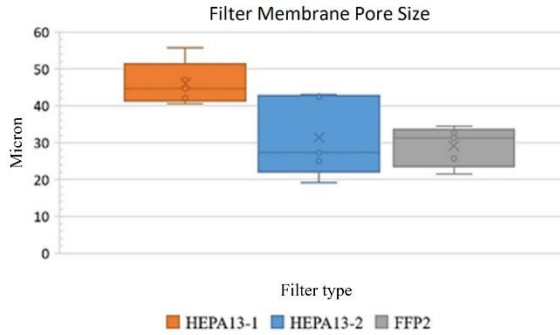
According to the porosity measurements of the filter membranes, a standard FFP2 filter membrane (thickness 200  $\mu$ ) was determined between 21.4  $\mu$  (min.) and 32.6  $\mu$  (max.) (n = 5). In addition, measurements were performed on two different HEPA13 filter membranes (thickness 1000  $\mu$ ): i) For HEPA13-1 (Philips, Marathon product) it was measured as 19.1  $\mu$  (min.) and 43  $\mu$  (max.), and ii) For HEPA13-2 (another HEPA13 from a different supplier) it was measured as 40.5  $\mu$  (min.) and 55.7  $\mu$  (max.) (n = 5). As a result, average porosity of 4.84  $\mu$  was determined for a standard FFP2 filter membrane and 5.34  $\mu$  for the

HEPA13-2 filter which is close to the FFP2 standard. Figure 4 illustrates the pore sizes of a standard FFP2 filter membrane and two different HEPA13 filters (Philips Marathon vacuum cleaner filter and another HEPA13 filter).

It was determined that 60 filter membranes could be obtained (1000  $\mu$  thick) in a single vacuum cleaner filter and the cost of a filter (Philips, Marathon) was 30 ₺. The total cost of the mask and its components were listed as below:

- i) Mask and sub-components – 7 ₺,

ii) Filter membrane - 0.5 ₺,  
 iii) Sealing apparatus (nasal cannula) - 1.25 ₺ and  
 iv) Rubber - as 0.25 ₺. In total, the manufacturing of a whole mask cost 9 ₺. Figure 5 illustrates the assembled mask prototype.

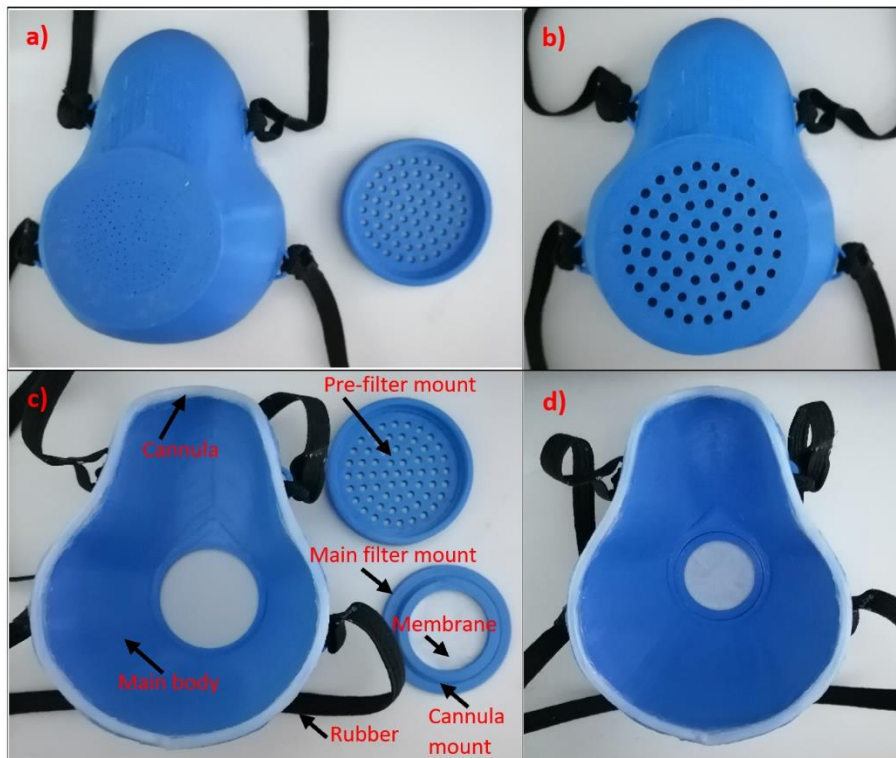


**Figure 4.** FFP2 and HEPA pore sizes (n=5).

The flexibility of the filament is important especially during the 3D printing of Mask 1 that is given in Tables 3. In addition, these flexible filaments should not be printed at normal and high speeds [53]. For this reason, masks in this group were excluded from the comparison chart given in Figure 3. Full face masks or masks that have additional eye protection apparatus were also not considered. Apart

from these, designs that only cover the mouth and nose, such as Mask 12, have too many components. Hence, their printing time is quite long and their components can cover almost the entire surface of the build plate. On the contrary, it was determined that models with a design such as Mask 17 are more suitable in terms of manufacturing planning and usage. In addition to this planning, the manufacturing costs of each mask model is also important. The current manufacturing time and cost of the Mask 17 is higher (3.19 and 1.1 times, respectively) than the developed mask model in this study. Moreover, the thickness of the mentioned model is 1.5 times less which may affect the durability and tightness.

The thick body structure may increase durability, especially in long-term use. An unwanted leakage, caused by the gaps between perimeters during the 3D printing process, may occur in models with thinner body structures such as Mask 11. Although the thickness of the body structure extends the printing time, the protection provided by the mask is more important, and thus it's recommended that the thickness value should be a minimum of 2 mm as a result of this evaluation. It was observed that 1 mm and thinner models even the separation of the model may crack from the build table after printing.



**Figure 5.** Completed mask prototype. Top view of assembled main filter apparatus only (a) and the assembled main filter and pre-filter apparatus (b). View of all unassembled (c) and assembled components (d).

Another important parameter is the attachable filter mount apparatus in mask models such as used in Mask 19. This apparatus is designed to be directly attached to the main body of the mask. Therefore, it may deform and may cause leakage during usage after several assemblies. On the other hand, the masks with screw mounts such as Mask 1 and Mask 17 prevent more leakage than the models such as Mask 19. In this study, in order to minimize the unwanted leakage, it was decided to connect the main body of the mask and the filter apparatus by screwing. Moreover, a cannula, a gasket, or a silicone component can be placed into the gap between these two parts to improve tightness. Custom fitting is crucial for each mask to provide better protection. As observed in many mask models except the Mask 3 and Mask 17, the main body structures of the models require to contact directly with the face that may cause skin irritation. As applied in Mask 17, it is recommended to use a silicone or a rubber component between the mask and the face to prevent this discomfort and skin irritation, especially during long-term use. The sealing component must be developed or preferred from a medical-grade material whose effects are well-known.

In addition to the mask design, the type and protection of the used filter membranes are important. Although the Coronavirus sizes are very small, such as 100 nm, protection tests for a standard FFP2 or a HEPA filter are defined as 300 nm (min.) particle sizes [57-58]. In this case, the pore sizes of the filter membranes, their thickness, and particle capture capabilities also play a crucial role. These abilities may be grouped as mechanical particle capture capability, other trapping features such as inertia effect, retention, blocking, and diffusion in filter membranes or electrostatic capture that can be created in fibers [59]. Functionality tests of all these features are carried out by experimental or simulation studies to reveal the protection quality of the filter membranes [60]. As a result of this research, it was observed that the HEPA13 filter membrane properties were close to a standard FFP2 filter membrane. However, it should be noted that even commercially available same filter membranes may have different pore sizes. Therefore, it is recommended to perform an experimental study based on the target pathogen sizes before usage.

Although FFP2 or HEPA standards are generally preferred on filter membranes in FDM-based mask prototypes, long-term protection is still uncertain. Even the FFP3 standard, it was determined that filter membranes prevent the risk of infection with an efficiency range of 94% to 99% during a 20-minute inhalation [61]. Therefore, Ultra Hepa Filter (ULPA) group, which is listed in Table 2, is recommended as filter membranes to increase the protectiveness of developed masks.

## 4. Conclusions

In this study, a more reliable, robust, and cheaper respirator was developed to fight against the pandemic. Furthermore, the fundamentals of mask design and manufacturing process were meticulously clarified to ensure the protectiveness of personal equipment. In particular, the manufacturing time and cost of FDM-based masks were significantly decreased. Moreover, the airtightness of the mask was improved via commercially available components.

## Acknowledgments

This study was financially supported by BAP Project (FHD-2020-2220) of Kocaeli University.

## Conflict of Interests

No conflict of interest was stated by the authors.

## Declaration of Ethical Standards

The authors of this article declare that the materials and methods used in this study do not require ethical committee permission and legal-special permission.

## References

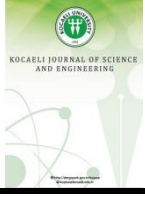
- [1] WHO, 2020. Naming the Coronavirus Disease (COVID-19) And the Virus That Causes It. [https://www.who.int/emergencies/diseases/novel-coronavirus-2019/technical-guidance/naming-the-coronavirus-disease-\(covid-2019\)-and-the-virus-that-causes-it](https://www.who.int/emergencies/diseases/novel-coronavirus-2019/technical-guidance/naming-the-coronavirus-disease-(covid-2019)-and-the-virus-that-causes-it). (Access Date: 20.11.2020).
- [2] Wikipedia, 2020. COVID-19 Pandemic. [https://en.wikipedia.org/wiki/COVID-19\\_pandemic](https://en.wikipedia.org/wiki/COVID-19_pandemic). (Access Date: 20.11.2020).
- [3] TR Ministry of Health Scientific Advisory Board Study, 2020. Covid-19 Adult Patient Treatment. [http://www.solunum.org.tr/TusadData/userfiles/file/covid-19\\_rehberi\\_eriskin\\_hasta\\_tedavisi.pdf](http://www.solunum.org.tr/TusadData/userfiles/file/covid-19_rehberi_eriskin_hasta_tedavisi.pdf). (Access Date: 20.11.2020).
- [4] Choong Y.Y.C., Tan H.W., Patel D.C., Choong W.T.N., Chen C.H., Low H.Y., Tan M.J., Patel C.D., Chua C.K., 2020. The Global Rise of 3D Printing During the COVID-19 Pandemic. *Nature Reviews Materials* **5**, pp. 637-639.
- [5] Ishack S., Lipner S.R., 2020. Applications of 3D Printing Technology to Address COVID-19 Related Supply Shortages. *The American Journal of Medicine* **2**, pp. 1-14.

- [6] FDA, 2020. FDA's Role in 3D Printing. <https://www.fda.gov/medical-devices/3d-printing-medical-devices/fdas-role-3d-printing>, (Access Date: 10.10.2020).
- [7] Clifton W., Damon A., Martin A.K., 2020. Considerations and Cautions for Three-Dimensional-Printed Personal Protective Equipment in the COVID-19 Crisis. *3D Printing and Additive Manufacturing* **7**, pp. 97-99.
- [8] CDC, 2020. Strategies for Optimizing the Supply of Facemasks. <https://www.cdc.gov/coronavirus/2019-ncov/hcp/ppe-strategy/face-masks.html>. (Access Date: 03.04.2020).
- [9] NIH, 2020. COVID-19 Supply Chain Response. <https://3dprint.nih.gov/collections/covid-19-response>. (Access Date: 03.04.2020).
- [10] Attaran M., 2020. 3D Printing Role in Filling the Critical Gap in the Medical Supply Chain During COVID-19 Pandemic. *American Journal of Industrial and Business Management* **10**, pp. 988-1001.
- [11] Ishack S., Lipner S.R., 2020. Applications of 3D Printing Technology to Address COVID-19 Related Supply Shortages. *The American Journal of Medicine* **133**, pp. 771-773.
- [12] Mostaghimi A., Antonini M.J., Plana D., Anderson P.D., Beller B., Boyer E.W., Fannin A., Freake J., Oakley R., Sinna M.S., Smith L., Van C., Yang H., Sorger P.K., LeBoeuf N.R., Yu S.H., 2020. Regulatory and Safety Considerations in Deploying a Locally Fabricated, Reusable Face Shield in a Hospital Responding to the Covid-19 Pandemic. *Med* **1**, pp. 1-18.
- [13] Long J., Gholizadeh H., Lu J., Bunt C., Seyfoddin A., 2017. Application of Fused Deposition Modelling (FDM) Method of 3D Printing in Drug Delivery. *Current Pharmaceutical Design* **23**, pp. 433-439.
- [14] Chen M.Y., Skewes J., Woodruff M.A., Dasgupta P., Rukin N.J., 2020. Multi-Colour Extrusion Fused Deposition Modelling: A Low-Cost 3D Printing Method for Anatomical Prostate Cancer Models. *Scientific Reports* **10**, pp. 1-5.
- [15] Rengier F., Mehndiratta A., Von Tengg-Kobligk H., Zechmann C., Unterhinninghofen R., Kauczor H., Giesel F., 2010. 3D Printing Based on Imaging Data: Review of Medical Applications. *International Journal of Computer Assisted Radiology and Surgery* **5**, pp. 335-341.
- [16] Ilardo R., Williams C., 2010. Design and Manufacture of a Formula SAE Intake System Using Fused Deposition Modeling and Fiber-Reinforced Composite Materials. *Rapid Prototyping Journal* **16**, pp. 174-179.
- [17] Shofner M., Lozano K., Rodríguez-Macias F., Barrera E., 2003. Nanofiber-Reinforced Polymers Prepared by Fused Deposition Modeling. *Journal of Applied Polymer Science* **89**, pp. 3081-3090.
- [18] Heller B., Smith D., Jack D., 2015. The Effects of Extrudate Swell, Nozzle Shape, And the Nozzle Convergence Zone on Fiber Orientation in Fused Deposition Modeling Nozzle Flow. American Society of Composites-30th Technical Conference, Michigan, USA, 28-30 September, pp. 1220-1236.
- [19] Neupane B., Giri B., 2020. Current Understanding on the Effectiveness of Face Masks and Respirators to Prevent the Spread of Respiratory Viruses. *enrXiv*, <https://doi.org/10.31224/osf.io/h3wgc>.
- [20] CDC - NIOSH - Respirator Fact Sheet. Understanding Respiratory Protection Against SARS, <https://www.cdc.gov/niosh/npptl/topics/respirators/fact-sheets/respsars.html>. (Access Date: 03.04.2020).
- [21] Wigglesworth N., 2019. Infection Control 5: Equipment for Facial and Respiratory Protection. *Nursing Times* **10**, pp. 30-32.
- [22] Deneysan, 2020. Havalandırma. [http://deneysan.com/Content/images/documents/havalandirma-3\\_63272884.pdf](http://deneysan.com/Content/images/documents/havalandirma-3_63272884.pdf). (Access Date: 03.04.2020).
- [23] Airfuji, 2020. Hepa Versus MERV Filters. <https://airfuji.com/hepa-vs-merv>. (Access Date: 10.06.2020).
- [24] He H., Gao M., Illés B., Molnar K., 2020. 3D Printed and Electrospun, Transparent, Hierarchical Polylactic Acid Mask Nanoporous Filter. *International Journal of Bioprinting* **6**, pp. 1-9.
- [25] Bulus E., Bulus G.S., Yakuphanoglu F., 2020. Production of Polylactic Acid-Activated Charcoal Nanofiber Membranes For COVID-19 Pandemic by Electrospinning Technique and Determination of Filtration Efficiency. *Journal of Materials and Electronic Devices* **4**, pp. 21-26.
- [26] Ahmed M.K., Afifi M., Uskoković V., 2020. Protecting Healthcare Workers During COVID-19 Pandemic with Nanotechnology: A Protocol for A New Device from Egypt. *Journal of Infection and Public Health* **13**, pp. 1243-1246.
- [27] Wikipedia, 2020. Air Filters. [https://en.wikipedia.org/wiki/Air\\_filter#Filter\\_classes](https://en.wikipedia.org/wiki/Air_filter#Filter_classes). (Access Date: 10.06.2020).

- [28]European Standard EN 1822-1:2009, High Efficiency Air Filters (EPA, HEPA and ULPA). <https://standards.iteh.ai/catalog/standards/cen/46f566b7-2405-4a14-988c-8436402d0975/en-1822-1-2009>. (Access Date: 10.06.2020).
- [29]Bosch, Elektrikli Süpürgeler. <https://www.bosch-home.com.tr/urun-listesi/elektrikli-supurgeler/toz-torbasiz-elektrikli-supurgeler/BGC41Q69>. (Access Date: 20.06.2020).
- [30]Fersan, Hepa Filtre Nedir. <https://www.bosch-home.com.tr/urun-listesi/elektrikli-supurgeler/toz-torbasiz-elektrikli-supurgeler/BGC41Q69>. (Access Date: 20.06.2020).
- [31]Tcharkhtchi A., Abbasnezhad N., Seydani M.Z., Zirak N., Farzaneh S., Shirinbayan M., 2020. An Overview of Filtration Efficiency Through the Masks: Mechanisms of the Aerosols Penetration. *Bioactive Materials* **6**, pp. 106-122.
- [32]BBC, 2020. Coronavirus: Robots Use Light Beams to Zap Hospital Viruses. *Journal of Infection and Public Health*. <https://www.bbc.com/news/business-51914722>. (Access Date: 08.07.2020).
- [33]Darnell M.E., Subbarao K., Feinstone S.M., Taylor D.R., 2004. Inactivation of the Coronavirus That Induces Severe Acute Respiratory Syndrome, SARS-CoV. *Journal of Virological Methods* **121**, pp. 85-91.
- [34]Cults, 2020. N95 Masks Against Coronavirus - Hack the Pandemic. <https://cults3d.com/en/3d-model/tool/n95-masks-against-coronavirus-covid19-hackthepandemic>. (Access Date: 10.07.2020).
- [35]Cults, 2020. N95 Masks Against Coronavirus - Hack the Pandemic. <https://cults3d.com/en/3d-model/tool/covid-19-mask-easy-to-print-no-support-filter-required>. (Access Date: 10.07.2020).
- [36]Cults, 2020. N95 Masks Against Coronavirus - Hack the Pandemic. <https://cults3d.com/en/3d-model/tool/covid-19-mask-easy-to-print-no-support-modified-version>. (Access Date: 10.07.2020).
- [37]Cults, 2020. N95 Masks Against Coronavirus - Hack the Pandemic. <https://cults3d.com/en/3d-model/tool/masque-de-protection-covid-19-epi-equipement-individuel-de-secours>. (Access Date: 10.07.2020).
- [38]Cults, 2020. N95 Masks Against Coronavirus - Hack the Pandemic. <https://cults3d.com/en/3d-model/tool/reusable-facial-mask-frame>. (Access Date: 10.07.2020).
- [39]Cults, 2020. N95 Masks Against Coronavirus - Hack the Pandemic. <https://cults3d.com/en/3d-model/fashion/respirator-breathing-mask-with-hepa-filter>. (Access Date: 10.07.2020).
- [40]Cults, 2020. N95 Masks Against Coronavirus - Hack the Pandemic. <https://cults3d.com/en/3d-model/various/mask-antivirus>. (Access Date: 10.07.2020).
- [41]Cults, 2020. N95 Masks Against Coronavirus - Hack the Pandemic. <https://cults3d.com/en/3d-model/tool/covid-19-mask-easy-to-print-no-support-filter-required>. (Access Date: 10.07.2020).
- [42]Cults, 2020. N95 Masks Against Coronavirus - Hack the Pandemic. <https://cults3d.com/en/3d-model/tool/h1-heavy-mask>. (Access Date: 10.07.2020).
- [43]Cults, 2020. N95 Masks Against Coronavirus - Hack the Pandemic. <https://cults3d.com/en/3d-model/various/masque-fmp-imalize-securite-covid-19-facile-a-imprimer-aucun-support-filtre-requis>. (Access Date: 10.07.2020).
- [44]Cults, 2020. N95 Masks Against Coronavirus - Hack the Pandemic. <https://cults3d.com/en/3d-model/various/vmo-mask-v2-coronavirus-covid-19>. (Access Date: 10.07.2020).
- [45]Cults, 2020. N95 Masks Against Coronavirus - Hack the Pandemic. <https://cults3d.com/en/3d-model/various/vmo-mask-v3-coronavirus-covid-19-improved-version>. (Access Date: 10.07.2020).
- [46]Cults, 2020. N95 Masks Against Coronavirus - Hack the Pandemic. <https://cults3d.com/en/3d-model/tool/nanohack-2-0-n95-masks-against-coronavirus-covid19-hackthepandemic>. (Access Date: 10.07.2020).
- [47]Cults, 2020. N95 Masks Against Coronavirus - Hack the Pandemic. <https://cults3d.com/en/3d-model/tool/masque-ffp2-reel-filtration-covid-19>. (Access Date: 10.07.2020).
- [48]Cults, 2020. N95 Masks Against Coronavirus - Hack the Pandemic. <https://cults3d.com/en/3d-model/gadget/respirator-mask-removable-filter>. (Access Date: 10.07.2020).
- [49]Cults, 2020. N95 Masks Against Coronavirus - Hack the Pandemic. <https://cults3d.com/en/3d-model/various/mask-l-n95-with-modular-filters-adult-version>. (Access Date: 10.07.2020).
- [50]Cults, 2020. N95 Masks Against Coronavirus - Hack the Pandemic. <https://cults3d.com/en/3d-model/various/reusable-mask-ppe-alternative-malamask>. (Access Date: 10.07.2020).

- [51]Cults, 2020. N95 Masks Against Coronavirus - Hack the Pandemic. <https://cults3d.com/en/3d-model/various/cov3d-v2-08-fdm-3d-print-optimised-mask-in-15-sizes-also-for-children>. (Access Date: 10.07.2020).
- [52]Cults, 2020. N95 Masks Against Coronavirus - Hack the Pandemic. <https://cults3d.com/en/3d-model/tool/another-cap-for-covid-19-mask>. (Access Date: 10.07.2020).
- [53]Novak J.I., Loy J., 2020. A Quantitative Analysis Of 3D Printed Face Shields and Masks During COVID-19. *Emerald Open Research* **2**, pp. 1-14.
- [54]Tino R., Moore R., Antoline S., Ravi P., Wake N., Ionita C.N., Morris J.M., Decker S.J., Sheikh A., Rybicki F.J., Chepelev, L.L., 2020. COVID-19 and the role of 3D printing in medicine. *3D Printing in Medicine* **6**, pp. 1-8.
- [55]WASP, 2020. 3D Printed Mask From 3D Scanning. <https://www.3dwasp.com/en/3d-printed-mask-from-3d-scanning>. (Access Date: 10.07.2020).
- [56]NIH, 2020. GLWTEchLLC. <https://3dprint.nih.gov/discover/3dpx-013363-0>. (Access Date: 10.07.2020).
- [57]Vaňková E., Kašparová P., Khun J., Machková A., Julák J., Sláma M., Hodek J., Ulrychová L., Weber J., Obrová K., Kosulin K., Lion T., Scholtz V., 2020. Polylactic Acid as A Suitable Material For 3D Printing of Protective Masks in Times Of COVID-19 Pandemic. *PeerJ* **8**, <https://doi.org/10.7717/peerj.10259>.
- [58]Leung W.W.F., Sun, Q., 2020. Electrostatic Charged Nanofiber Filter for Filtering Airborne Novel Coronavirus (COVID-19) And Nano-Aerosols. *Separation and Purification Technology* **116886**, pp. 1-17.
- [59]Pedro M., 2020. Filter Considerations in the COVID-19 Era. [https://www.vyaire.com/sites/default/files/2020-06/vyr-gbl-2000294-filter-considerations-in-the-covid-19-era-wp\\_final.pdf](https://www.vyaire.com/sites/default/files/2020-06/vyr-gbl-2000294-filter-considerations-in-the-covid-19-era-wp_final.pdf). (Access Date: 10.10.2020).
- [60]Ortiz L.W., Soderholm S.C., Valdez F.O., 1988. Penetration of Respirator Filters by An Asbestos Aerosol. *American Industrial Hygiene Association Journal* **49**, pp. 451-460.
- [61]Wilson A. M., Abney S. E., King M. F., Weir M. H., López-García M., Sexton J. D., Reynolds K. A., 1988. COVID-19 and Non-Traditional Mask Use: How Do Various Materials Compare in Reducing the Infection Risk for Mask Wearers? *The Journal of Hospital Infection* **105**, pp. 640-642.
- [62]Darnell M. E., Subbarao K., Feinstone S. M., Taylor D. R., 2004. Inactivation of The Coronavirus That Induces Severe Acute Respiratory Syndrome. *Journal of Virological Methods* **121**, pp. 85-91.





## Evaluation of Industry 4.0 Applications for Agriculture using AHP Methodology

Melda Güliz ATEŞ<sup>1</sup> , Yıldız ŞAHİN<sup>2,\*</sup> 

<sup>1</sup> Industrial Engineering, Kocaeli University, Kocaeli, 41100, Turkey, **ORCID:** 0000-0002-2243-9642

<sup>2</sup> Industrial Engineering, Kocaeli University, Kocaeli, 41100, Turkey, **ORCID:** 0000-0002-6283-5340

### Article Info

#### Research paper

Received : July 15, 2020

Accepted : February 6, 2021

#### Keywords

Agriculture

Agriculture 4.0

AHP

Industry 4.0

Industry 4.0 Applications

### Abstract

In today's world because of increasing competition, shifting customer demands and expectations firms have to shorten their time-to-market, increase their flexibility and efficiency. Industry 4.0 applications as meet these requirements gain popularity. Awareness of the necessity of Industry 4.0 applications for excellent customer experience and great innovation capacity and studies searching advantageous applications for related sectors are increasing day by day. In this context, the agriculture sector, like other sectors, adapts to the changing conditions within the scope of Industry 4.0, and the concept of Agriculture 4.0, which includes digital agricultural technologies, appears. This study provides a detailed framework for the transition from Industry 4.0 to Agriculture 4.0 and digital agricultural tools. In addition, it is aimed to contribute to the literature by choosing the best alternative by evaluating these digital agricultural tools with the Analytical Hierarchy Process method according to cost, income, applicability and practicality criteria.

## 1. Introduction

Industry 4.0 represents the newest level of digital solutions offered by new production understanding and current technological developments, where concepts of speed, flexibility, efficiency, cost and innovation come to the fore. With increasing competition and changing customer expectations in today's world, companies should shorten their time to market, be flexible and increase their efficiency in order to achieve sustainable success. At this point, Industry 4.0 creates new production processes that communicate with each other, collect and process real-time big data and make decisions with autonomous mechanisms. <sup>1</sup>Cyber-physical systems aim to create "Smart Factories" of Industry 4.0 which includes the Internet of Things (IoT) and cloud computing technology [1]. In smart factories, cyber-physical systems observe physical processes, create a virtual copy of the physical world and make the final decision through distributed decision mechanisms. With IoT technology, cyber-physical systems communicate with each other and machine-machine, machine-human

collaborations are established in real-time, and instant data and information are transmitted to internal and external participants in the value chain of the organization through internet services [2].

Industry 4.0 refers to the 4th Industrial Revolution, which includes intelligent, connected and decentralized production (Figure 1). The first industrial revolution (Industry 1.0) emerged with the introduction of steam power in mechanical systems. The second industrial revolution (Industry 2.0) started with electricity, assembly lines and mass production. The third industrial revolution (Industry 3.0) was accomplished by replacing people working in the production line of computerized production and automation, robots and machines, and the introduction of information technologies. Today, with the fourth industrial revolution (Industry 4.0), computers and automation come together with a brand-new structure and equipped with machine learning algorithms, computer systems control robots with a minimum human contribution [3].

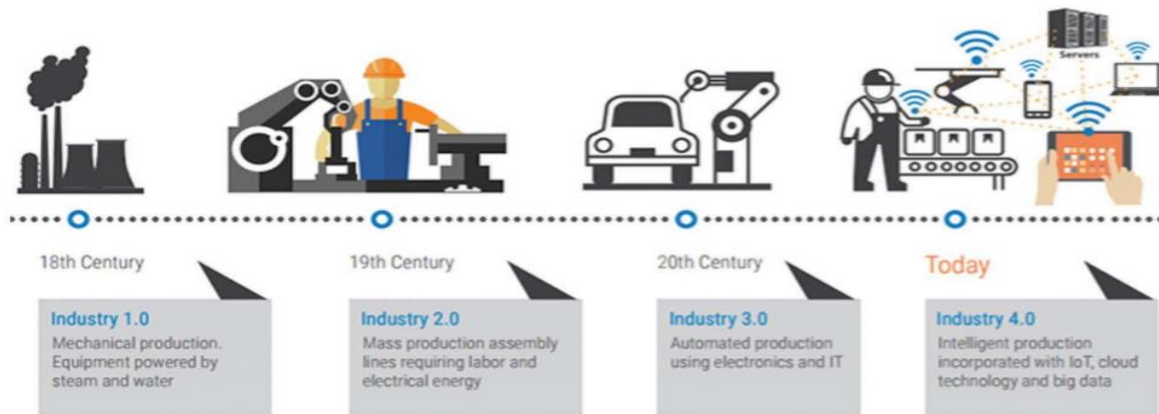
The concept of Industry 4.0 was first mentioned at the Hannover Fair in Germany in 2011 and Germany and the

\* Corresponding Author: [meldaguliz.ates@kocaeli.edu.tr](mailto:meldaguliz.ates@kocaeli.edu.tr)



US, which lost their production power to countries like China and India, determined this reducing manpower

impact on the production model as their new industrial strategy [4].



**Figure 1.** Industrial revolutions (Source [3])

In this context, the agriculture sector, like other sectors, adapts to the changing conditions within the scope of Industry 4.0, and the concept of Agriculture 4.0, which includes digital agricultural technologies, appears. This transformation is actually a necessary step to take against the threats expected in the future, because the world population will be more than 9.6 billion by 2050, according to the report titled "World Population Expectation" prepared by the United Nations (UN). That will cause a 70% increase in food consumption and also agricultural production is projected to decrease by 2% in the next decade, as 12 million agricultural lands deteriorated every year. The observations of the last five years indicate the loss of an average of 5.2 million hectares of forest land each year [5]. Smart and sustainable agriculture practices with Agriculture 4.0 technologies aim to be environmentally friendly, to achieve high productivity with fewer resources, and to be economical and practical.

In this study, the transition process from Industry 4.0 to Agriculture 4.0 and new technologies related to digital agriculture will be discussed, and the evaluation of digital agriculture technologies with the analytical hierarchy process (AHP) method will be carried out according to the cost, income, applicability and practicality criteria.

### 1.1. From Industry 4.0 to Agriculture 4.0

In the age of Industry 4.0, digital technologies developed and used thanks to the integration of data and the connectivity of their resources have developed highly efficient and sustainable production models. A more efficient and sustainable structure in the agricultural sector is considered as a natural result of the transfer of the Industry 4.0 approach to this sector [6]. As expected, the agricultural sector is changing like other sectors and is

becoming much more technology and knowledge-intensive. Behind this, the concern of offering sustainable and affordable prices and more crops to the growing population with fewer resources in the coming periods lies and digital/smart agriculture principles are offered as a solution to this problem [7-8]. Traditional production methods turn into modern, productive and innovative forms, farmers realize the increasing importance of managerial activities and harmony with nature as well as production [9]. The meaning of the agricultural sector today shifted to smart agriculture, nature-friendly and water-saving agriculture, efficient agriculture and digital agriculture is the most necessary, effective and most appropriate approach for this transformation [10].

Digital agriculture is not the result of an instantly developing process, it has followed a path parallel to the development stages of the industrial revolution and this process has brought us to today's "Agriculture 4.0" [1]:

-Agriculture 1.0: It is a labor-intensive and low-yielding form of agriculture carried out with animal power in the early 20th century.

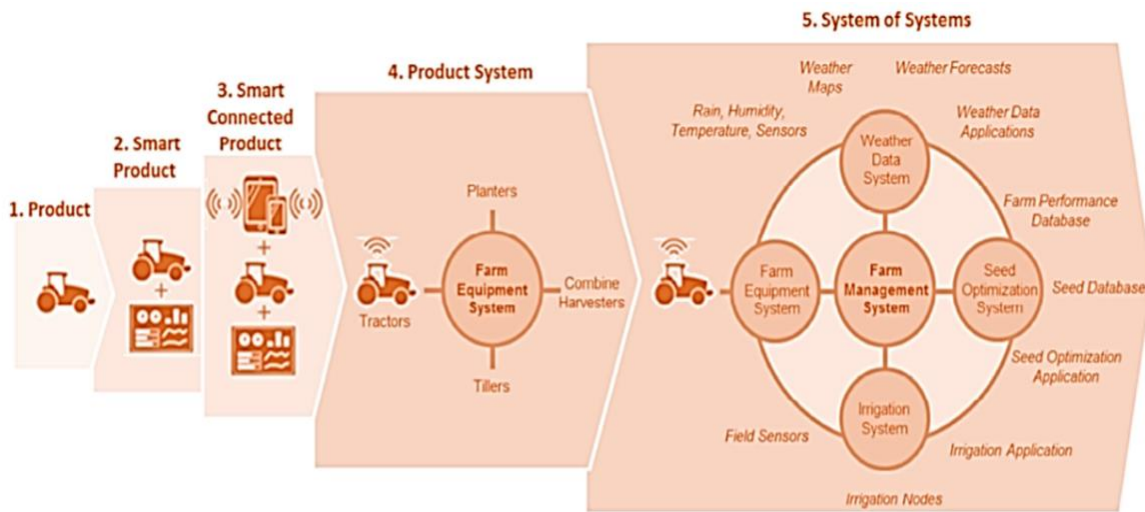
- Agriculture 2.0: Started with the use of combustion engines and tractors in agriculture, another feature of this period is high volume production with synthetic pesticides and fertilizers with low cost.

- Agriculture 3.0: Precision agriculture practices started with the opening of military GPS (Global Positioning System) signals for public use. Precision agriculture is defined as the management of variability in order to increase productivity and minimize the impact of environmental factors. With GPS signals and satellite images, terrain features, organic matter contents, moisture and nitrogen levels, crop efficiency, etc. can be measured. Similarly, decision support systems and agricultural software related to instant maps have been developed.

- Agriculture 4.0: In the 2010s with the development

of cheap and advanced sensors, actuators, microprocessors; high bandwidth in the cellular communication system;

cloud-based information communication technology and big data analytics led connected agricultural practices.



**Figure 2.** Agriculture 4.0 (Source [11])

Digital agriculture, as a knowledge-based agriculture model, provides support to the manufacturer in management of resources, the efficiency of business operations and decision making by the collection and processing of high-precision, instant and personalized data with the technological tools offered by Industry 4.0, How agricultural components come together in the Agriculture 4.0 concept is summarized in Figure 2.

Internet of Things (IoT), one of the most important technologies of Industry 4.0, is the main component of the related agricultural practices in Agriculture 4.0. IoT is based on the natural environment and any measurable physical size, such as temperature, humidity, pH, gas rates, light intensity. The raw data collected by various sensors placed in the product area are transmitted to cloud computing systems for storage using wireless gateways or other methods required for human-machine, machine-machine communication. The data in the cloud environment is transmitted to the farmers so that they can make better decisions directly or by processing [8-12]. With sensor technology, farmers are given detailed information on the fertilizer type they need to use, weather and soil conditions, irrigation and mineral amount, estimated harvest time, and this way, it is aimed to obtain high-level efficiency by managing their resources correctly [13]. An exemplary study on reducing water consumption with IoT was carried out with Bosh smart technology used in olive groves in Spain. With the wireless sensors placed on the trees, precise irrigation is made according to the weather conditions and actual needs. Similarly, Rajakumar [14] and Kumar and Ramasamy [15] have developed digital systems that automatically start and shut off irrigation if the humidity level is low with the soil moisture sensor and instantly transfer the current measurements via

the IoT module. Again, by monitoring the soil properties and environmental factors with sensors, studies to find the ideal environment conditions for systems and plants that take automatic action have become prominent in recent years [16-17]. Another usage area of IoT and sensors is the monitoring of livestock and animal products [13-16]. With RFID technology counting and monitoring of animals, keeping the statistics in the process from birth to sale and providing security with the tracking mechanism has become extremely easy [18]. German CLASS company proposes a proactive approach by informing the producers via SMS with sensors attached to animals during pregnancy or disease situations. Following the herd with the Connected Herd Management application, the animal herds can be followed instantly [19]. The use of IoT in the agricultural sector has increased the functionality of the existing tools by making the physical environment a part of the information flow, and the collection and processing of a wide variety of information have accelerated the development of the agricultural sector from greenhouse to animal husbandry [20]. According to the research carried out by Business Insider, while 30 million objects in agriculture are interconnected in 2015, this figure is projected to increase to 75 million in 2020, which also indicates a 20% growth in the economy.

According to the report published by the United Nations, two-thirds of the population will live in urban areas by 2050, which will reduce its agricultural workforce potential. The importance of autonomous systems, one of the new digital solutions to reduce the workload of farmers, is increasing with this statistic. With the developing object detection and radar technology, the developments in autonomous vehicle technology increase the applicability and decrease the costs. Robotic and autonomous vehicles,

which are among the components of Industry 4.0, have been transferred to the agriculture sector in a similar way, and agricultural vehicle applications that automatically recognize and talk to each other have started to appear with Agriculture 4.0 [11]. Agricultural robots aim to increase productivity by automating standardized and repetitive work (such as harvesting, mowing, pruning, seeding, spraying, phenotyping, packaging) for farmers [21]. While autonomous systems in agriculture and robotics are defined as the application process of robotics, automatic control and artificial intelligence techniques in all kinds of agricultural production -including farmbots and farm drones- one of the most important technologies is drones, which are small unmanned vehicles with cloud connections and cameras [12-13]. Drones, which can display the entire production area and take instant action, as well as carry loads such as fertilizer, water, increase work efficiency and reduce costs. In the Agriculture 4.0 report published by Oliver Wyman in 2018, drones have given wide coverage and usage areas of this technology shared as 3-D mapping, soil and field analysis, providing data for the best planting area decision, sowing, fertilizing, irrigation, spraying activities, harvest imaging and harvest health screening. Hektaş agriculture firm in Turkey started to collect significant information on optimum plant growing conditions via drone and sensor technology and create a library by analyzing the collected information [22].

## 2. Materials and Methods

The development of digital agriculture in our country has started to be supported by state policies, and an action plan and roadmap have been created for the Agriculture 4.0 transformation. The number of producers that support and nurture this strategy and keep pace with digital transformation is increasing. Thus, the decision to make the right technology investment for the manufacturer is becoming more and more critical day by day. As what kind of factors or variables need to be considered for agricultural policy and decision-makers is a challenging topic mostly economical and technical factors have been seen as the main criteria for agricultural investment decisions [23-25]. In this context, an AHP study based on cost, income, applicability and practicality criteria is conducted for both agriculture and animal husbandry sectors.

### 2.1. Analytical Hierarchy Process (AHP)

Analytical Hierarchy Process (AHP) was designed by Thomas L. Saaty in the 1970s to solve complex decision-making problems involving multiple criteria. AHP is based

on analyzing the problem with a hierarchical model consisting of goals, criteria and alternatives and reaching the appropriate solution with pairwise comparisons. It is an approach that can solve large-scale, dynamic and complex multi-criteria decision-making problems [26]. The stages of the AHP method can be summarized as [27]:

- Defining the problem, determining the main goal
- Determination of decision criteria
- Determination of decision alternatives
- Creating the hierarchical structure of the problem
- Pairwise comparison of criteria
- Pairwise comparison of alternatives and calculation of their priorities according to criteria
- Selection of the highest priority alternative

The scale 1-9 of Saaty is used to perform pairwise comparisons (Table 1), and to determine whether the comparisons are consistent, the consistency ratio (CR) should be calculated for each matrix after the comparison matrices are configured. However, if the CR value is less than 0.10, pairwise comparisons can be said to be consistent and the highest priority alternative can be decided.

**Table 1.** The comparison scale in AHP (Source [28])

Importance Level	Definition
1	Equal importance
3	Weak importance of one over another
5	Essential or strong importance
7	Demonstrated importance
9	Absolute importance
2,4,6,8	Intermediate values between the two adjacent judgements

### 2.2. Hierarchy Models and Application

Following the process steps of the AHP method, two separate applications were carried out for the agriculture and animal husbandry sectors.

-In the determination of the main target, which is the first step, the target has been defined as “Selection of the best Agriculture 4.0 technology for the agriculture sector” and “Selection of the best Agriculture 4.0 technology for animal husbandry sector”.

-Both literature review and expert opinions were consulted during the determination of criteria and alternatives, where the criteria were determined as cost, return, applicability and practicality for both sectors (with different weights). While the alternatives for the agricultural sector were a drone, soil sensor and autonomous tractor technology, animal sensor, associated herd application and milk scanner technology alternatives

were evaluated for the animal husbandry sector.

-Pairwise comparisons were made by three experts, who are academics with PhD in the agricultural area. Experts opinions were collected via mailing (as an excel sheet) with the request of pairwise comparison of criteria and pairwise comparison of alternatives and calculation of their priorities according to criteria. Expert evaluations were singularized using the geometric mean method and a compromise value was obtained.

-Super Decisions package program was used in the implementation of the AHP method.

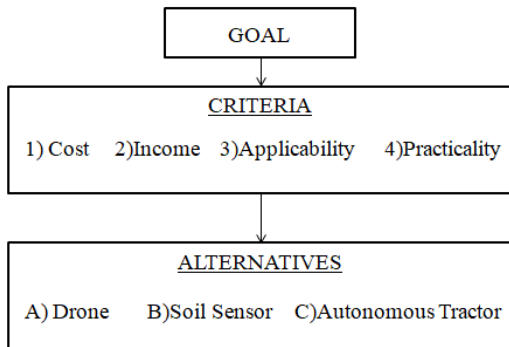


Figure 3. Hierarchy model for agriculture

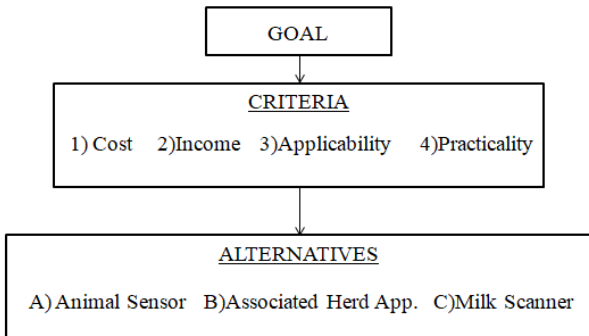


Figure 4. Hierarchy model for animal husbandry

### 3. Results and Discussion

According to the analysis conducted with Super Decisions software, the priority values for criteria and rankings of alternatives have been obtained for two sectors. For agriculture income was found as the most important criteria and followed by the criteria cost, applicability, practicality respectively. Similarly, despite the different limiting values, the orders of the criteria for animal husbandry have been obtained as income, cost, applicability, practicality respectively. In the selection of the best alternative, the soil sensor, one of the Agriculture 4.0 technologies for the agricultural sector, came to the fore with its cost advantage and applicability and was chosen as the best alternative within the criteria. Similarly,

for the animal husbandry sector, it was decided on the sensor technology attached to the animals as the best alternative with its cost advantage and the ability to provide fast returns.

Table 2. Priorities of criteria for agriculture

Criteria	Normalized by Cluster	Limiting
Income	0,564	0,282
Cost	0,255	0,128
Applicability	0,113	0,056
Practicality	0,068	0,034

Table 3. Priorities of criteria for animal husbandry

Criteria	Normalized by Cluster	Limiting
Income	0,503	0,251
Cost	0,285	0,143
Applicability	0,114	0,057
Practicality	0,098	0,049

Table 4. Results for alternatives for agriculture

Alternatives	Ideal	Normal	Raw	Rank
Soil Sensor	1	0,575	0,287	1
Drone	0,562	0,323	0,161	2
Autonomous Tractor	0,179	0,103	0,051	3

Table 5. Results for alternatives for animal husbandry

Alternatives	Ideal	Normal	Raw	Rank
Animal Sensor	1	0,465	0,233	1
Milk Scanner	0,643	0,299	0,15	2
Associated Herd Application	0,506	0,235	0,117	3

### 4. Conclusions

Due to the paradigm shift based on changing customer demand and expectations for gaining competitive advantage companies focused on being flexible, fast and efficient. Industry 4.0 applications serve these needs with their digitalized tools and emerge as a concept that increases its popularity. Similarly, the agriculture sector adapts to changing conditions within the scope of Industry 4.0, and the Agriculture 4.0 concept, which includes digital agriculture technologies, stands out especially in terms of optimum use of resources in the face of expected population growth. In this study, the transition process from Industry 4.0 to Agriculture 4.0 and new technologies

of digital agriculture are mentioned.

Although there are studies that presents conceptual frameworks on Agriculture 4.0, need for analytical approaches on the area is emerging. In this context, this study aims to close a gap by presenting an AHP based decision making approach on digital agriculture technologies for agriculture and animal husbandry sectors. For the decision-making process criteria were obtained as income, cost, applicability and practicality due to the literature review and field experts' opinion. Similarly, alternatives for digital solutions were gathered from literature and chosen with field experts. As the result of the study, it has been decided that soil sensor technology is the best alternative for the agricultural sector, where the technological infrastructure and the availability of the necessary information bring the cost advantage. Similarly, in the animal husbandry sector, the sensor technology attached to the animals is obtained as the best alternative with its cost advantage and fast return.

When the outputs of the study are considered from a managerial point of view, it has come to the forefront that the income and cost balance (criteria) have priority at the investment point. At this point, it is usual to proceed with an alternative that can provide a fast return on investment and offer a cost advantage. While sensor technology is the backbone of Agriculture 4.0, it has become the top priority alternative with the cost advantage of its prevalence and applicability.

### Conflict of Interests

No conflict of interest was stated by the authors.

### Declaration of Ethical Standards

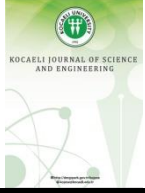
The authors of this article declares that the materials and methods used in this study do not require ethical committee permission and legal-special permission.

### References

- [1] Kovács, I., Husti, I., 2018. The role of digitalization in the agricultural 4.0 – how to connect the industry 4.0 to agriculture?. *Hungarian Agricultural Engineering*, pp.38-42.
- [2] Tong-Ke F., 2017. Smart Agriculture Based on Cloud Computing and IOT. *Journal of Convergence Information Technology*, **8**(2), pp.210-216.
- [3] Husti, I., Daroczi, M., Kovacs, I., 2017. Towards sustainable agriculture and biosystems engineering book Edited by: Anikó Nyéki, Attila J. Kovács, Gábor Milics.
- [4] EBSO, 2015. Sanayi 4.0. Retrieved from [http://www.ebso.org.tr/ebsoimedia/documents/sanayi-40\\_88510761.pdf](http://www.ebso.org.tr/ebsoimedia/documents/sanayi-40_88510761.pdf)
- [5] Kirkaya, A., 2020. Akıllı tarım teknolojileri uygulamaları. Retrieved from [https://www.researchgate.net/publication/339029285\\_AKILLI\\_TARIM\\_TEKNOLOJILERI\\_UYGULAMALARI](https://www.researchgate.net/publication/339029285_AKILLI_TARIM_TEKNOLOJILERI_UYGULAMALARI)
- [6] Corallo, A., Latino, M.E., Menegoli, M., 2018. From Industry 4.0 to Agriculture 4.0: A Framework to Manage Product Data in Agri-Food Supply Chain for Voluntary Traceability. *World Academy of Science, Engineering and Technology, International Journal of Nutrition and Food Engineering*, **12**, pp.146-150.
- [7] Ozdogan, B., Gacar, A., Aktaş, H., 2017. Digital Agriculture Practices in The Context of Agriculture 4.0. *Journal of Economics, Finance and Accounting*. **4**. 184-191. 10.17261/Pressacademia.2017.448.
- [8] Duman, B., Ozsoy, K., 2019. Endüstri 4.0 perspektifinde akıllı tarım. Retrieved from [https://www.researchgate.net/publication/334234038\\_ENDUSTRI\\_40\\_PERSPEKTIFINDE\\_AKILLI\\_TARIM\\_SMART\\_AGRICULTURE\\_IN\\_INDUSTRY\\_40\\_PERSPECTIVE](https://www.researchgate.net/publication/334234038_ENDUSTRI_40_PERSPEKTIFINDE_AKILLI_TARIM_SMART_AGRICULTURE_IN_INDUSTRY_40_PERSPECTIVE)
- [9] Sørensen, C. G., Fountas, S., Nash, E., Pesonen, L., Bochtis, D., Pedersen, S. M., Basso, B., Blackmore, S. B., 2010. Conceptual Model of a Future Farm Management Information System, *Computers and Electronics in Agriculture*, **72**(1), pp.37-47.
- [10] Yane, D., 2010. Research and Analysis about System of Digital Agriculture Based on a Network Platform, In *International Conference on Computer and Computing Technologies in Agriculture*, Springer Berlin Heidelberg. pp.274-282.
- [11] Zambon, I., Cecchini, M., Egidi, G., Saporito, M., Colantoni, A., 2019. Revolution 4.0: Industry vs. Agriculture in a Future Development for SMEs. *Processes*. **7**. 36. 10.3390/pr7010036.
- [12] Kalkışım, A., Akkaş, M., Yucedag, I., 2019. Nesnelerin İnterneti ve Nesnelerinin İnternetinin Tarım Alanında Kullanımı. Retrieved from [https://www.researchgate.net/publication/336020647\\_NESNELERIN\\_INTERNETI\\_VE\\_NESNELERIN\\_INTERNETININ\\_TARIM\\_ALANINDA\\_KULLANIMI](https://www.researchgate.net/publication/336020647_NESNELERIN_INTERNETI_VE_NESNELERIN_INTERNETININ_TARIM_ALANINDA_KULLANIMI)
- [13] Kılavuz, E, Erdem, İ., 2019. Dünyada Tarım 4.0 Uygulamaları ve Türk Tarımının Dönüşümü. *Social Sciences*, **14**(4), pp.133-157.



- [14] Rajakumar, G., Sankari, M.S., Shunmugapriya, D., Maheswari, S.P.U., 2018. "Iot Based Smart Agricultural Monitoring System", *Asian Journal of Applied Science and Technology (AJAST)*, **2**(2), pp.474-480.
- [15] Kumar, V., Ramasamy, R., 2017. "Implementation of Iot In Smart Irrigation System Using Arduino Processor", *International Journal of Civil Engineering and Technology (IJCIET)*.
- [16] Meola, A., 2016. "Why IoT, big data & smart farming are the future of agriculture", <https://www.businessinsider.com/internet-of-things-smart-agriculture-2016-10>.
- [17] Suma, N., Samson, S.R., Saranya, S., Shanmugapriya, G., Subhashri, R., 2017. "IOT Based Smart Agriculture Monitoring System" *International Journal on Recent and Innovation Trends in Computing and Communication*, **5**(2), pp.177-181.
- [18] Doknić, V., 2014. "Internet of Things Greenhouse Monitoring and Automation System, Summer term."
- [19] Akay, M., 2018. "Endüstri 4.0 ile Akıllı Tarıma Geçiş." Retrieved from [https://www.researchgate.net/publication/326550785\\_ENDUSTRI\\_40\\_ILE\\_AKILLI\\_TARIMA\\_GECIS](https://www.researchgate.net/publication/326550785_ENDUSTRI_40_ILE_AKILLI_TARIMA_GECIS)
- [20] Kaloxylos, A., Eigenmann, R., Teye, F., Politopoulou, Z., Wolfert, S., Shrank, C., Dlinger, M., Lampropoulou, I., Antoniou E., Pesonen, L., Nicole, H., 2012. "Farm Management Systems and The Future Internet Era, Computers and Electronics in Agriculture", **89**, pp.130-144.
- [21] Oliver Wyman Report., 2018. "Agriculture 4.0: The Future of Farming technology."
- [22] Kirkaya, A., 2020. "Akıllı tarım teknolojileri uygulamaları." Retrieved from [https://www.researchgate.net/publication/339029285\\_AKILLI\\_TARIM\\_TEKNOLOJILERI\\_UYGULAMALARI](https://www.researchgate.net/publication/339029285_AKILLI_TARIM_TEKNOLOJILERI_UYGULAMALARI)
- [23] Yanli, Z., 2009. "An Introduction to the Development and Regulation of Agricultural Insurance in China." *Geneva Pap. Risk Insur. Issues Pract.*, **34**, pp.78-84.
- [24] Pinstrup-Andersen, P., Shimokawa, S., 2006. "Rural Infrastructure and Agricultural Development; World Bank: Washington, DC, USA. Available online: [http://siteresources.worldbank.org/INTDECABCTO/K2006/Resources/Per\\_Pinstrup\\_Andersen\\_Rural\\_Infrastructure.pdf](http://siteresources.worldbank.org/INTDECABCTO/K2006/Resources/Per_Pinstrup_Andersen_Rural_Infrastructure.pdf)
- [25] Amadi, B.C., 1998. "The impact of rural road construction on agricultural development: An empirical study of Anambra state in nigeria." *Agricultural System*, **27**, pp.1-9.
- [26] Kaplan, R., 2010. "AHP Yöntemiyle Tedarikçi Seçimi: Perakende Sektöründe Bir Uygulama", Master's Thesis (Yüksek Lisans Tezi), İstanbul Teknik Üniversitesi, Fen Bilimleri Enstitüsü, İstanbul.
- [27] Esen, H. Ö., 2008. "Applied Operational Research" ("Uygulamalı Yöneylem Araştırması"), (S. Tolun, Ed.), Çağlayan Kitabevi.



## Investigation of Stability Changes in a Neural Field Model

Berrak ÖZGÜR<sup>1,\*</sup>

<sup>1</sup> Izmir Democracy University, Department of Mathematics, Izmir, 35140, Turkey, **ORCID:** 0000-0002-9709-7376

### Article Info

#### Research paper

Received : January 04, 2021

Accepted : February 08, 2021

### Abstract

In this paper, the stability analysis of the neural field model is studied. The special case for three neuron populations is considered. The work is conducted by finding the characteristic equation of the system first and then investigating the characteristic roots of the third-order equation by using the Routh-Hurwitz criterion and Sturm sequence. The main analysis is given in two parts considering the nonexistence and existence of the delay term. Some basic stability criteria in terms of coefficients of the system are given in the theorems.

### Keywords

Characteristic Equation  
Neural Field Model  
Routh-Hurwitz Criterion  
Stability Analysis  
Sturm Sequence

## 1. Introduction

The term ‘dynamical system’ is used to determine a system varying with respect to time. In applied mathematics, in order to understand the general construction for a real-world phenomenon and analyse its future state, mathematical models are used. Differential equations, difference equations and functional equations are frequently used when writing mathematical models for dynamical systems representing the real phenomena. Hence, the important analyses related to them can be made by using convenient mathematical methods.

In sciences such as biology, engineering, economics, since time is very important, we generally use a time delay in writing more realistic models. The theory of delay differential equations has an important role in such fields.

The scientists aimed to model the activity of large neuron populations in the brain, use the neural field models. These models are constructed using integro-

differential equations including a time delay. For the basic facts in neural field models, one can refer to the studies given in [1,2]. Besides these studies, the stability analysis of the neural field model and the existence and uniqueness of their solutions are studied in some papers [3-15].

In stability analysis, obtaining the characteristic equation of the system and determining the characteristic roots construct the important part. There are some studies on investigation of the stability analysis for this model including functional analysis and numerical methods [7,9,10]. In [11-15] the analysis is made by using the D-curves method and the Routh-Hurwitz criterion.

In this study, we are interested in the stability of a neural field model for three neuron populations. The general overview of the study is given in the following; the model is given in Section 2. The stability properties for the model are given in Section 3. The roles of the system parameters on the stability of the model are shown. This analysis is made by using the Sturm sequence since the corresponding characteristic equation of the model is third order. The conclusion of this study is in Section 4.

\* Corresponding Author: [berrak.ozgur@idu.edu.tr](mailto:berrak.ozgur@idu.edu.tr)



### 2. Neural Field Model

The scientists use neural field equations to model dynamics of mean membrane potential for  $p$  neural populations on the space  $\Omega \subset R^d$ . This model given in [6,7,9,10] is given below

$$\left(\frac{d}{dt} + l_i\right) V_i(t, r) = \sum_{j=1}^p \int_{\Omega} J_{ij}(r, \bar{r}) S[\sigma_j(V_j(t - \tau_{ij}(r, \bar{r}), \bar{r}) - h_j)] d\bar{r} + I_i^{ext}(r, t), \quad t \geq 0, \quad 1 \leq i \leq p$$

$$V_i(t, r) = \phi_i(t, r), \quad t \in [-T, 0] \tag{1}$$

Here, we consider this model for three neuron populations ( $p = 3$ ). The synaptic inputs for large groups of neurons at position  $x$  and time  $t$  are represented by the functions  $V_1(x, t)$ ,  $V_2(x, t)$  and  $V_3(x, t)$ . We consider  $\Omega = \left[-\frac{\pi}{2}, \frac{\pi}{2}\right]$ . The relations of neurons on different populations are shown by the functions  $J_{ij}(x, y)$ . Some of the relations among them are restricted. The stability analysis is made in the special case that  $J_{12}(x, y) \neq 0$ ,  $J_{21}(x, y) \neq 0$ ,  $J_{23}(x, y) \neq 0$ ,  $J_{32}(x, y) \neq 0$ . In this research, the delay term is considered constant as  $\tau(x, y) = \tau$ . Hence the linearized model near  $(0,0,0)$  is given below. For this model the functions  $U_1(x, t)$ ,  $U_2(x, t)$  and  $U_3(x, t)$  are used.

$$\frac{d}{dt} U_1(x, t) + l_1 U_1(x, t) = \sigma_2 s_1 \int_{-\frac{\pi}{2}}^{\frac{\pi}{2}} J_{12}(x, y) U_2(y, t - \tau(x, y)) dy$$

$$\frac{d}{dt} U_2(x, t) + l_2 U_2(x, t) = \sigma_1 s_1 \int_{-\frac{\pi}{2}}^{\frac{\pi}{2}} J_{21}(x, y) U_1(y, t - \tau(x, y)) dy + \sigma_3 s_1 \int_{-\frac{\pi}{2}}^{\frac{\pi}{2}} J_{23}(x, y) U_3(y, t - \tau(x, y)) dy$$

$$\frac{d}{dt} U_3(x, t) + l_3 U_3(x, t) = \sigma_2 s_1 \int_{-\frac{\pi}{2}}^{\frac{\pi}{2}} J_{32}(x, y) U_2(y, t - \tau(x, y)) dy \tag{2}$$

### 3. Stability Analysis

Considering the Fourier method, we are looking for the solutions as  $U_1(x, t) = e^{ikx} u_1(t)$ ,  $U_2(x, t) = e^{ikx} u_2(t)$ ,  $U_3(x, t) = e^{ikx} u_3(t)$ . Here  $u_1(t) = c_1 e^{\lambda t}$ ,  $u_2(t) = c_2 e^{\lambda t}$  and  $u_3(t) = c_3 e^{\lambda t}$ . Writing them in the system (2), we get the following system

$$\lambda e^{ikx} u_1(t) + l_1 e^{ikx} u_1(t) = \sigma_2 s_1 e^{-\lambda \tau} u_2(t) \int_{-\frac{\pi}{2}}^{\frac{\pi}{2}} J_{12}(x, y) e^{iky} dy$$

$$\lambda e^{ikx} u_2(t) + l_2 e^{ikx} u_2(t) = \sigma_1 s_1 e^{-\lambda \tau} u_1(t) \int_{-\frac{\pi}{2}}^{\frac{\pi}{2}} J_{21}(x, y) e^{iky} dy + \sigma_3 s_1 e^{-\lambda \tau} u_3(t) \int_{-\frac{\pi}{2}}^{\frac{\pi}{2}} J_{23}(x, y) e^{iky} dy$$

$$\lambda e^{ikx} u_3(t) + l_3 e^{ikx} u_3(t) = \sigma_2 s_1 e^{-\lambda \tau} u_2(t) \int_{-\frac{\pi}{2}}^{\frac{\pi}{2}} J_{32}(x, y) e^{iky} dy \tag{3}$$

The solutions of the system are the functions  $\cos(2nx)$  and  $\sin(2nx)$  [9]. Hence we have

$$\lambda u_1(t) + l_1 u_1(t) = \sigma_2 s_1 e^{-\lambda \tau} u_2(t) \int_{-\frac{\pi}{2}}^{\frac{\pi}{2}} J_{12}(x, y) e^{iky} dy$$

$$\lambda u_2(t) + l_2 u_2(t) = \sigma_1 s_1 e^{-\lambda \tau} u_1(t) \int_{-\frac{\pi}{2}}^{\frac{\pi}{2}} J_{21}(x, y) e^{iky} dy + \sigma_3 s_1 e^{-\lambda \tau} u_3(t) \int_{-\frac{\pi}{2}}^{\frac{\pi}{2}} J_{23}(x, y) e^{iky} dy$$

$$\lambda u_3(t) + l_3 u_3(t) = \sigma_2 s_1 e^{-\lambda \tau} u_2(t) \int_{-\frac{\pi}{2}}^{\frac{\pi}{2}} J_{32}(x, y) e^{iky} dy \tag{4}$$

Considering the coefficient determinant of this system with respect to  $u_1(t)$ ,  $u_2(t)$  and  $u_3(t)$ , we get the following characteristic equation arranged in terms of the powers of  $\lambda$

$$\lambda^3 + (l_1 + l_2 + l_3)\lambda^2 + (l_2 l_3 + l_1 l_3 + l_1 l_2)\lambda + l_1 l_2 l_3 - K_1 K_3 F_3 F_4 e^{-2\lambda \tau} (\lambda + l_1) - K_1 K_2 F_1 F_2 e^{-2\lambda \tau} (\lambda + l_3) = 0 \tag{5}$$

where  $K_1 = \sigma_2 s_1$ ,  $K_2 = \sigma_1 s_1$ ,  $K_3 = \sigma_3 s_1$ ,

$$F_1 = \int_{-\frac{\pi}{2}}^{\frac{\pi}{2}} J_{12}(x, y) e^{iky} dy,$$

$$F_2 = \int_{-\frac{\pi}{2}}^{\frac{\pi}{2}} J_{21}(x, y) e^{iky} dy,$$

$$F_3 = \int_{-\frac{\pi}{2}}^{\frac{\pi}{2}} J_{23}(x, y) e^{iky} dy,$$

$$F_4 = \int_{-\frac{\pi}{2}}^{\frac{\pi}{2}} J_{32}(x, y) e^{iky} dy$$

If there is no delay term in the system, i.e.,  $\tau = 0$ , the characteristic equation turns into the following form

$$\lambda^3 + (l_1 + l_2 + l_3)\lambda^2 + (l_2l_3 + l_1l_3 + l_1l_2 - K_1K_3F_3F_4 - K_1K_2F_1F_2)\lambda + l_1l_2l_3 - K_1K_3F_3F_4l_1 - K_1K_2F_1F_2l_3 = 0 \quad (6)$$

According to the Routh-Hurwitz criterion, we may give the following theorem.

Theorem: Consider the system (2). If the following conditions are satisfied

$$l_1 + l_2 + l_3 > 0 ,$$

$$l_1l_2l_3 - K_1K_3F_3F_4l_1 - K_1K_2F_1F_2l_3 > 0$$

and

$$(l_1 + l_2 + l_3)(l_2l_3 + l_1l_3 + l_1l_2 - K_1K_3F_3F_4 - K_1K_2F_1F_2) - (l_1l_2l_3 - K_1K_3F_3F_4l_1 - K_1K_2F_1F_2l_3) > 0$$

then the system is stable near (0,0,0) in the absence of delay term.

Proof: If the conditions given above are satisfied then, according to the Routh-Hurwitz criterion, all roots of the characteristic equation have negative real parts and the system is stable near (0,0,0) in the absence of delay term.

In case of existence of a delay term, we apply the procedure given in [16]. Because of the critical delays, some characteristic roots change from having negative real parts to having positive real parts. For this reason, we will examine the purely imaginary roots  $\lambda = i\sigma$ . To get the characteristic equation and see such a change, we substitute  $\lambda = i\sigma$  in Eq. (5) , and separating the real and imaginary parts, we get

$$-\sigma^2(l_1 + l_2 + l_3) + l_1l_2l_3 - K_1K_3F_3F_4\sigma\sin(2\sigma\tau) - K_1K_3F_3F_4l_1\cos(2\sigma\tau) - K_1K_2F_1F_2\sigma\sin(2\sigma\tau) - K_1K_2F_1F_2l_3\cos(2\sigma\tau) = 0 \quad (7)$$

$$-\sigma^3 + \sigma(l_2l_3 + l_1l_3 + l_1l_2) - K_1K_3F_3F_4\sigma\cos(2\sigma\tau) + K_1K_3F_3F_4l_1\sin(2\sigma\tau) - K_1K_2F_1F_2\sigma\cos(2\sigma\tau) + K_1K_2F_1F_2l_3\sin(2\sigma\tau) = 0 \quad (8)$$

Rearranging them we get the following two equations

$$-\sigma^2(l_1 + l_2 + l_3) + l_1l_2l_3 = K_1K_3F_3F_4\sigma\sin(2\sigma\tau) + K_1K_3F_3F_4l_1\cos(2\sigma\tau) + K_1K_2F_1F_2\sigma\sin(2\sigma\tau) + K_1K_2F_1F_2l_3\cos(2\sigma\tau) \quad (9)$$

$$-\sigma^3 + \sigma(l_2l_3 + l_1l_3 + l_1l_2) = K_1K_3F_3F_4\sigma\cos(2\sigma\tau) - K_1K_3F_3F_4l_1\sin(2\sigma\tau) + K_1K_2F_1F_2\sigma\cos(2\sigma\tau) - K_1K_2F_1F_2l_3\sin(2\sigma\tau) \quad (10)$$

Taking squares of both sides in these two equations and adding them we get the polynomial equation given below

$$\sigma^6 + (l_1^2 + l_2^2 + l_3^2)\sigma^4 + (l_2^2l_3^2 + l_1^2l_3^2 + l_1^2l_2^2 - K_1^2K_3^2F_3^2F_4^2 - 2K_1^2K_2K_3F_1F_2F_3F_4 - K_1^2K_2^2F_1^2F_2^2)\sigma^2 + l_1^2l_2^2l_3^2 - K_1^2K_3^2F_3^2F_4^2l_1^2 - 2K_1^2K_2K_3F_1F_2F_3F_4l_1l_3 - K_1^2K_2^2F_1^2F_2^2l_3^2 = 0 \quad (11)$$

Now following the Routh-Hurwitz criterion, we replace  $\mu$  by  $\sigma^2$ . Hence we have the following third-order polynomial equation to carry the stability analysis for the model.

$$\mu^3 + (l_1^2 + l_2^2 + l_3^2)\mu^2 + (l_2^2l_3^2 + l_1^2l_3^2 + l_1^2l_2^2 - K_1^2K_3^2F_3^2F_4^2 - 2K_1^2K_2K_3F_1F_2F_3F_4 - K_1^2K_2^2F_1^2F_2^2)\mu + l_1^2l_2^2l_3^2 - K_1^2K_3^2F_3^2F_4^2l_1^2 - 2K_1^2K_2K_3F_1F_2F_3F_4l_1l_3 - K_1^2K_2^2F_1^2F_2^2l_3^2 = 0 \quad (12)$$

For simplicity, we call the coefficients

$$\begin{aligned} A &= l_1^2 + l_2^2 + l_3^2 \\ B &= l_2^2l_3^2 + l_1^2l_3^2 + l_1^2l_2^2 - K_1^2K_3^2F_3^2F_4^2 - 2K_1^2K_2K_3F_1F_2F_3F_4 - K_1^2K_2^2F_1^2F_2^2 \\ C &= l_1^2l_2^2l_3^2 - K_1^2K_3^2F_3^2F_4^2l_1^2 - 2K_1^2K_2K_3F_1F_2F_3F_4l_1l_3 - K_1^2K_2^2F_1^2F_2^2l_3^2 \end{aligned} \quad (13)$$

Since the leading coefficient is positive, a positive real root may occur in two cases.

i) If  $C < 0$  then the positive real root occurs.

ii) If  $C > 0$  then a negative real root is guaranteed. To analyze the possibility to have two positive real roots, we use the Sturm sequence of the polynomial in Eq. (12).

The details of the method of Sturm sequence are constructed by determining whether a positive real root exists. After finding the functions in the Sturm sequence, the sign changes in endpoints of the considered interval must be determined. The number gives us the number of

real roots. After this step, the conditions must be analyzed to see the positive real root.

We will follow the procedure given in [16]. Let us start with the polynomials

$$f_0 = \mu^3 + A\mu^2 + B\mu + C$$

and

$$f_1 = 3\mu^2 + 2A\mu + B$$

where  $f_1 = f_0'$ . Applying the division algorithm

$$f_0 = q_0f_1 + f_2$$

$$f_1 = q_1f_2 + f_3$$

we have

$$f_2 = \left(\frac{2}{9}A^2 - \frac{2}{3}B\right)\mu + C - \frac{1}{9}AB$$

$$f_3 = -\frac{9}{4} \frac{4B^3 - A^2B^2 - 18ABC + 4CA^3 + 27C^2}{(A^2 - 3B)^2}$$

By considering the sign changes at each endpoint of the interval  $(-\infty, \infty)$ , we may construct the following table given in [16] to have three sign changes, hence three real roots for the case (ii).

**Table 1.** The sign changes for the Sturm sequence.

	$-\infty$	$\infty$
$f_0$	-	+
$f_1$	+	+
$f_2$	-	+
$f_3$	+	+

In order to get this table we need the following conditions,

$$A^2 - 3B > 0$$

and

$$4(B^2 - 3AC)(A^2 - 3B) - (9C - AB)^2 > 0$$

where the constants  $A, B, C$  are determined as in (13).

And for the case (ii), there exists one positive real root if  $A < 0$  or  $A > 0$  and  $B < 0$  [16].

We will conclude this part by the following theorem based on the theorem in [16] in case of a delay term exists.

**Theorem:** Consider the characteristic equation (5) for the system (2) with a delay term. The system is unstable near  $(0,0,0)$  if and only if  $A, B$  and  $C$  are not all positive and either  $C < 0$ , or  $C > 0$ ,  $A^2 - 3B > 0$  and  $4(B^2 - 3AC)(A^2 - 3B) - (9C - AB)^2 > 0$  is satisfied where  $A, B$  and  $C$  are given in (13).

**Proof:** In the existence of the conditions given above, we have three real characteristic roots and one of them is positive. Hence the system becomes unstable.

#### 4. Conclusion

In this study, the stability properties of a neural field model are constructed in a special case. The linearized model for three neuron populations is considered and is investigated for the stability in an algebraic way. The main idea here is to determine the roots of the characteristic equation. Since the characteristic equation is third-order, the Routh-Hurwitz criterion and the Sturm sequence are used. These two methods give the chance to make the analysis in an efficient way. As shown in this study, the stability properties in terms of the coefficients on the system are determined in a quick way by two theorems.

#### Conflict of Interests

No conflict of interest was stated by the authors.

#### Acknowledgements

The author would like to thank the editor and the reviewers for their valuable suggestions and comments.

#### Declaration of Ethical Standards

The authors of this article declares that the materials and methods used in this study do not require ethical committee permission and legal-special permission.

#### References

- [1] Wilson H., Cowan J., 1973. A Mathematical Theory of the Functional Dynamics of Cortical and Thalamic Nervous Tissue. *Biological Cybernetics*, **13**(2), pp. 55-80.

- [2] Amari S.I., 1977. Dynamics of Pattern Formation in Lateral-inhibition Type Neural Fields. *Biological Cybernetics*, **27**(2), pp. 77-87.
- [3] Coombes S., 2005. Waves, Bumps, and Patterns in Neural Field Theories. *Biological Cybernetics*, **93**(2), pp. 91-108.
- [4] Atay F.M., Hutt A., 2006. Stability and Bifurcations in Neural Fields with Finite Propagation Speed and General Connectivity. *Siam Journal on Mathematical Analysis*, **5**(4), pp. 670-698.
- [5] Coombes S., Venkov N.A., Shiau L., Bojak L., Liley D.T.J., Laing C.R., 2007. Modeling Electrocortical Activity Through Improved Local Approximations of Integral Neural Field Equations. *Physical Review E*, **76**, 051901.
- [6] Faye G., Faugeras O., 2010. Some Theoretical and Numerical Results for Delayed Neural Field Equations. *Physica D: Nonlinear Phenomena*, **239**(9), pp. 561-578.
- [7] Veltz R., Faugeras O., 2011. Stability of the Stationary Solutions of Neural Field Equations with Propagation Delay. *Journal of Mathematical Neuroscience*, **1**, 1, pp. 1-28.
- [8] Van Gils S.A., Janssens S.G., Kuznetsov Yu. A., Visser S., 2013. On Local Bifurcations in Neural Field Models with Transmission Delays. *Journal of Mathematical Biology*, **66**(4), pp. 837-887.
- [9] Veltz R., 2013. Interplay Between Synaptic Delays and Propagation Delays in Neural Field Equations. *Siam Journal of Applied Dynamical Systems*, **12**(3), pp. 1566-1612.
- [10] Veltz R. Faugeras O., 2013. A Center Manifold Result for Delayed Neural Fields Equations. *Siam Journal on Mathematical Analysis*, **45**(3), pp. 1527-1562.
- [11] Özgür B., Demir A., 2016. Some Stability Charts of a Neural Field Model of Two Neural Populations. *Communications in Mathematics and Applications*, **7**(2), pp. 159-166.
- [12] Özgür B., Demir A., Erman S., 2018. A Note on the Stability of a Neural Field Model. *Hacettepe Journal of Mathematics and Statistics*, **47**(6), pp. 1495-1502.
- [13] Özgür B., Demir A., 2018. On the Stability of Two Neuron Populations Interacting with Each Other. *Rocky Mountain Journal of Mathematics*, **48**(7), pp. 2337-2346.
- [14] Özgür B., 2019. Some stability notes of a neural field model. *IDES 2019 International Design and Engineering Symposium*, İzmir, Turkey, 10-12 October, pp. 123-126.
- [15] Özgür B., 2020. Stability Switches in a Neural Field Model: An Algebraic Study on the Parameters. *Sakarya University Journal of Science*, **24**(1), pp. 178-182.
- [16] Forde J., Nelson P., 2004. Applications of Sturm Sequences to Bifurcation Analysis of Delay Differential Equation Models. *Journal of Mathematical Analysis and Applications*, **300**, pp. 273-284.





## Synthesis and Antioxidant Activities of Novel Naphthalimide Derivatives

Ufuk YILDIZ<sup>1,\*</sup> <sup>1</sup> Department of Chemistry, Zonguldak Bülent Ecevit University, Zonguldak, 67100, Turkey, **ORCID:** 0000-0002-0419-0011

### Article Info

#### Research paper

Received : October 25, 2020

Accepted : February 11, 2021

### Keywords

Antioxidant

DPPH

Naphthalimide

Peroxide

### Abstract

In this study, synthesis and characterization of naphthalimide derivatives containing both amide and urea groups were performed and their antioxidant activities were determined. 4-*R*-1 8-naphthalic anhydride (*R* = -H, -NO<sub>2</sub> or -NH<sub>2</sub>) with different functional groups has been chosen as the precursor and reacted with 5,6-diamino-1*H*-benzo[*d*]imidazol-2(3*H*)-one to synthesize the targeted naphthalimide derivatives. ESI-MS and <sup>1</sup>H-NMR techniques have been used to characterize the molecules. Antioxidant activities of compounds have been determined by DPPH and peroxide radical scavenging methods.

## 1. Introduction

Antioxidants are molecules that can inhibit the oxidation of other molecules after the release of free radicals and prevent what is left [1]. Designing and developing compounds that can exhibit antioxidant activity is a very interesting field of study, as such compounds can help prevent many diseases such as stroke, diabetes, and many types of cancer by relieving oxidative stress [2, 3]. Many types of natural compounds and different vitamins obtained from plants are used extensively in many industries such as food and cosmetics. Therefore, there is considerable scientific interest in discovering effective synthetic antioxidants.

Amide derivatives are an important chemical group displaying many biological activities [4-6]. For example, anilides are widely used in medicine, pharmacy, biology and other related fields due to their biological activities such as anti-bacterial, anti-fungal, anti-infectious, and anesthetic. Various anilides have also found a broad of

applicability as bioactive species (antimicrobial, antioxidant, and antatherosclerotic agents) [7]. At the same time, synthetic amide derivatives can show strong antioxidant activity [7, 8].

Urea and thiourea are important functional groups in many natural products and drug intermediates. Urea and thiourea derivatives have many promising biological activities such as herbicide, antimicrobial, antioxidant, antiviral, anti-HIV and antitumor activity [9-13]. It is known that molecules with urea functional groups show enzyme inhibition and promising antioxidant activity [14, 15].

In this study, it is aimed to synthesize the compounds which could have high antioxidant activity due to including both urea and amide functional group (Figure 1). Thus, naphthalimide derivatives with different *R*-groups have been synthesized and their antioxidant activities have been examined.

\* Corresponding Author: [ufukyildiz@beun.edu.tr](mailto:ufukyildiz@beun.edu.tr)



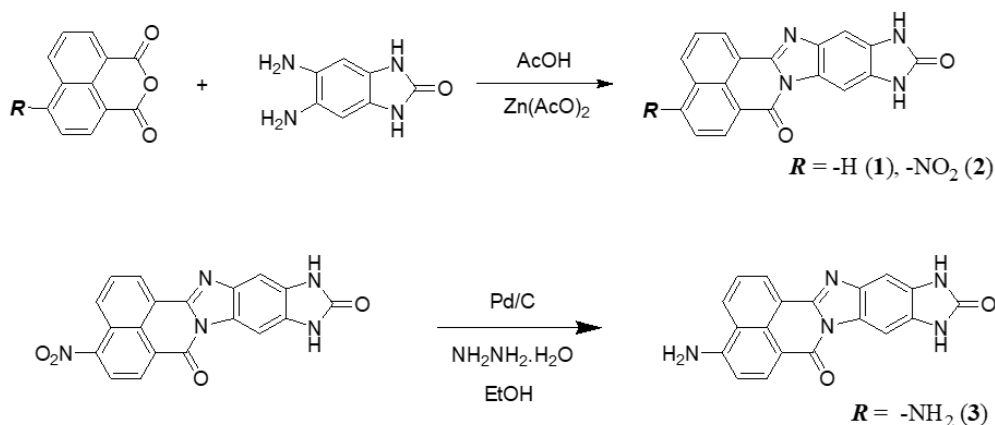


Figure 1. General synthesis procedure for compounds.

## 2. Materials and Methods

### 2.1. Chemicals and Instruments

All chemicals used were of analytical grade and obtained from Sigma-Aldrich unless otherwise stated. UV-Vis absorption measurements were carried out using Varian Cary 100 spectrophotometer device. Proton Nuclear Magnetic Resonance Spectroscopy ( $^1\text{H}$  NMR) was measured on a Bruker Ultra Shield Plus spectrometer, with chemical shifts reported as parts per million (in  $\text{DMSO-d}_6/\text{CDCl}_3$ , TMS as an internal standard).

### 2.2. Synthesis of Compounds

#### 2.2.1. Synthesis of 1

1 mmol (198 mg) 1,8-naphthalic anhydride was dissolved in 30 ml of acetic acid and 1 mmol (164 mg) 5,6-diamino-1H-benzo [*d*] imidazol-2(3H)-one was added to the balloon. After adding 1 equivalent of zinc acetate to the mixture, it was boiled at 130 °C under reflux overnight. After the reaction was completed, the balloon was then taken over the heater and cooled to room temperature. Precipitation was formed by the addition of crushed ice. The precipitate formed was filtered under vacuum and washed sequentially with acetone, ethanol and ether. The commercially available compound obtained was characterized by electrospray ionization mass spectrometry (ESI-MS) and  $^1\text{H}$ -NMR techniques. Yield: 68%. M.p.: 165 °C. ESI-MS:  $m/z = 327.0$  [M+H] (Fig. A.1).  $^1\text{H}$ NMR (600 MHz,  $\text{DMSO-d}_6$   $\delta$ , ppm): 10.87 (s, 1H, NH), 10.80 (s, 1H, NH), 8.62 (m, 2H, CH), 8.46 (d, 1H, CH), 8.27 (d, 1H, CH), 7.94 (s, 1H, CH), 7.94 (s, 1H, CH), 7.87 (t, 1H, CH), 7.84 (t, 1H, CH), (Fig. A.2).

#### 2.2.2. Synthesis of 2

Synthesis of compound 2 was achieved by the same way, using 1 mmol (243 mg) 4-nitro-1,8-naphthalic anhydride. Yield: 59%. M.p.: 173 °C. ESI-MS:  $m/z = 372.0$  [M+H] (Fig. A.3).  $^1\text{H}$ NMR (600 MHz,  $\text{DMSO-d}_6$   $\delta$ , ppm): 10.84 (s, 1H, NH), 8.80+8.60 (d, 2H, CH), 8.75 (s, 1H, CH), 8.05+8.01 (t, 2H, CH), 7.89 (s, 1H, CH), 7.44+7.37 (m, 2H, CH), 7.28 (s, 1H, CH) (Fig. A.4).

#### 2.2.3. Synthesis of 3

Compound 2 was used as a reagent in the reaction. 110 mg of 2 was taken into the flask and dissolved in 50 ml of ethanol by boiling. 0.5 g of Pd/C and excess of hydrazine hydrate were added. The mixture was boiled under reflux for 6 hours, then filtered while hot and the Pd/C was removed. The remaining solution was cooled to room temperature and ether was added. The precipitate formed was filtered and washed sequentially with cold acetone and ether. The product was characterized by mass and NMR techniques. Yield: 52%. M.p.: 178 °C. ESI-MS:  $m/z = 341.7$  [M+H] (Fig. A.5).  $^1\text{H}$ NMR (600 MHz,  $\text{DMSO-d}_6$   $\delta$ , ppm): 10.88 (s, 1H, NH), 10.81 (s, 1H, NH), 8.75+8.72+8.62 (m, 2H, CH), 8.50+8.48+8.42 (m, 2H, CH), 8.27+8.21+8.05+8.01 (m, 3H, CH), 7.95 (s, 1H, CH), 7.31 (s, 1H, CH) (Fig. A.6).

## 2.3. Antioxidant Assays

### 2.3.1. 1,1-diphenyl-2-picrylhydrazyl (DPPH) radical scavenging activity

DPPH method previously reported in the literature was modified and applied [16]. DPPH radical absorbs at 517 nm wavelength. Stabilized DPPH was determined by following the absorbance at this wavelength. In the study, solutions of DPPH (0.5 mM) and compounds (0, 10, 20,

40, 80 and 100  $\mu\text{M}$ ) were prepared by dissolving in ethanol. 1.8 mL of DPPH solution was well mixed with 0.2 mL of a solution of the compound. Absorbance at 517 nm of the resulting solution (DPPH + samples) was recorded after incubation for half an hour in dark. The abilities of compounds to stabilize DPPH radical was examined using the formula;

$$\text{DPPH \%} = (A_c - A_s) / A_c \times 100 \quad (1)$$

where  $A_c$  is absorbance of control and  $A_s$  is absorbance of sample mixture at 517 nm. The required concentration of compounds to stabilize the half of the DPPH radical ( $\text{IC}_{50}$ ) was calculated.

### 2.3.2. Hydrogen Peroxide Scavenging Activity

The  $\text{H}_2\text{O}_2$  scavenging abilities of the compounds were determined according to the literature [17]. 0.6 mL of 40 mM  $\text{H}_2\text{O}_2$  solution (pH 7.4) was well mixed with the 100, 250, and 500  $\mu\text{g/mL}$  of the samples. The absorbance of prepared mixtures at 230 nm were recorded after incubation for 10 min. The abilities of compounds to scavenge the peroxide radicals was examined using the formula;

$$\text{H}_2\text{O}_2 \% = (A_c - A_s) / A_c \times 100$$

where  $A_c$  is absorbance of control and  $A_s$  is absorbance of sample mixture at 230 nm.

## 3. Results and Discussion

### 3.1. Synthesis of the compounds

$^1\text{H}$  NMR spectroscopy and ESI-MS spectroscopy techniques were used to analyse the structure of the compounds. The ESI-MS result for compound 1 (Figure S1) (327.0 (M+H)) directly matches with the calculated molecular weight (356.3 g/mol). When the  $^1\text{H}$  NMR spectrum of 1 is examined, number of protons derived from  $^1\text{H}$  NMR spectrum is compatible with the targeted molecule. The chemical shifts of the protons numbered 7 and 8 (Fig.S2) were observed at different ppm values due to the fact that the proton number 7 is attached to a partially positive carbon as a result of conjugation. Likewise, protons attached to nitrogen atoms have very close chemical shift values to each other but at separate

ppm values due to differences in charge distribution. When the structure is examined completely, the chemical shift of all protons is in the expected region and confirms the structure.

When the mass distribution of compound 2 is examined, the high peak appeared at  $m/z = 372$  directly confirms the structure as the M+H molecular ion peak. The  $^1\text{H}$  NMR spectrum of 2 shows that the compound was synthesized as two different isomers as expected (Fig. A.7). Number of integrated protons directly matches with the structure of the targeted molecule. Since the carbon atom to which the proton number 4 is attached is adjacent to the carbon attached to the electron withdrawing nitro group, the chemical shift value has increased up to 8.8 ppm. Since TFA was used together with DMSO as a solvent in the spectrum, one of the nitrogen protons 8 and 9 could not be observed. The  $^1\text{H}$  NMR spectrum of the compound suggests that 2 has been synthesized as its two isomers mixture with the ratio of 56% and 44%, while the triplets of the proton 2 gave twin signals at 8.05 and 8.00 ppm.

ESI-MS spectra of 3 indicated that the molecular weight of the compound is 341.3 g/mol as supposed. The  $^1\text{H}$  NMR spectrum of 3 is similar to the spectrum of 2. The  $^1\text{H}$  NMR spectrum of the compound suggests that 3 has been synthesized as its two isomers as a continuation of 2 with the ratio of 56% and 44%

### 3.2. Antioxidant Activities

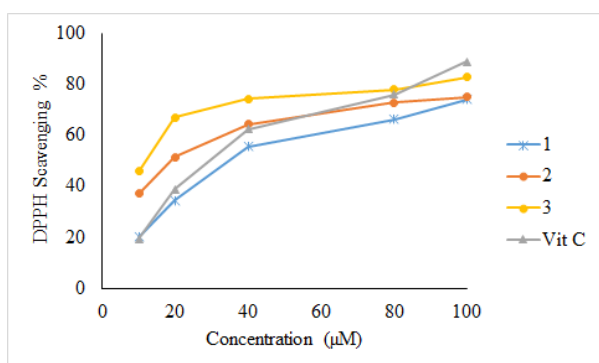
Elimination of reactive species is an issue that is taken into consideration, as it causes various health problems by damaging the biochemical molecules in the organism. The task of the compounds that provide protection against cancer by showing antioxidant activity is to stabilize free radicals. This process occurs when compounds donate either a single electron or hydrogen atom to free radicals [18]. In this study, DPPH and  $\text{H}_2\text{O}_2$  methods were used, which give results much faster than other methods. All the newly synthesized compounds showed potent to moderate radical scavenging activities at all concentrations.

DPPH radical scavenging activity of compounds is related to their tendency to donate hydrogen or single electron [19]. The results of percentage inhibition of the DPPH radical by synthesized compounds and standard antioxidant Vit C with different concentrations were represented in Figure 2. The  $\text{IC}_{50}$  values calculated by using graph were illustrated in Table 1.

**Table 1.** IC<sub>50</sub> and total scavenging percentages of compounds.

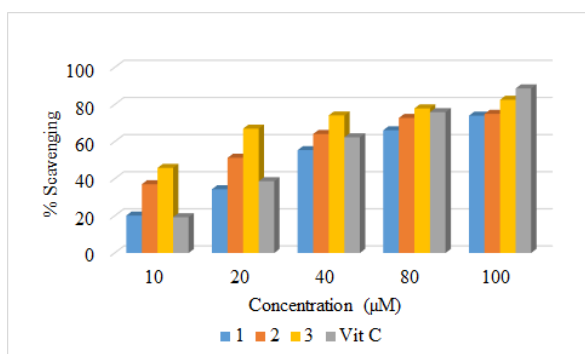
Compound	DPPH		H <sub>2</sub> O <sub>2</sub>	
	IC <sub>50</sub> (μM)	Tot. Scavenging %	IC <sub>50</sub> (μg/mL)	Tot. Scavenging %
1	35.1	73.9	550.2	48.7
2	18.7	74.9	487.2	51.6
3	12.3	82.6	251.1	66.7
Vit C	39.2	88	409.5	58

IC<sub>50</sub> value of DPPH for Vit C used as standard antioxidant was calculated as 39.2 μM while IC<sub>50</sub> value for all compounds were greater than Vit C. The NH<sub>2</sub> functional group in compound **3** increased antioxidant activity with 12.3 μM due IC<sub>50</sub> value due to increasing the possibility of H-donating.



**Figure 2.** Antioxidant activities of compounds by DPPH method.

Comparative DPPH scavenging percentages of compounds for different concentrations are shown in figure 3. These results indicated that total scavenging activity of compounds were lower than Vit C.

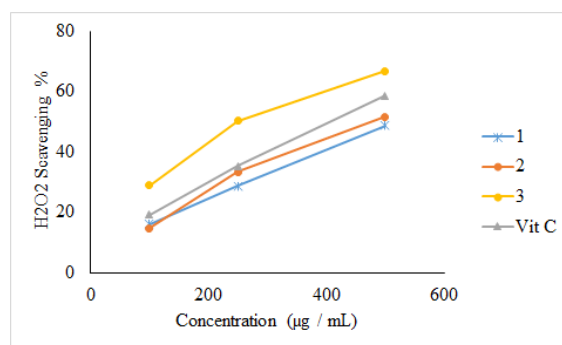


**Figure 3.** Percentage inhibition of DPPH scavenging activity of synthesized compounds in comparison to Vit C.

Synthesized compounds **1–3** were screened for in vitro scavenging activity utilizing hydrogen peroxide. These tested compounds showed moderate hydrogen

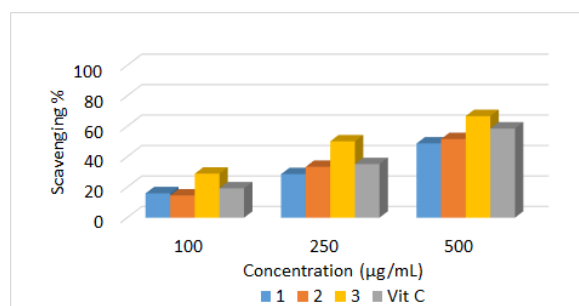
peroxide scavenging activity.

The ability compound **1** and **2** to scavenge hydrogen peroxide were lower than Vit C but compound **3** had a better IC<sub>50</sub> with 251.1 μg/mL (Fig.4). Scavenging activities of compounds were dose-dependent and increased with concentration.



**Figure 4.** Antioxidant activities of compounds by H<sub>2</sub>O<sub>2</sub> method.

Total hydrogen peroxide radical scavenging percentage of compounds at 500 μg/mL were 48.7 for **1**, 51.6 for **2** and 66.7 for **3** (Fig.5). Similar to the DPPH method, compound **3** could scavenge H<sub>2</sub>O<sub>2</sub> radicals as effective as well-known antioxidant Vit C.



**Figure 5.** Percentage inhibition of hydrogen peroxide scavenging activity of synthesized compounds in comparison to Vit C.

#### 4. Conclusions

As a result, the antioxidant activities of the newly synthesized naphthalimide derivatives were determined by

DPPH and H<sub>2</sub>O<sub>2</sub> methods. Adding functional group for single electron and –H donating just as nitro (compound **2**) and amino (compound **3**) prominently enhanced the antioxidant capacity. The availability of these new naphthalimide derivatives would facilitate further investigations of their applications in food and pharmaceutical industries.

### Declaration of Ethical Standards

The author(s) of this article declare that the materials and methods used in this study do not require ethical committee permission and/or legal-special permission.

### Conflict of Interest

The authors declare that they have no known competing financial interests or personal relationships that could have appeared to influence the work reported in this paper.

### Acknowledgements

We are grateful for the support of Zonguldak Bulent Ecevit University with grant 2019-72118496-02.

### References

- [1] Cornelli U., 2009. Antioxidant use in nutraceuticals. *Clinics in Dermatology* **27**(2), p. 175-194.
- [2] Giugliano D., Ceriello A., and Paolisso G., 1995. Diabetes mellitus, hypertension, and cardiovascular disease: Which role for oxidative stress? *Metabolism* **44**(3), p. 363-368.
- [3] Reuter S., Gupta S.C., Chaturvedi M.M., and Aggarwal B.B., 2010. Oxidative stress, inflammation, and cancer: How are they linked? *Free Radical Biology and Medicine* **49**(11), p. 1603-1616.
- [4] Saeedi M., Goli F., Mahdavi M., Dehghan G., Faramarzi M.A., Foroumadi A., and Shafiee A., 2014. Synthesis and Biological Investigation of some Novel Sulfonamide and Amide Derivatives Containing Coumarin Moieties. *Iran J Pharm Res* **13**(3), p. 881-92.
- [5] Huczyński A., Janczak J., Stefańska J., Antoszczak M., and Brzezinski B., 2012. Synthesis and antimicrobial activity of amide derivatives of polyether antibiotic—salinomycin. *Bioorganic & Medicinal Chemistry Letters* **22**(14), p. 4697-4702.
- [6] Narasimhan B., Belsare D., Pharande D., Mourya V., and Dhake A., 2004. Esters, amides and substituted derivatives of cinnamic acid: synthesis, antimicrobial activity and QSAR investigations. *Eur J Med Chem* **39**(10), p. 827-34.
- [7] Kamat J.P. and Devasagayam T.P., 1999. Nicotinamide (vitamin B3) as an effective antioxidant against oxidative damage in rat brain mitochondria. *Redox report : communications in free radical research* **4**(4), p. 179-184.
- [8] Malki F., Touati A., and Moulay S. *Comparative Study of Antioxidant Activity of Some Amides*. 2017.
- [9] Yonova P.A. and Stoilkova G.M., 2004. Synthesis and biological activity of urea and thiourea derivatives from 2-aminoheterocyclic compounds. *Journal of Plant Growth Regulation* **23**(4), p. 280-291.
- [10] Abdel-Rahman H.M. and Morsy M.A., 2007. Novel benzothiazolyl urea and thiourea derivatives with potential cytotoxic and antimicrobial activities. *Journal of Enzyme Inhibition and Medicinal Chemistry* **22**(1), p. 57-64.
- [11] Shusheng Z., Tianrong Z., Kun C., Youfeng X., and Bo Y., 2008. Simple and efficient synthesis of novel glycosyl thiourea derivatives as potential antitumor agents. *European Journal of Medicinal Chemistry* **43**(12), p. 2778-2783.
- [12] Özgeriş B., Akbaba Y., Özdemir Ö., Türkez H., Göksu S., 2017. Synthesis and Anticancer Activity of Novel Ureas and Sulfamides Incorporating 1-Aminotetralins. *Archives of Medical Research* **48** (6), p. 513-519.
- [13] Özgeriş B., 2021. Design, synthesis, characterization, and biological evaluation of nicotinoyl thioureas as antimicrobial and antioxidant agents. *The Journal of Antibiotics*. <https://doi.org/10.1038/s41429-020-00399-7>
- [14] Aksu K., Özgeriş B., Taslimi P., Naderi A., Gülçin İ., and Göksu S., 2016. Antioxidant Activity, Acetylcholinesterase, and Carbonic Anhydrase Inhibitory Properties of Novel Ureas Derived from Phenethylamines. *Archiv der Pharmazie* **349**(12), p. 944-954.
- [15] Bhaskara Reddy M.V., Srinivasulu D., Peddanna K., Apparao C., and Ramesh P., 2015. Synthesis and Antioxidant Activity of New Thiazole Analogues Possessing Urea, Thiourea, and

Selenourea Functionality. Synthetic Communications **45**(22), p. 2592-2600.

- [16] Özel A., Barut B., Demirbaş Ü., and Biyiklioglu Z., 2016. Investigation of DNA binding, DNA photocleavage, topoisomerase I inhibition and antioxidant activities of water soluble titanium(IV) phthalocyanine compounds. *Journal of Photochemistry and Photobiology B: Biology* **157**, p. 32-38.
- [17] Al-Amiery A.A., Al-Majedy Y.K., Kadhum A.A.H., and Mohamad A.B., 2015. Hydrogen

Peroxide Scavenging Activity of Novel Coumarins Synthesized Using Different Approaches. *PLOS ONE* **10**(7), p. e0132175.

- [18] Soare J.R., Dinis T.C.P., Cunha A.P., and Almeida L., 1997. Antioxidant Activities of Some Extracts of *Thymus zygis*. *Free Radical Research* **26**(5), p. 469-478.
- [19] Blois M.S., 1958. Antioxidant Determinations by the Use of a Stable Free Radical. *Nature* **181**(4617), p. 1199-1200.

## Appendices

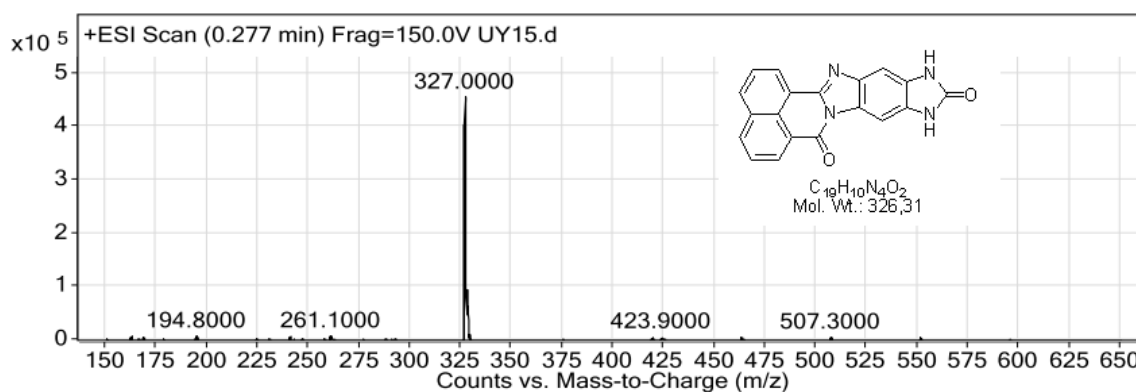


Figure A.1 ESI-MS spectrum for 1.

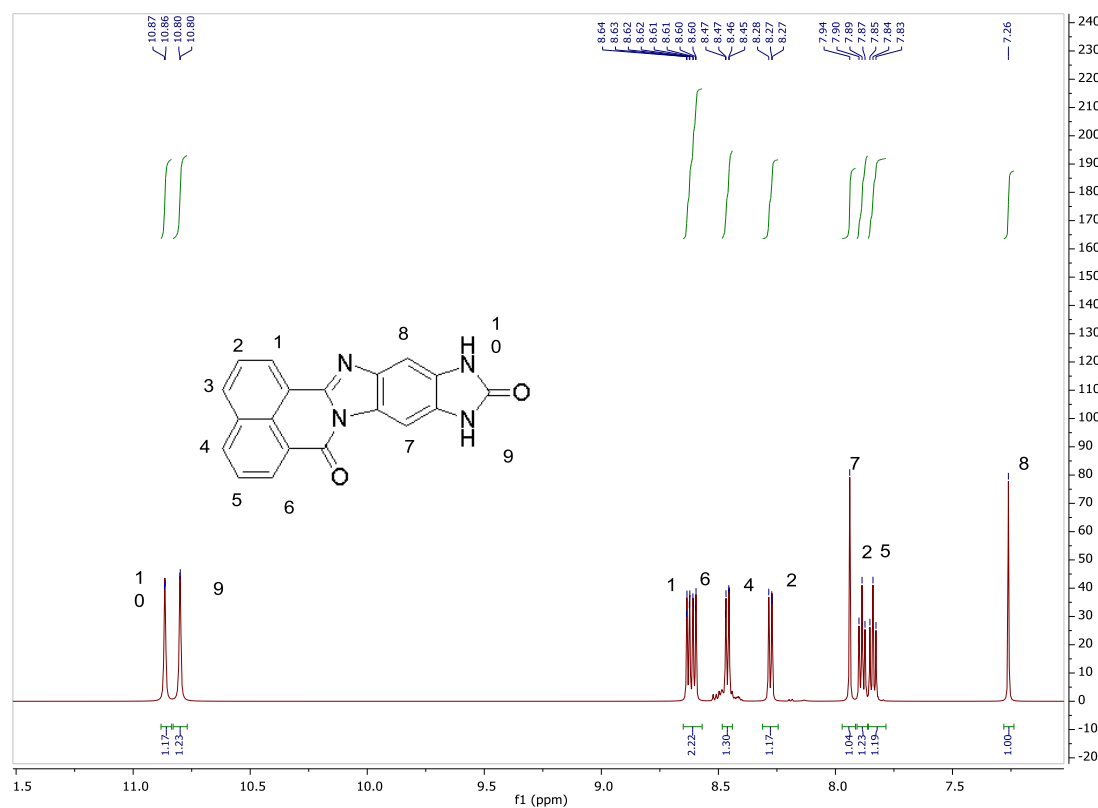


Figure A.2 <sup>1</sup>H-NMR spectrum for 1.

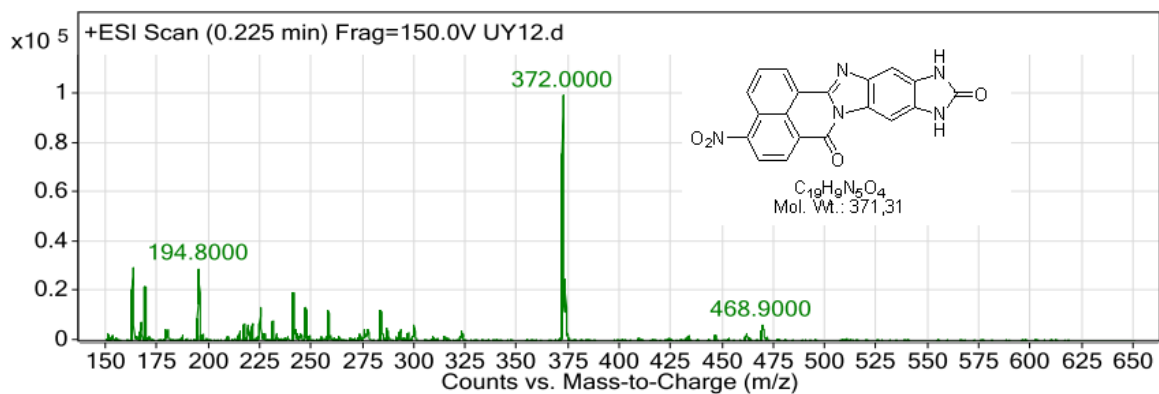


Figure A.3 ESI-MS spectrum for 2.

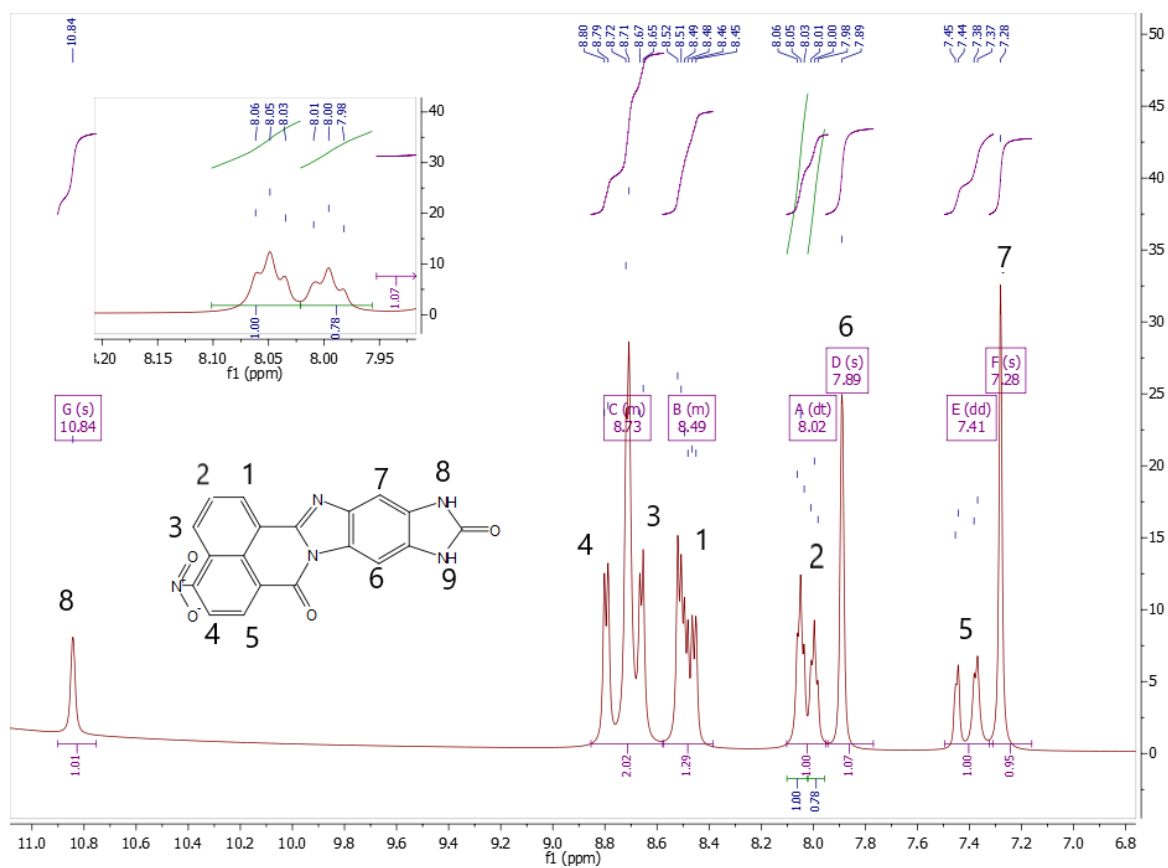


Figure A.4  $^1H$ -NMR spectrum for 2.

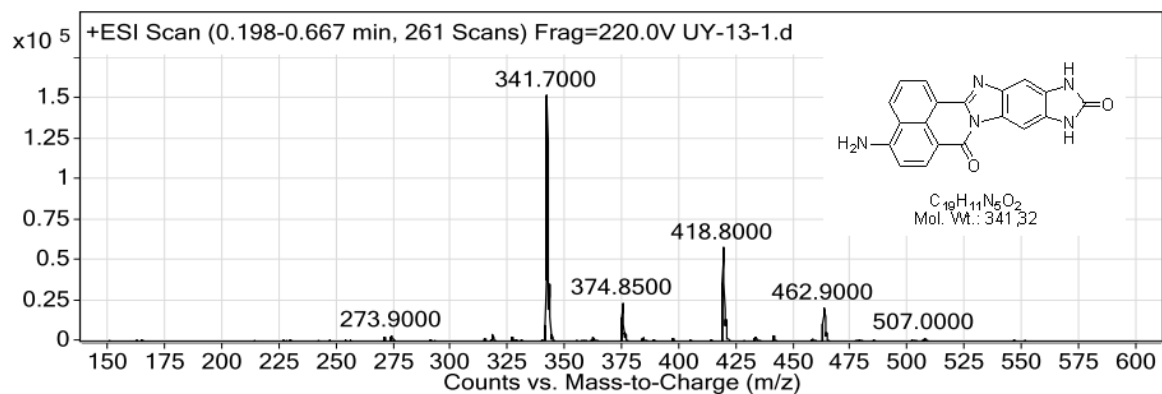
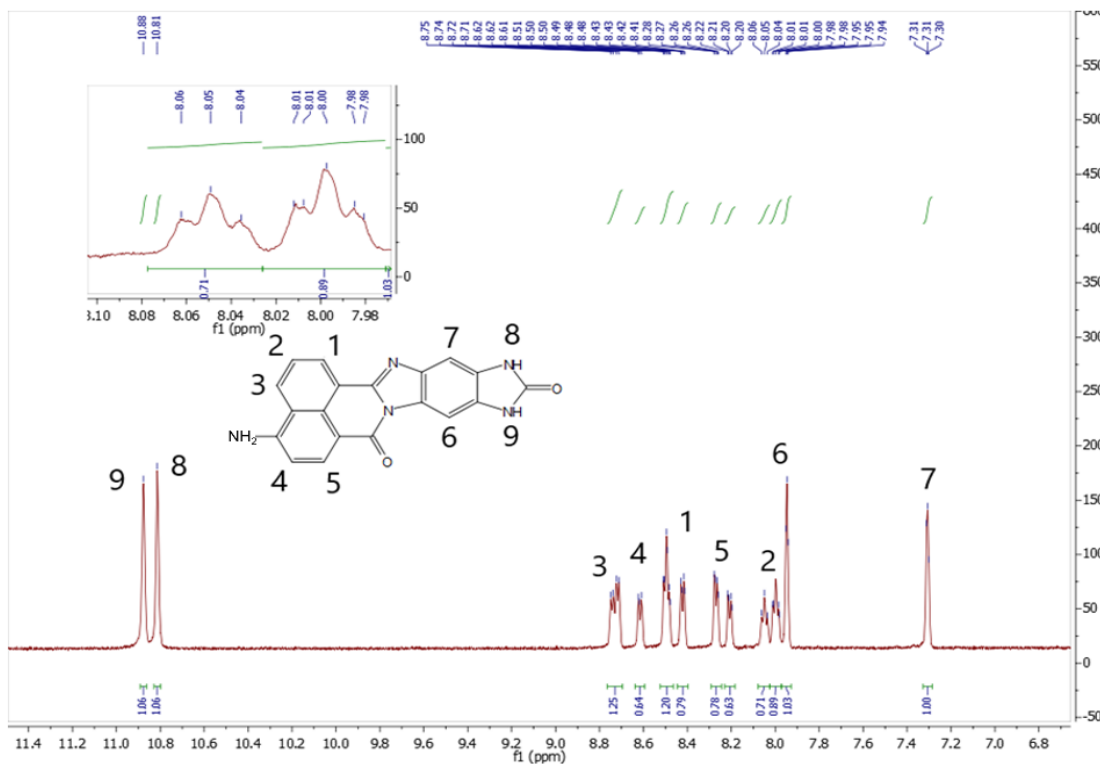
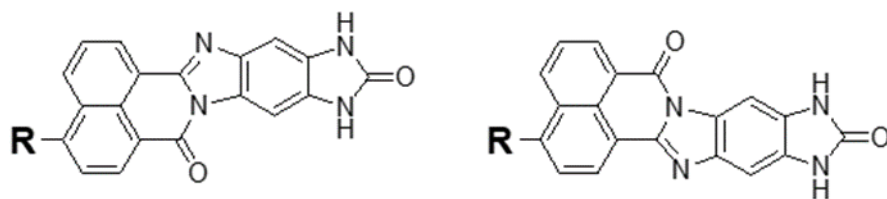


Figure A.5 ESI-MS spectrum for 3.





**Figure A.6**  $^1\text{H-NMR}$  spectrum for **3**



**Figure A.7** The structures of possible isomers.



# An Investigation on Provincial Production & Consumption of Electric Energy: A Case Analysis for Ankara

Mert ÖKTEN <sup>1,\*</sup>

<sup>1</sup> Department of Energy Systems Engineering, Manisa Celal Bayar University, Manisa, 45400, Turkey, **ORCID:** 0000-0003-0077-4471

## Article Info

### Research paper

Received : September 28, 2020

Accepted : February 18, 2021

### Keywords

Ankara  
Decarbonisation  
Electric Energy  
Renewable Energy

## Abstract

Energy is one of the most important factors affecting the country's economy in developing countries. Factors such as interdependent relations, external dependence in primary energy sources such as natural gas and oil, international treaties to reduce carbon emissions, and the amount and availability of domestic conventional resources lead countries to renewable energy sources. In this study, the production sources and sectoral consumption places of the electric energy in Ankara in 2019 were examined. In addition, the share of renewable energy sources in production has been investigated. Economic and environmental analysis of electric energy consumption has been made. As a result, it was determined that 9.55 TWh of electricity was produced in 2019, and this value meets 68% of the 14 TWh consumption value.

## 1. Introduction

Energy is the basic requirement of life, which enables the formation of socioeconomic activities in the modern world. Fossil fuels that meet most of this need compared to the increasing energy need on a global basis are gradually decreasing. In the world, especially in the twentieth century, the intensive use of fossil fuels such as oil, coal and natural gas have caused the effects of ozone depletion, acid rain and global warming [1]. It is also known that fossil fuels will be an ultimate reserve and these fuels will run out in the coming years. Nature with limited resources makes fossil fuel-based energy consumption unsustainable. As a result, humanity has increased the trend towards renewable energy based on nature.

Renewable energy is an important issue today and is expected to continue to play an important role globally in the future. Today, most countries are developing policies and trying to set accessible targets in this area. Renewable energy has an important place in meeting the energy needs of countries with domestic resources, reducing dependency on foreign resources, diversifying resources with ensuring

sustainable energy use and minimizing the damages caused by energy consumption [2].

Renewable energy can be classified as solar energy, wind energy, hydraulic power energy, geothermal energy, biofuel energy, hydrogen energy, wave and current energy and tidal energy as seen in Table 1.

**Table 1.** Energy sources.

Renewable E.S.		Non-Renewable E.S.	
Hydrogen	Wind	Oil (LPG, Gasoline, Diesel)	Nuclear (Thorium, Uranium, Plutonium)
Solar	Hydraulic	Coal (Lignite, Coal, Charcoal, Coke, Air Gas)	Methane hydrate
Geothermal	Wave		Natural gas (LNG)
Biofuel (Biomass, Biodiesel/ Bioethanol, Biogas)	Tidal	Unconventional natural gas (Sand gas, Coal mine methane, Shale (rock) gas)	

Approximately 20% of the energy consumed in the world today is obtained from renewable sources. Currently, despite the high dependence on fossil fuels, renewable

\* Corresponding Author: mert.okten@cbu.edu.tr



energy use has been increasing steadily over the years. In recent years, Turkey is following the global trend of significant progress in the field of renewable energy. According to data from 2019, the share of electricity production in renewable energy in Turkey was 44% [3].

Fossil fuels are the energy source that has originated from living organisms such as animal and plant remained under the ground for millions of years. These are fuels formed by the fossilization under high pressure in airless environments in the layers of the Earth's crust. Fossil fuels can be used in various fields such as operating factories, electricity generation, operating vehicles, comfort heating and meeting kitchen needs.

On the other hand, climate change has become one of the most important reasons to support renewable energy. Climate change is the most controversial and known environmental problem today. Climate change occurs with a combination of natural and anthropogenic factors that slowly increase the temperature in the atmosphere. The global warming pollution is constantly measured, and CO<sub>2</sub> equivalent gases are given to all gases causing the climate change. Renewable energy such as fossil energy is used as electricity generation, heat generation and vehicle fuels. One of the latest developments common to all renewable energy sources is that different technologies are expected to emerge in the future. In recent years, renewable energy transfer and CO<sub>2</sub> capture technologies have been developed [4].

The natural process that causes the gases in the earth's atmosphere to be permeable to the incoming sun rays and to be less permeable to the rays reflected from the ground, and to cause the place to heat up more than normal, is called the greenhouse effect. Global warming is the phenomenon of increasing the temperature of the earth by intensive increase in greenhouse gases (CO<sub>2</sub>, CH<sub>4</sub>, N<sub>2</sub>O, O<sub>3</sub>, CFCs and H<sub>2</sub>O) as a result of unnatural activities [5]. Supply-demand imbalances in the quality of energy causes additional CO<sub>2</sub> emissions due to exergy destruction and these exergy destructions are not possible to return. CO<sub>2</sub> emission amounts for different energy sources are given in Table 2 [6]. In this table, emission values generated by renewable energy sources result from the installation of plants, production and assembly of materials and waste disposal processes.

**Table 2.** CO<sub>2</sub> emission of different energy sources.

Energy Sources	CO <sub>2</sub> Emissions (ton / GWh)
Natural Gas	499
Lignite	1054
Coal	888
Fuel-Oil	733
Nuclear	66
Hydraulic	26
Geothermal	38
Solar PV	85
Wind	26
Biofuel	45

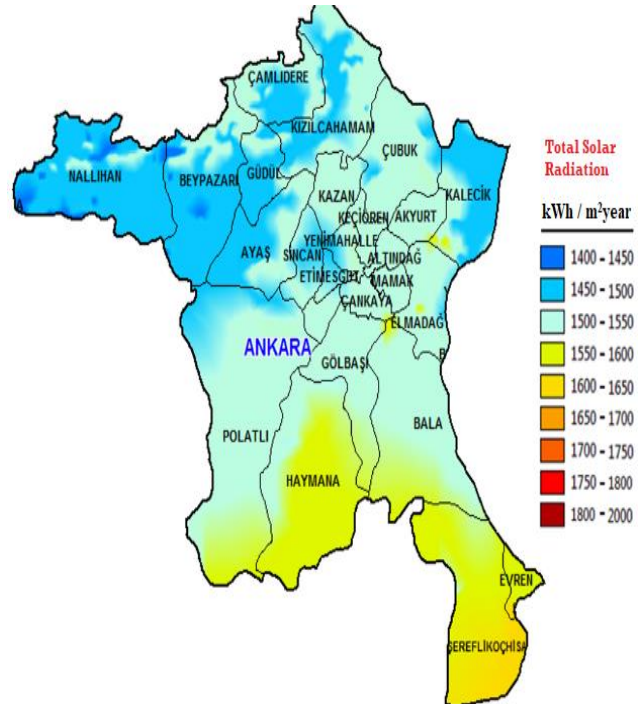
When we examine the literature on energy analysis, the scarcity of resources is remarkable. Bastianoni et al. stated that the energy sector is responsible for 92% of the total greenhouse gas production by evaluating the thermodynamic analysis of Ravenna region of Italy and the entropy waste production of greenhouse gases [7]. Liu et al. conducted an energy analysis of the ecological economic system for Liaoning province and stated that non-renewable resources constitute 74% of the total consumed energy [8]. In a similar study performed in Turkey level, it was found that energy production in Karabük province can meet 45% of its power consumption, and the share of renewable energy in the total energy production has been calculated as 32% [9].

To better understand energy sources and their end use, energy flow diagrams, also called Sankey diagrams, are created that visualize complex relationships [10].

In this study, the place of traditional and renewable energy sources in Ankara in terms of production and distribution of energy consumption to the usage areas as well as environmental and economic analysis of energy production and consumption was investigated.

## 2. Method

Turkey, in terms of solar potential is quite favorable compared to European countries. The average annual sunbathing time of Ankara is 2506 hours, and the average annual solar radiation is 1389 Wh/m<sup>2</sup> [11]. Figure 1 shows Ankara's solar energy potential [12].



**Figure 1.** Ankara global solar radiation distribution.

When the sunshine duration values (hours) and global radiation values (kWh/m<sup>2</sup>/day) given in Figure 2 are analyzed, it is observed that the solar radiation values differ during the year and months and increase in the south and east and increase in July-August [13].

Sun rays come to the city center of Ankara (39.56 N, 32.52 E) with the lowest angle of 26.7° (in winter), the steepest 73.5° (in summer), 61.9° in spring and 39.5° in autumn. Kocer et al. (2016) calculated the annual optimum angle of inclination for Ankara provinces and districts as

34° ±1. In addition, it was calculated as 15 and 56° for six-month periods, and 62°, 23°, 6° and 49° for seasonal (winter, spring, summer, autumn) periods, respectively, and solar radiation values were found for optimum slope angles [14]. Although Ankara had 27 MW solar power plant installed capacity as of 2019, the ratio Ankara in Turkey's installed capacity is only 0.5% [15]. Figure 3 shows the wind power plant installable areas of Ankara.

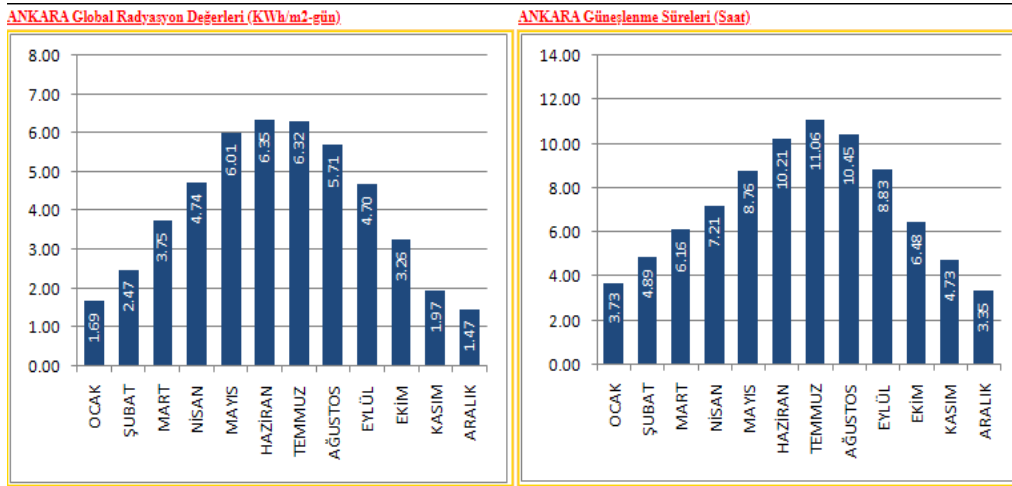


Figure 2. Ankara province global radiation values (kWh/m<sup>2</sup>/day) and sunshine time (hours).

For economic Renewable Energy Source (RES) investment, a wind speed of 7 m/s or more and a capacity factor of 35% or more are required [16]. Average absolute percentage errors for the test data in the wind speed estimation made in MATLAB by taking the historical 30 years wind speed, humidity, pressure, temperature and precipitation amount data obtained from the General Directorate of Meteorology Affairs for sample districts in Ankara province are 9,48% for Çubuk, 7,77% for Keçiören, 7,88% for Polatlı, 6,83% for Bala, 8,02% for Şereflikoçhisar and 5,41% for Haymana [17].

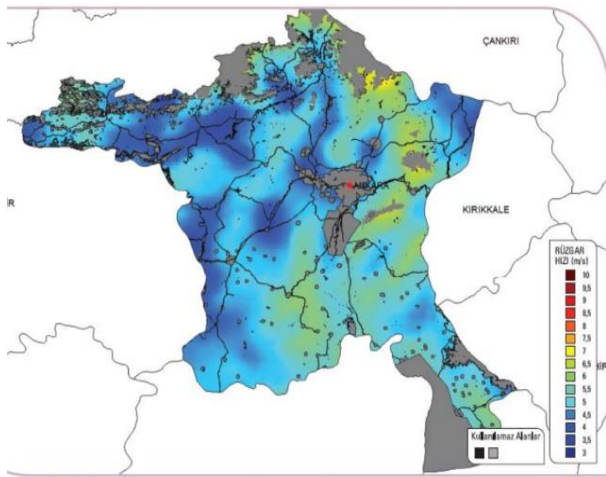


Figure 3. Wind power plant installable areas of Ankara.

Although there is no wind power plant currently installed in Ankara, there are projects planned to be built.

The theoretical hydroelectric potential of our hydraulic resources, which holds the most important place in the renewable energy potential of our country, is 433 billion kWh, and the technically available hydroelectric potential is 216 billion kWh and the economic hydroelectric energy potential is 140 billion kWh / year [18]. Although Ankara had a hydroelectric power plant installed capacity of 304 MW by the year 2019, the ratio of Ankara in Turkey's installed capacity was 1.07% [19].

Biofuel energy is fuel obtained from recently living organisms. Organic substances and biogas yield in biofuel production are given in Table 3, equivalent energy values for animal/plant waste amounts for Ankara province are given in Table 4 and equivalent for municipal and forest residues energy values are given in Table 5 [20].

Table 3. Organic matter and biogas yields.

Organic Matter Type	Biogas Yield (m <sup>3</sup> / ton)	Source
Cattle Manure	45	[21]
Kitchen Waste	30	[22]
Small Cattle Manure	60	[23]

**Table 3.** (Cont.) Organic matter and biogas yields.

Organic Matter Type	Biogas Yield (m <sup>3</sup> / ton)	Source
Domesticated Poultry Manure	70-90	[24]
Wastewater Treatment Sludge	310-800	[25]
Food Waste	50-480	[22]
Vegetable and Fruit Waste	45-110	[21]
Agricultural Wastes	20	[24]
Poultry Manure	310-620	[23]
Sugar Beet Meal	147,1	[26]

**Table 4.** Equivalent energy values for animal/plant waste amounts.

	Number of Animals (Pieces) / Crop Production (Ton)	Waste Amount (Ton)	Energy Equivalent (TOE/ Year)
Cattle	13.631.000	17.469.453	15.376.587
Small Cattle	10.652.000	12.376.785	3.525.390
Poultry	13.956.000	3.429.963	2.699.417
Field Crop	23.707.000	22.360.580	18.950.380
Garden Plant	43.498.000	7.686.060	4.598.154
Vegetables	27.161.000	23.036.800	18.009.426

**Table 5.** Equivalent energy values for municipal and forest residues.

Municipal Wastes	
Amount of Municipal Waste Suitable for Biomethanization (Ton/Year)	926.598
Amount of Municipal Waste Suitable for Incineration (Ton/Year)	758.125
Forest Wastes	
Industrially Not Evaluated (Ster/Year)	64.481
Total Energy Equivalent (TOE/Year)	14.508

According to the data obtained from the studies conducted, the kitchen waste value per capita is approximately 1 kg [21]. 60% of this waste is organic waste. Organic waste amount from Ankara is given in Table 6. Ankara's 2019 population was 5,639,076 [27]. According to this information, the total kitchen waste potential is approximately 5,639 megatons. The amount of gas per person in the domestic wastewater treatment plant varies between 15-22 liters / person. The methane percentage of the gas generated is 65%, and its energy value is 22.4 MJ / m<sup>3</sup> [28].

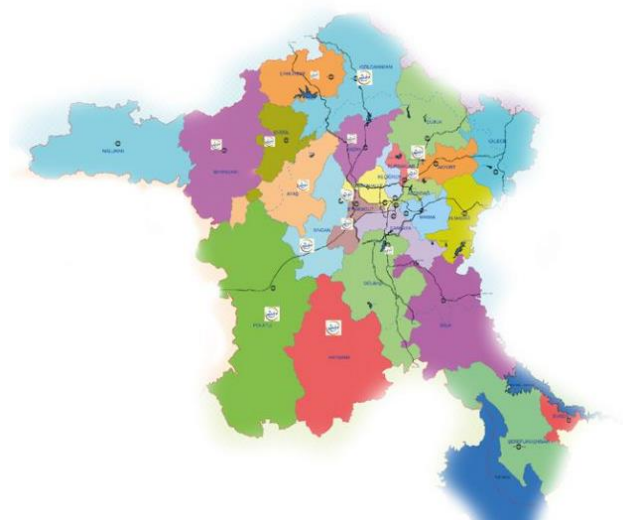
**Table 6.** Organic waste amount in Ankara province.

Organic Waste Type	Total Amount of Organic Waste (TOE / Day)
Kitchen Waste	5,60
Wastewater Treatment Sludge Waste	858,70
Agricultural Waste	113.857,40
Animal Fertilizer Waste	59.181,90
Forest Waste	39,70
Municipal Waste	2,10
Total	173.945,49

Although Ankara had 61 MW biomass power plant installed capacity as of 2019, the ratio Ankara in Turkey's installed capacity is 7.44% [29].

Similarly, Ankara had 1958 MW thermal power plant installed capacity as of 2019, and the ratio of Ankara in Turkey's installed capacity is 4.18% [30-31].

Residential heating, greenhouse cultivation and industry are involved in the direct use of geothermal energy. It is seen that geothermal energy is used in residential heating and tourism in Ankara as depicted in Figure 4. Geothermal energy is at 80 °C, and 2500 houses are heated in Kızılcahamam, a district of Ankara. Thermal tourism and balneology applications of geothermal energy are also available in Haymana. Energy efficiency can be achieved in the districts by increasing the use in Ankara's Ayaş, Beypazarı, Çamlıdere, Çubuk, Etimesgut, Gölbaşı, Güdül, Haymana, Kahramankazan, Kızılcahamam, Mamak, Polatlı, Pursaklar, Sincan and Yenimahalle districts that have geothermal energy [32-33].

**Figure 4.** Geothermal energy map of Ankara province.

### 3. Research Results

The share of renewable energy-based power generation in the licensed power plants in Turkey is 45%



(38,425.02 MW) as seen in Figure 5. The biggest share among these resources is hydraulic energy with 34% (28,494.4 MW). Hydraulic energy is followed by wind energy with 9% (7,520.3 MW) and geothermal energy with 2% (1,514.7 MW). The largest share in non-renewable energy sources belongs to natural gas with 31% (25,935.43 MW).

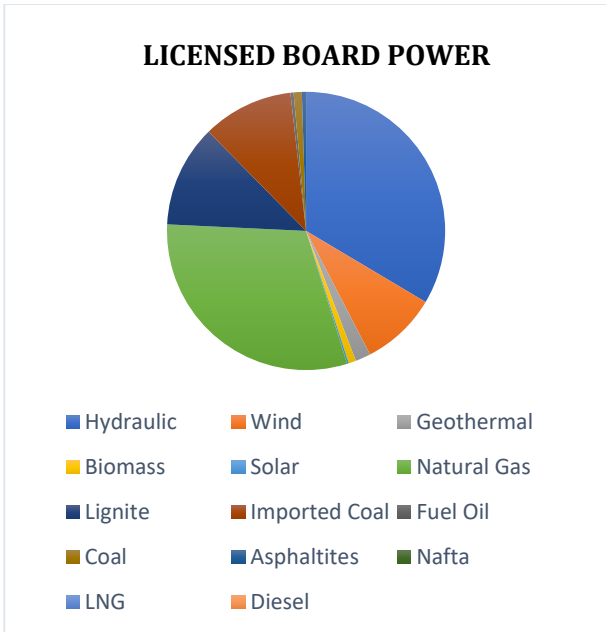


Figure 5. Turkey licensed potential installed capacity of 2019.

In the unlicensed power generation plants, the biggest share has solar (photovoltaic) energy with 97% (5,666.25 MW) as seen in Figure 6.

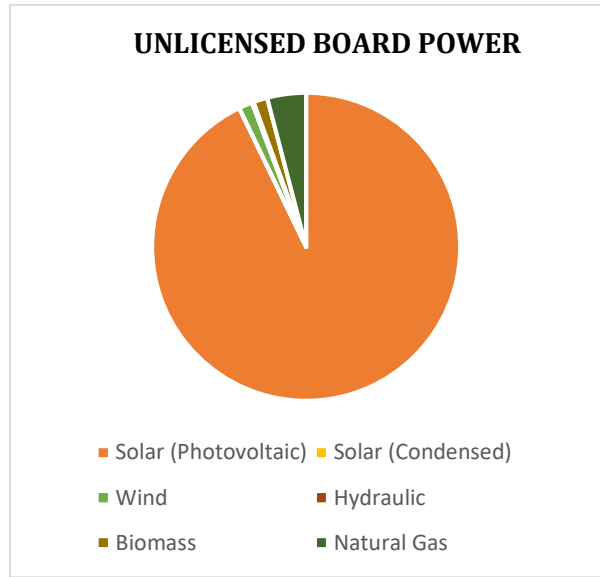


Figure 6. Turkey unlicensed potential installed capacity of 2019.

Hydraulic power comes first in renewable licensed electricity generation. As can be seen in Figure 7, an increase in the production amount is observed with the increase in the water carrying capacity of the rivers especially in the spring months. Natural gas and imported coal lead to the production of electricity from the non-renewable energy sources as shown in Figure 8.

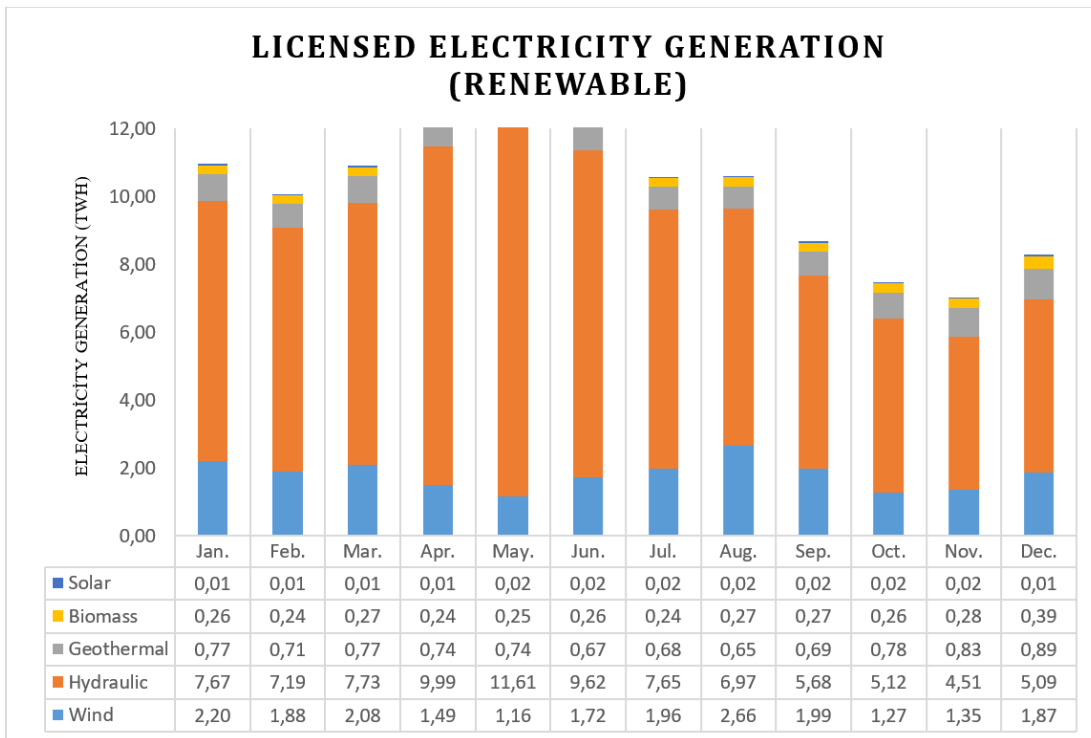


Figure 7. Licensed production of electricity from renewable energy in Turkey in 2019.

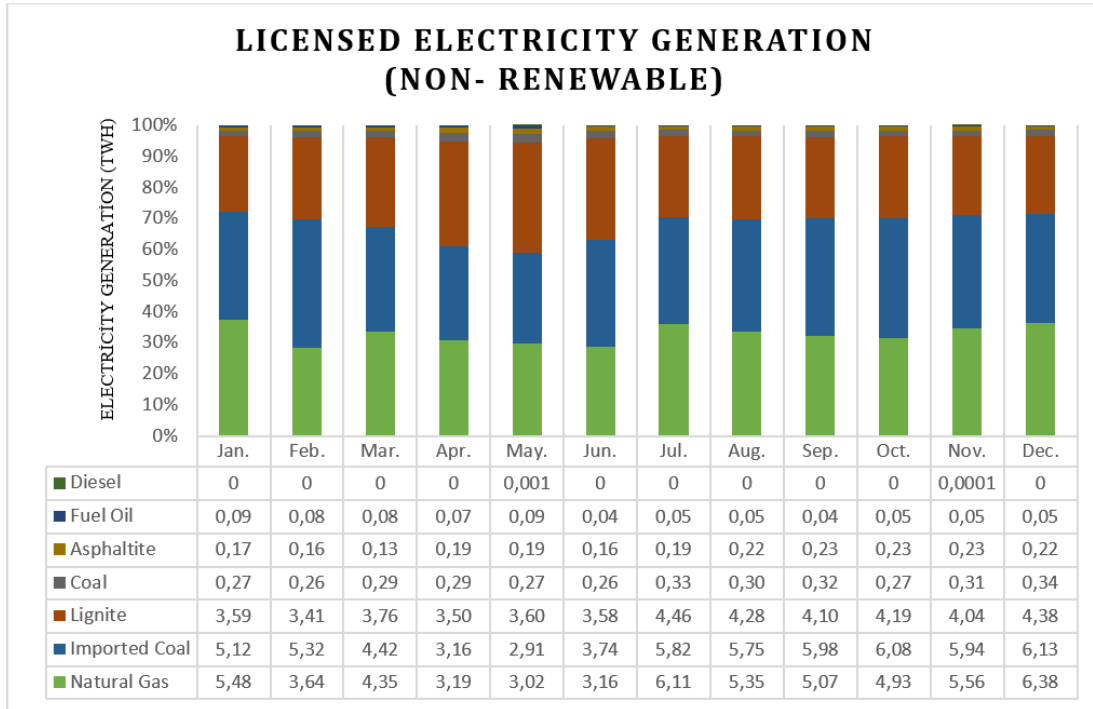


Figure 8. Licensed production of electricity from non-renewable energy in Turkey in 2019.

Electricity generation in Ankara was 9.55 TWh annually as reported in detail in Figure 9. This value refers to 3% of Turkey's equivalent production [34].

Photovoltaic solar energy has the largest share in unlicensed installed power as shown in Figure 10.

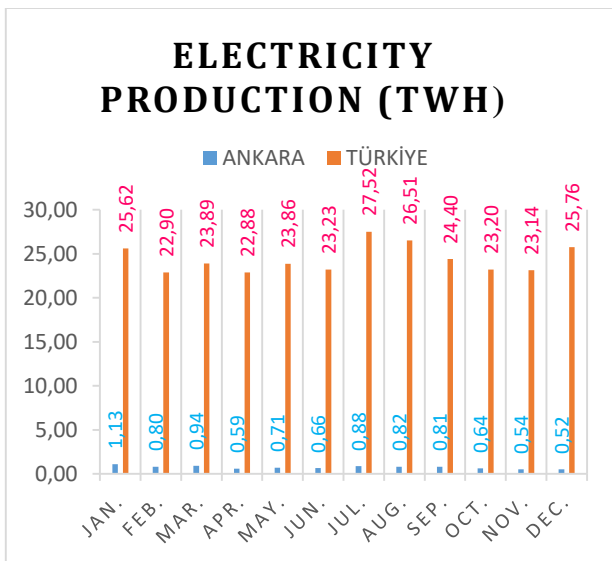


Figure 9. Electricity production in Ankara, 2019.

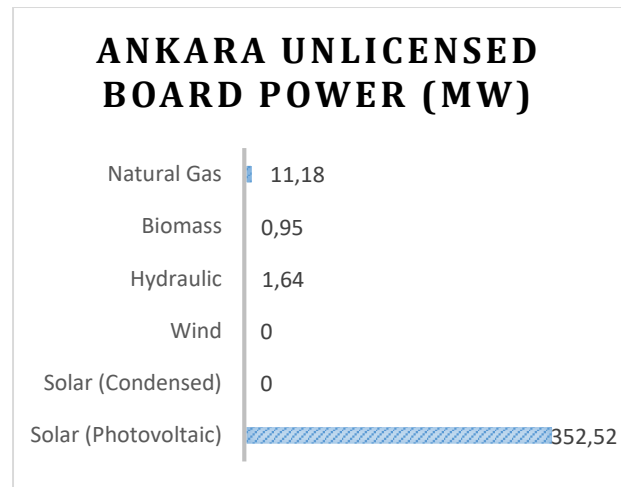


Figure 10. Ankara 2019 unlicensed installed power.



Ankara's annual electrical energy consumption was 14 TWh as reported in detail in Figure 11.

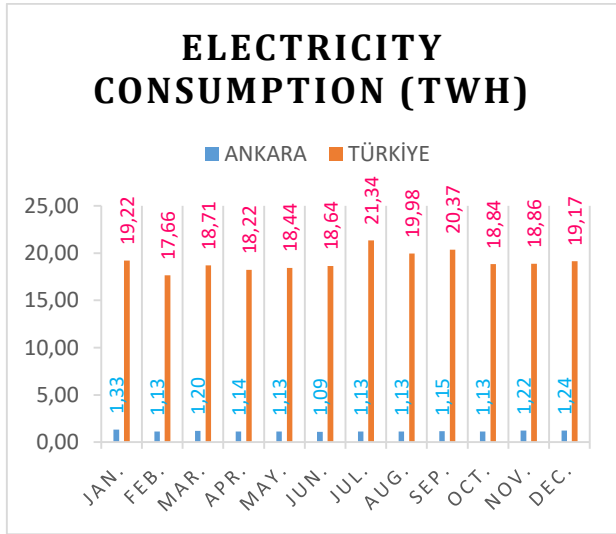


Figure 11. Electricity consumption in Ankara, 2019.

In Turkey, the share of electric energy usage was 6%. Of this consumption, 30% is in industry (Figure 12a), 38% is in the commercial (Figure 12b), 29% is in dwellings (Figure 12c), 2% in illumination (Figure 12d), and 1% in agricultural irrigation (Figure 12e) is used.

It is seen from the graphs that electricity consumption is distributed proportionally throughout the year in industrial, commercial and residential buildings. This usage decreases due to the increase in day length in summer months, and agricultural irrigation increases because of hot summer temperatures.

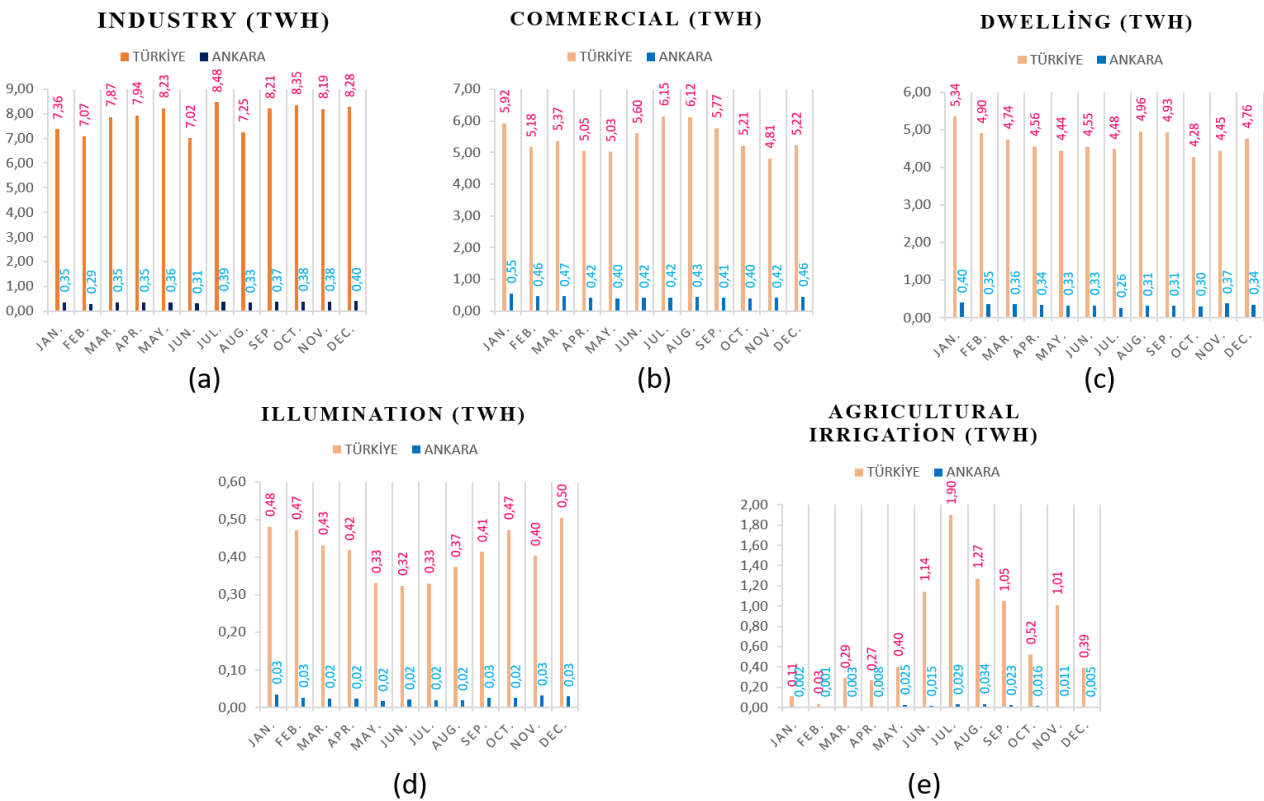


Figure 12. Distribution of electrical energy usage by sectors in Ankara, 2019.

In Figure 13, the electricity production & consumption values for Ankara in 2019 are shown on the Sankey diagram. In 2019, the electricity consumption of Ankara was

provided by 0.8 TWh from self-licensed generation, 8.75 TWh from self-licensed generation, and 4.45 TWh from the interconnected network.

# Ankara

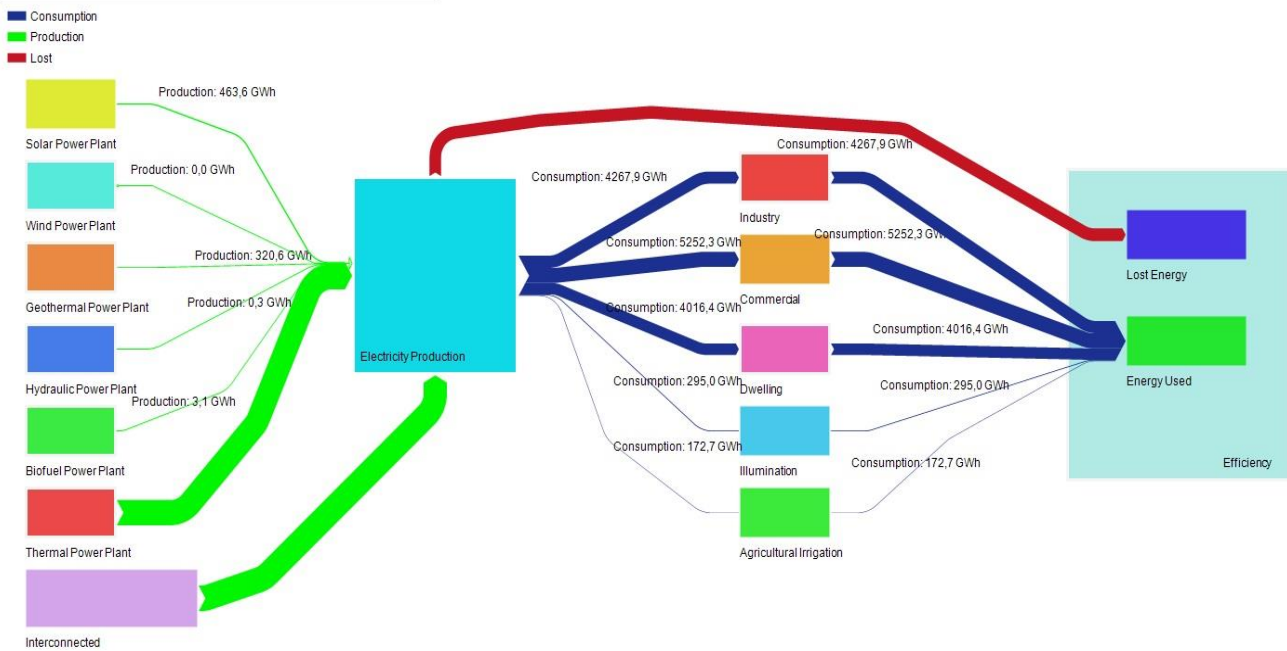


Figure 13. Ankara 2019 electricity production/consumption values SANKEY diagram.

## 4. Conclusion

Ankara's electricity production and consumption in 2019 were 9.55 TWh and 14 TWh, respectively, and the ratio of electricity production to electricity consumption is 68%.

Ankara's 787.6 GWh of electricity generation in 2019 was from renewable energy sources. 22,934 tons of CO<sub>2</sub> emission occurred in the consumption of electricity produced from these sources. Considering that other consumption of 13,216.4 GWh was from fossil origin sources in 2019, approximately 11 million tons of CO<sub>2</sub> emission occurred from these sources.

While Enerjisa Ankara Başkent electricity unit price in 2019 was 0.5375 TL/kWh for dwellings including taxes, this value is 0.7148 TL/kWh for commercial houses [35]. It is known that electricity consumption is 4.3 million MWh for dwellings and illumination and 9.7 million MWh for commercial, industrial and agricultural irrigation. While there was a pricing of 2.3 billion TL for dwellings and illumination, this expense was 6.9 billion TL in industry, commercial and agricultural irrigation.

Efforts should be made to reduce losses and leakages that occur during the transmission and distribution of electrical energy. Projects developed within the framework of the energy efficiency law should be supported. Solar energy use should be encouraged, especially in organized industrial zones and street lighting.

It is thought that Ankara, which is in a central

location close to energy resources, can reduce existing CO<sub>2</sub> emissions with its support programs to renewable energy sources. It is expected that the rooftop PV panels will become the green cities that produce their own energy by producing electricity from renewable energy sources such as the widespread use of geothermal resources in regional heating and electricity production.

## Declaration of Ethical Standards

The materials and methods used in this study do not require ethical committee permission and/or legal-special permission.

## Conflict of Interest

The authors declare that they have no known competing financial interests or personal relationships that could have appeared to influence the work reported in this paper.

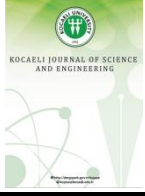
## References

- [1] Kaushik, S.C., Reddy, V.S., Tyagi, S.K., 2011. Energy and Exergy Analyses of Thermal Power Plants: A Review, *Renew. Sustain. Energy Rev.* pp. 1857–1872.
- [2] Kaushik, S.C., Singh, O.K., 2014. Estimation of Chemical Exergy of Solid, Liquid and Gaseous Fuels Used in Thermal Power Plants, *J. Therm. Anal.*

- Calorim. 115 pp. 903–908.
- [3] T.C. Enerji ve Tabii Kaynaklar Bakanlığı, Türkiye Elektrik Enerjisi Tüketimi, <https://enerji.gov.tr/bilgi-merkezi-enerji-elektrik>, (Access Date:22.11.2020).
- [4] Nehrenheim, E., 2018. Introduction to Renewable Energy, volume 1 pp 405-406 <https://doi.org/10.1016/B978-0-12-809665-9.09138-2>.
- [5] Bayraç, H., 2010. Enerji Kullanımının Küresel Isınmaya Etkisi ve Önleyici Politikalar. Eskişehir Osmangazi Üniversitesi Sosyal Bilimler Dergisi, 11 (2), 229-259.
- [6] World Nuclear Association, 2011. Comparison of Lifecycle Greenhouse Gas Emissions of Various Electricity Generation Sources.
- [7] Bastianoni, S., Marchettini, N., Panzieri, M., Ridolfi, R., 2002. Thermodynamic Analysis of The Province of Ravenna (Italy), Ann Chim., 92(9), 771-81.
- [8] Liu, H., Wang, Q., Li, XJ., Song, Y., Li, GJ., 2008. Energy Analysis of Ecological–Economic System in Liaoning Province, Chinese Journal of Applied Ecology, 19(3), 627–33.
- [9] Şevik, S., 2017. Provincial Energy Balance Analysis: Karabük Sample. Gazi Üniversitesi Fen Bilimleri Dergisi Part C: Tasarım ve Teknoloji, 5 (4), 71-85.
- [10] Simon, A.J., Belles, R.D., 2011. Estimated State-level energy flows in 2008, Lawrence Livermore National Lab., United States.
- [11] Sensoy, S., Ulupınar, Y., Demircan, M., Alan, I., Bostan, PA., 2010. Modeling Solar Energy Potential in Turkey, BALWOIS, Republic of Macedonia: Ohrid, 25, 29.
- [12] T.C. Enerji ve Tabii Kaynaklar Bakanlığı, Güneş Enerjisi Potansiyel Atlası (GEPA), <https://gepa.enerji.gov.tr/MyCalculator/pages/6.aspx> (Access Date:22.11.2020).
- [13] Şevik, S., Isı Pompası ve Güneş Kolektörünün Birlikte Kullanıldığı, Isıtma ve Kurutma Amaçlı Sıcak Hava Üretim Sisteminin Tasarımı, İmalatı ve Deneysel İncelenmesi, Doktora Tezi, 2011. Gazi Üniversitesi Fen Bilimleri Enstitüsü, Ankara.
- [14] Koçer, A., Şevik, S., Güngör, A., 2016. Ankara ve İlçeleri İçin Güneş Kolektörü Optimum Eğim Açısının Belirlenmesi, Uludağ University Journal of The Faculty of Engineering, 21 (1), 63-78.
- [15] Ankara Güneş Enerjisi Santralleri, <https://www.enerjibes.com/turkiye-gunes-enerjisi-santralleri/>, (Access Date:22.11.2020).
- [16] T.C. Enerji ve Tabii Kaynaklar Bakanlığı, Rüzgâr Enerjisi Potansiyel Atlası (REPA), <https://repa.enerji.gov.tr/REPA/ANKARA-REPA.pdf> (Access Date:22.11.2020).
- [17] Altınsoy, M., Bal, G., 2019. Uzun Dönem Rüzgâr Hızı Tahmininde Yapay Sinir Ağlarının Kullanımı ve Performans İncelemesi. Mesleki Bilimler Dergisi (MBD), 8 (1) , 21-28.
- [18] T.C. Enerji ve Tabii Kaynaklar Bakanlığı, Hidrolik Enerji, <https://enerji.gov.tr/bilgi-merkezi-enerji-hidrolik> (Access Date:22.11.2020).
- [19] Ankara Hidroelektrik Enerjisi Santralleri, <https://www.enerjibes.com/turkiye-hes-santralleri/>, (Access Date:22.11.2020).
- [20] T.C. Enerji ve Tabii Kaynaklar Bakanlığı, Enerji İşleri Genel Müdürlüğü (EİGM), Biyokütle Enerjisi Potansiyel Atlası (BEPA), <https://bepa.enerji.gov.tr>, (Access Date:22.11.2020).
- [21] Türkiye’de Atıklardan Enerji Üretimi ve Biyogaz, [http://www.tarimsal.com/makaleler/Turkiye\\_Atiklar\\_dan\\_Enerji\\_uretimi\\_ve\\_biyogaz.htm](http://www.tarimsal.com/makaleler/Turkiye_Atiklar_dan_Enerji_uretimi_ve_biyogaz.htm), (Access Date:22.11.2020).
- [22] T.C. Çevre ve Şehircilik Bakanlığı, Suluova Biyogaz Tesisinin Teknik-Ekonomik Esaslarına İlişkin Rapor, Türk Alman Biyogaz Projesi, Ankara, (Access Date:22.11.2020).
- [23] Koçer N.N., Öner C., Sugözü İ., 2006. Türkiye’de Hayvancılık Potansiyeli ve Biyogaz Üretimi, Doğu Anadolu Bölgesi Araştırmaları, Türkiye.
- [24] Aybek A., Üçok S., Bilgili M.E., İspir M.A., 2015. Kahramanmaraş İlinde Bazı Tarımsal Atıkların Biyogaz Enerji Potansiyelinin Belirlenerek Sayısal Haritalarının Oluşturulması, U.Ü. Ziraat Fakültesi Dergisi, 29 (2): 25-37.
- [25] Koçar G., Eryaşar A., Ersöz Ö., Arıcı Ş., Durmuş A., 2010. Biyogaz Teknolojileri, Ege Üniversitesi Basımevi, İzmir.
- [26] Biyogaz Verimi, <http://www.soleaenerji.com/biyogaz-verimi/>, (Access Date:22.11.2020).
- [27] Ankara Nüfusu, <http://www.nufusu.com/il/ankara-nufusu>, (Access Date:22.11.2020).
- [28] Kaya D., Eysel Kaynaklı Arıtma Çamurlarının Biyogaz Üretiminde Kullanımının Değerlendirilmesi, 2010. ICCI- Uluslararası Enerji

ve Çevre Fuarı ve Konferansı, İstanbul.

- [29] Ankara Biyoyakıt Enerjisi Santralleri, <https://www.enerjibes.com/turkiye-biyokutle-santralleri/>, (Access Date:22.11.2020).
- [30] Ankara Termik Enerjisi Santralleri, <https://www.enerjibes.com/turkiye-termik-santralleri/>, (Access Date:22.11.2020).
- [31] Ankara Doğalgaz Enerjisi Santralleri, <https://tr.wikipedia.org/wiki/Ankara#Enerji>, (Access Date:22.11.2020).
- [32] Ankara Jeotermal Enerji Potansiyeli, [https://www.ankaraka.org.tr/tr/ankarada-yenilenebilir-enerji-konusunda-kumelenme-analizi\\_3754.html](https://www.ankaraka.org.tr/tr/ankarada-yenilenebilir-enerji-konusunda-kumelenme-analizi_3754.html), (Access Date:22.11.2020).
- [33] Ankara Jeotermal Enerji Haritası, <https://www.ankara.bel.tr/jeotermal/>, (Access Date:22.11.2020).
- [34] EPDK Elektrik Yıllık Sektör Raporları, <https://www.epdk.gov.tr/Detay/Icerik/3-0-24/elektrikyillik-sektor-raporu>, (Access Date:22.11.2020).
- [35] Enerjisa Ankara-Başkent Elektrik Birim Fiyat ve Tarifeleri, <https://gazelektrik.com/tedarikciler/enerjisa-ankara/birim-fiyat>, (Access Date:22.11.2020).



# Fault Maintenance and Repair Application Based on Augmented Reality Technology in Electrical Distribution Systems

Gokmen HASANCEBI <sup>1</sup> , E. Mustafa YEGIN <sup>2</sup> , Korhan KARAARSLAN <sup>3,\*</sup> 

<sup>1</sup> Sakarya Electricity Distribution Company, Kocaeli, 41310, Turkey, **ORCID:** 0000-0002-2799-3052

<sup>2</sup> Department of Electrical Engineering, Kocaeli University, Kocaeli, 41380, Turkey, **ORCID:** 0000-0002-1665-3132

<sup>3</sup> Department of Electrical Engineering, Kocaeli University, Kocaeli, 41380, Turkey, **ORCID:** 0000-0001-7109-3636

## Abstract

### Article Info

#### Research paper

Received : February 3, 2021

Accepted : March 11, 2021

#### Keywords

Augmented Reality  
Fault Scenario  
Object Recognition  
SCADA

This study presents an AR technology-based software that will work on mobile platforms and the pilot application of this software to solve the possible problems that may be experienced other than routine maintenance activities on protection/control panels and devices in SCADA centers. AR is essentially an information technology that provides the ability to present digital data and images in the same environment as our real world through its visualization, instruction/guidance, and interaction capabilities. Object recognition methods, necessary software, and infrastructure requirements are mentioned in this study in order to benefit from these advantages of AR technology correctly. Different scenarios have been created by using AR for possible failures in automation panels in a distribution center with a telemetry system. Finally, an exemplary scenario in the study is realized in a distribution center located in the SEDAŞ area of responsibility.

## 1. Introduction

The continuous increase in demand for electrical energy is an important part of our lives today. Thus, the amount of energy consumed per capita is shown as an indicator of every country's development level. The increase in energy demand has created a more reliable and high-quality energy concept known as "power quality" in electrical engineering. To meet the continuous and high-quality energy demand of consumers, it is necessary to take action quickly and safely against possible problems in electrical energy systems. In this context, it is thought that the use of information technologies to resolve problems rapidly in SCADA systems and to improve the quality of service for electricity distribution companies will have a positive impact on the maintenance/repair (MR) processes.

There is an essential inconsistency between the rich digital data presented to us and the physical world in which we apply. Although, the physical world is three-dimensional (3D), digital data affects our decisions but practices are

happening in two dimensions. The difference in dimensions must be mentally eliminated, and turning the digital data into the 3D real world. Augmented Reality (AR) technology can eliminate the obligation because it has the ability to present digital data and images in the same environment like the real world [1].

In the future, it is inevitable that all kinds of structures and industries, from educational institutions to social institutions, will be affected by AR technology. AR will change our decision mechanisms and learning styles. In addition, AR will change the way companies train their employees, deliver services, design their products, manage value chains, and compete. AR is an information technology that has visualization, instruction/guidance, and interaction capabilities that can make certain changes.

Through the visualization feature, it is ensured that the interior parts of a product, which are impossible to see under normal conditions, are made visible. For example, a medical device company that converts vein temperature data into images on the patient's skin reports a 350% increase in the

\* Corresponding Author: [korhan.karaarslan@kocaeli.edu.tr](mailto:korhan.karaarslan@kocaeli.edu.tr)



rate of venipuncture on the first attempt [2].

The instruction, training, and guidance processes required to increase productivity and service quality, ensure occupational safety, and take quick action are redefined with AR. It is difficult to follow written instructions/directions during the manufacturing phase. Training sessions are expensive and time-consuming, as well as creating space and equipment is required. AR can overcome such problems in a real physical environment with an array of real-time visual instructions. Boeing Company used AR technology in training for a process that included 50 step assembly drawings and found that training time was reduced by 30% compared to traditional training time [3]. In addition, AR-based devices can send images to an expert who is not in the field, and thus the performance of the personnel in the field can be increased and costs can be saved.

AR technology offers a virtual control panel that is projected directly on the product, instead of using physical control elements such as buttons, valves, and touch screens. Thus, it enables users to manage products remotely. With AR-based devices, it is possible to control the product through hand gestures and voice commands.

Although initially AR technology was used in limited areas, it is used in many areas in a short time in parallel with technological developments (increase in processor capacities and image quality in cameras). In addition, the availability of end-user hardware such as wearable AR systems and smart glasses (Magic Leap, Microsoft HoloLens, etc.), has increased this usage much faster. Currently, the areas where AR technology is mostly used are games, educational applications, advertising and marketing, architectural and construction applications, health, routing and travel applications, military equipment, and industry 4.0 applications [4-14].

The electricity sector is leading those industries that are not yet using AR technology enough. Because of the literature review, it has been determined that the applications of AR technology in the electric energy sector are also limited. Virtual Reality (VR) applications were included in the first studies [15-18]. While digital data are superimposed on the real world in AR applications, the real world is simulated in a computer environment in VR applications. An application showing the appearance of the basic elements in a transformer substation, the functions of these elements, and how to perform the switching operations were conducted by [15] for the purpose of personnel training. Another study describes how VR technology can be used to visualize electrical power systems and how to make professional educational activities more effective. For this purpose, a study was conducted for expert staff involved in the diagnosis, MR of complex machines such as transformers and generators [16]. In 2013, an application developed for a transformer center provided the opportunity

for visitors to navigate in a virtual environment. In addition, the user was enabled to perform real-time operations with real data obtained from the field [17]. With a VR application of electrical tests performed in substations, the aim of using this technique was to increase the number of electrical technicians and train the undergraduate students [18].

In the following years, VR applications were replaced with AR applications. In a study where AR technology is used in the electricity energy sector, a typical 220 kV transformer substation in Shanghai Electricity Grid was selected as a pilot application. AR models of primary and secondary equipment were created to improve the operations and MR training [19]. In 2017, the French electricity distribution company Edenis implemented an AR application consisting of a series of instructions in order to facilitate the use of low voltage control panels and medium voltage devices as well as to reduce possible errors. The same distribution company also implemented an application that enables the field staff to easily locate the fault in underground cables using smart glasses [20, 21]. In another study in which AR technology was used, a mobile application was made to determine and monitor the amount of sag in overhead transmission and distribution lines [22].

As can be seen from the results of the literature review, AR technology, which has a limited number of applications in electrical energy systems, is also underutilized in electrical energy systems in our country. In order to take an advantage of AR technology, a research and development project was carried out in a distribution substation located in the area of responsibility of Sakarya Electricity Distribution Corporation (SEDAS). This project, for the use of AR technology, forms the basis of the proposed study. In the project, the aim is to develop an AR technology-based application on mobile platforms to be used in MR operations of SCADA systems and to support on-field technical teams with quick diagnosis using this application.

The following part of the study mentions the methods of object recognition, the necessary needs for software and infrastructure, which will be used in the AR application. The third section contains an example scenario for an AR application designed for possible failures on the automation panels of the remote terminal unit (RTU) and the data concentrator unit (DCU) belonging to the distribution substation. Achievements with the application are described in the fourth part.

## 2. Materials and Methods

Some applications are relatively simple according to complex and instruction-based AR applications, such as furniture and decoration applications that allow you to



visualize objects in different configurations and settings, using simple content for objects to obtain the necessary digital content. However, complex applications use advanced recognition techniques and AR applications to digitalize objects in a more precise and detailed way.

## 2.1. Object Recognition Methods

Various methods have been developed to recognize objects in AR applications. These methods are based on image processing, which is the principle of digitizing the image and converting it into a form that computers can understand. Target recognition is made by taking useful parts of the objects transferred to digital form. The useful parts have distinct details of the object. It is important to analyze the object well and choose a recognition method. In short, the details of the object inform us which recognition method will be chosen. In this study, three different object recognition methods and an advanced object recognition program are used.

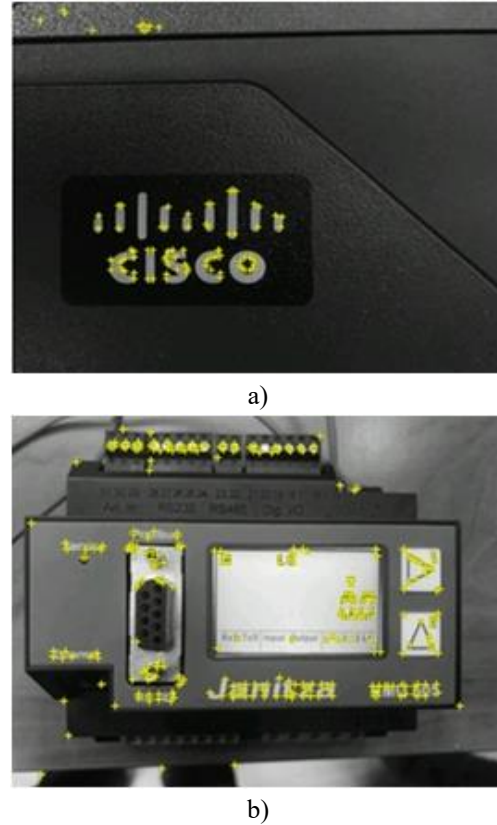
In the early stages of the development of the AR application, it is planned to use the photographs of the objects to create target images. However, the fact that each element in SCADA panels needs to be photographed individually and has shown that the success rate of this recognition process will be affected negatively. Moreover, it has been found that a large number of photographs are required since the photography has to be taken from many angles. Instead of this approach, it is decided to photograph each of the devices on the panels (Energy quality recorder, W-automat, RTU, modem, ...) independently, regardless of the SCADA cabinet and panels.

For this purpose, Vuforia program is used as an object recognition program in the AR application which is proposed to be designed. Vuforia is a library that provides the ability to recognize images or objects through image processing technology and develop AR applications according to the location of the objects in the real world. Objects located in the real world can be identified using the three different object recognition methods discussed below.

### 2.1.1. Image Target

In this method, the photo of the target object is taken and digitalized. The captured image is loaded into the object recognition program database. It is desired that the uploaded images have planar features that provide sufficient detail that can be detected by the program. Images do not need to be divided into special black-and-white zones or contain conventional reference marks, such as quick response codes (QR). The image is graded by analyzing the natural features of the image. The rating is to show the detection level of the

object and its traceability by the system. An image without enough detail and pattern is graded with a low score, while an image with different shapes, texts, characters, and patterns that do not repeat itself is rated with a high score. Other recognition methods are tried for objects with low grading scores. In Figure 1, images of two different objects graded with low and high scores are given.



**Figure 1.** Rating image target a) Low-scored image b) High-scored image.

For the image target method, a database must first be created within the Vuforia application. There are three different database types of Vuforia, which are specified as device, cloud, and vumark. These databases are shown in Figure 2 by taking a screenshot of Vuforia.

After selecting a suitable database for the application, the image target we want to recognize is loaded into the created database. There are different types of image targets that Vuforia offers to the user for object recognition. The target selection screen for two-dimensional objects, 3D cubic objects, 3D cylindrical objects, and other 3D objects that do not comply with this classification is shown in Figure 3. Once the loading process of the image target is finished, the rating of the image target can be seen as in Figure 1. After this process, the database created by Vuforia becomes available in the project where the application is developed.



### 2.1.2. Object Scan

The method, which is used to recognize objects that are not very large, is for situations where the image target method is insufficient. The proposed study is used primarily to recognize the objects that can be scanned. Real objects are scanned and digitized with an application installed on mobile devices. Digital data is loaded into the database of the object recognition program, as in the image target method, and the objects are recognized. Scanning is carried out by rotating 360 degrees around the object. Thus, recognizing the target from different angles is presented.

For the object scan method, the three-dimension object scanner application running on the Android operating system within Vuforia is used. By running the application, the object placed on the image is scanned. After the scanning process is completed, the created file is loaded into the database by selecting the "3D Object" model. Figure 4 shows the RTU digitalization used in SCADA panels by the object scan method.

### 2.1.3. Model Target

Real objects are not used in this recognition method. 3D models of objects drawn using computer-aided design (CAD) programs are used. The 3D model is loaded into a converter program and converted into a format that the object recognition program can understand. In short, digital data is transformed into another form of digital data. This transformation program gives us an output showing the external lines of the object. In practice, when these lines are overlapped on the real object, the recognition process takes place. This method can be used for objects that do not have sufficient detail on their surface, do not contain patterns, and have CAD drawings. The size of the object is not important in this method. Even a car with a 3D CAD drawing can be easily recognized by this method.

Vuforia includes a program that enables the recognition of 3D drawing models in order to create a model target. The CAD drawing in the supported extension is transferred into the project by running this program, which is called the model target generator. After the CAD model object is transferred into the project, the angle we want to recognize the object is determined and the project output of the target file is saved in the computer. Figure 5 shows a visual of this process.

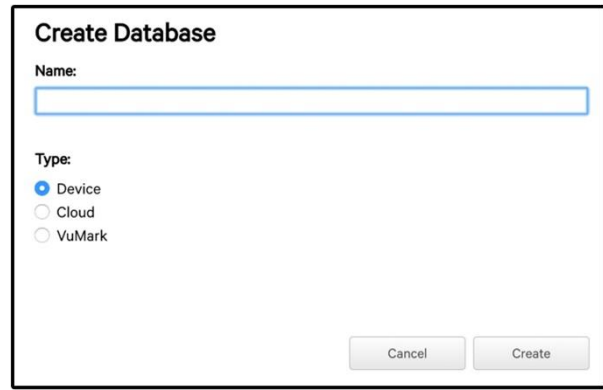


Figure 2. Creating a database in Vuforia.

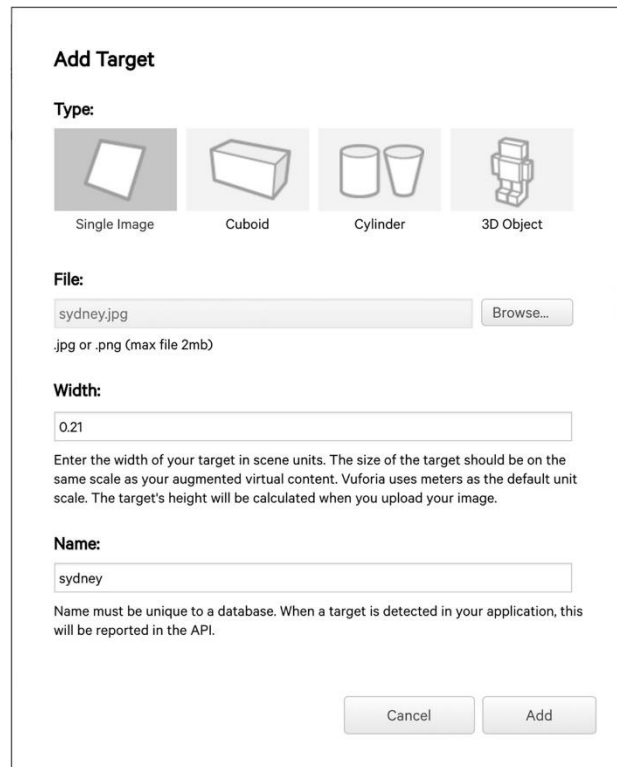


Figure 3. Adding image target in Vuforia.

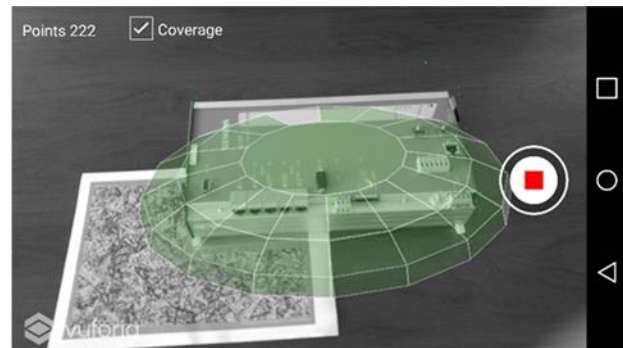


Figure 4. Object scanning for an RTU.

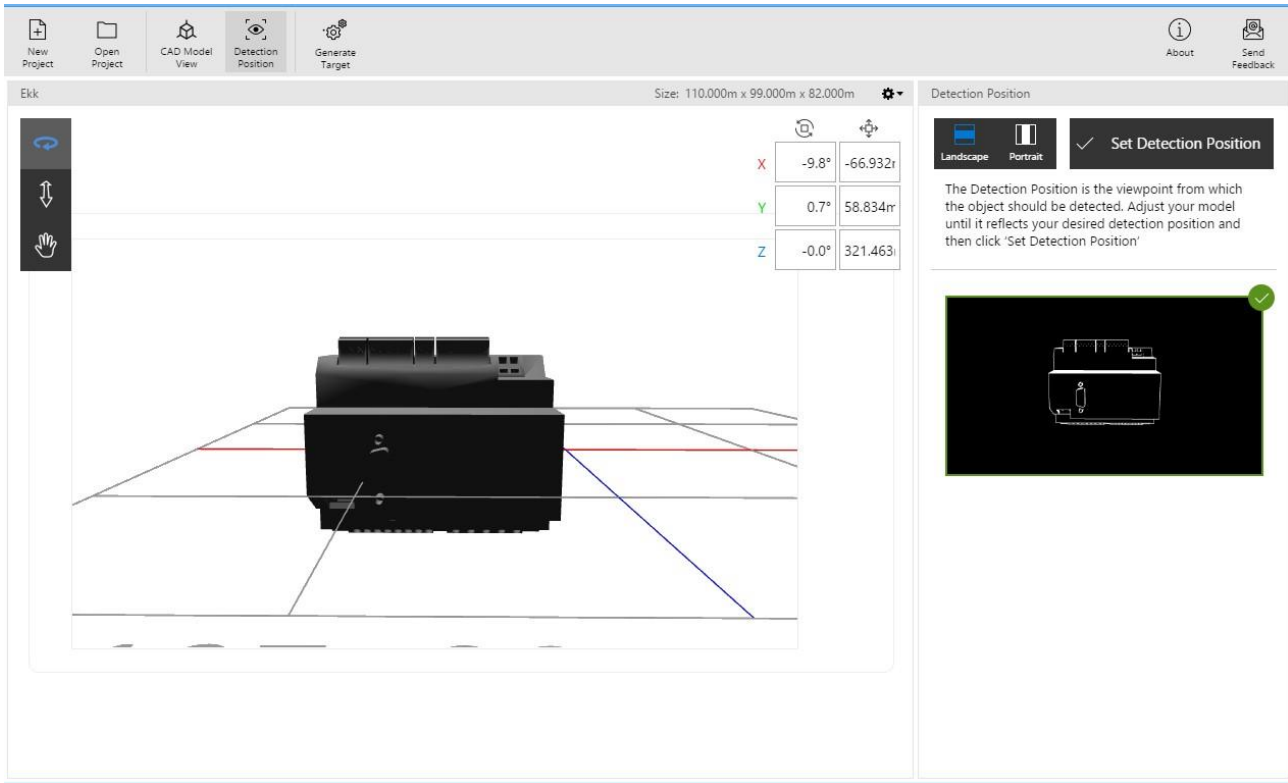


Figure 5. Object recognition with CAD drawing.

### 2.2. AR Development Tool

In the proposed study, ARKit software is used, which enables the determined objects that are detected and the AR processes start when the camera captures the objects. The library, called Object Scanner in the software, scans 360 degrees of the reference object placed on a flat surface. Once the scanning process is completed, the file with the extension ".arobject" is placed in the project in which the

AR application is developed in order to find the scanned object. The steps of this process performed for the energy quality analyzer (EQA) located in the panels in the SCADA center are shown in Figure 6. Objects in the project file are recognized by the relevant library through the Image Tracking module within ARKit, and reference objects are tracked as long as they are in the camera image. By using this module, horizontal-vertical planes and identified objects can be recognized quickly.

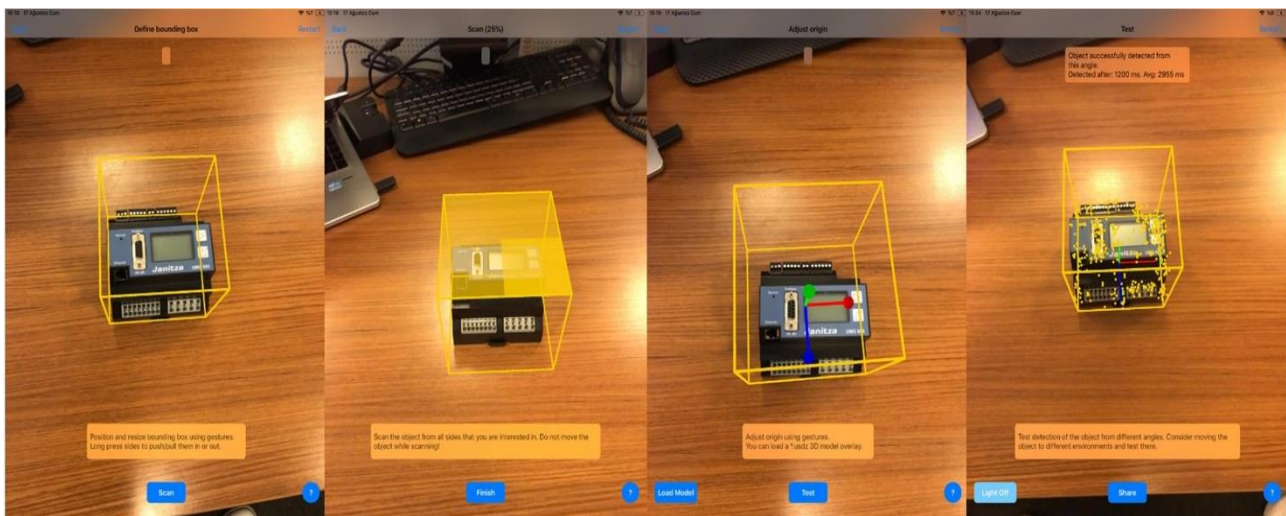


Figure 6. Scanning EQA.

### 2.3. Server and Database

The AR application actually does not need a web server and can run independently on a device (tablet, phone). However, it requires a webserver to collect and report the valuable data generated on the device in a central database. In addition, the user name and password information to be used by the people who will use the AR application to log in to the application are also defined through the web interface. This information is sent to devices via web services. Therefore, the AR application needs a web server to be able to exchange data with a central database and generate reports.

In the proposed study, two databases are created. First case, when there is no communication network available, the system produces data over the device database. In the presence of a communication network, the system design is made in such a way that the data stored on the device are transmitted to the central database. Data are written to the device database after the user action. Buttons are shown to the user at each step. When these buttons are clicked, data are stored in the device database. Second case, when the problem can not be solved, and the information about the

fault is stored on the device database. Therefore, when the communication network is provided, the information starts transmitting to the central database.

### 3. Results and Discussion

The facts that the department of SCADA development/maintenance (DM) team in SEDAS, headquartered in Gebze, has to travel in a wide area covering Kocaeli-Bolu-Düzce-Sakarya provinces for automation panel faults in SCADA cabinets of distribution centers with telemetry system, and the field maintenance teams do not have the experience to fix these faults are the most important starting point of the AR application proposed in this study. A system software has been implemented to work on AR technology-based mobile platforms that can take action more quickly and safely in order to solve possible problems that may occur in automation panels other than routine maintenance activities, reduce of occupational accidents, shorten of personnel hired adaptation period, minimize operational errors and raise the rate of resource utilization. A flowchart is used to create software is shown in Figure 7

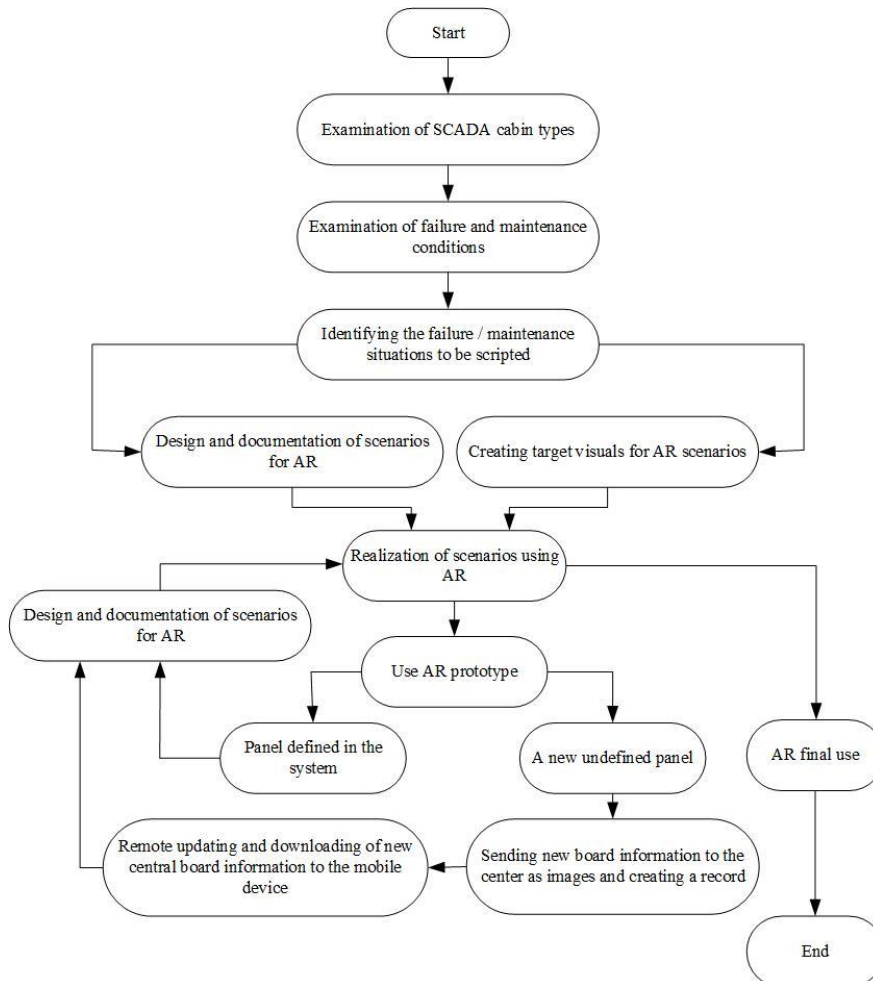


Figure 7. The roadmap of developed AR application.

In the first stage, panels in SCADA cabinets are examined and MR scenarios are created for possible faults in these panels. A workflow scenario is drawn for each case. By analyzing the AR requirements of the Android platform on which the software environment is developed, the visuals are used to determine the SCADA cabinet which has been made recognizable by the application.

In the next step, screen designs are made for possible failure scenarios individually that may occur in the RTU and DCU automation panels of distribution centers. Scenarios are recorded for each step. Scenario steps, screen messages, buttons on the screen, and information about the next screen display can be defined systematically in this way. "RTU/IO-BOX Automat Tripped", "No EQA Communication", "RTU EQA W-AUTO Control", "Rectifier Mainboard Replacement", "Rectifier AC Failure", "Rectifier Fan Failure", "No Communication", "RTU Module Failure" and "On/Off Failure" states are the names of the scenarios whose screen designs are realized. As an example, the screenshots designed for the "Rectifier Motherboard Replacement" scenarios are shown together in Figure 8.

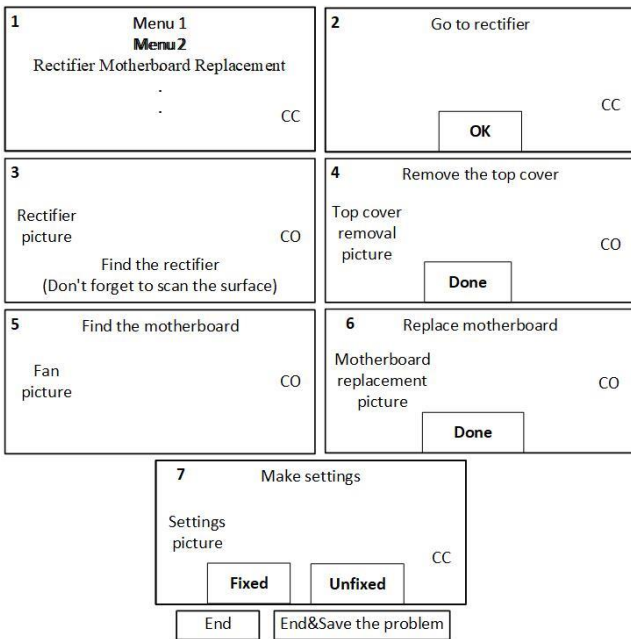


Figure 8. Rectifier motherboard replacement.

Two different recording procedures are made during the operation of the system. In every step of the application, during the interaction with the operator, the recording process is made and information such as the work number, scenario number, and time spent at each step, the buttons pressed at each step are kept. In this way, reports can be made on which scenarios work more (frequency of the problem), which steps are spent longer, and which problem the faults are mostly caused. In cases where the existing fault cannot be solved, records are stored to find out why the

problem could not be solved.

In addition, a scenario record has been created for each scenario. The steps of each scenario, the messages and buttons that will appear on the screen, and the next step information when each button is pressed can be systematically defined in this way. The scenarios in the application are operated over ".json" extension files. The code text in this file is collected under two basic tags as "Scenario" and "Steps". In Figure 9, there is a part of the codes belonging to the ".json" file created for the "No Communication with EQA" scenario.

The scenario tag holds the information of the scenario name and scenario number. The step tag, on the other hand, holds the data used in the operation of the scenario steps. These data include the index used to access the sequence information in the series, step number, work order to be made, work order detail, whether the AR camera will be operated or not, the button to be displayed to the user in the work step, the number of the next work steps to go when the relevant button is clicked, and other scenarios information if there is any. Information obtained from these tags is reflected on user screens.

```

1  { "Scenario":{ 29  {
2  "Title":"EKK Haberleşme Yok", 30  "Index":1,
3  "No":2, 31  "No":2,
4  "Index":1 32  "Title":"Hücre Yüzeyini Tara",
5  }, 33  "Description":",
6  }, 34  "TrackImage":false,
7  "Steps":[ 35  "TrackImageName":null,
8  { 36  "Input":{
9  "Index":0, 37  {
10 "No":1", 38  "Item":"BtnOk",
11 "Title":"Hücreye Git Kapağı Aç", 39  "NextStep":2
12 "Description":", 40  },
13 "TrackImage":false, 41  {
14 "TrackImageName":", 42  "Item":"BtnBack",
15 "Input":{ 43  "NextStep":999
16 { 44  }
17 "Item":"BtnOk", 45  },
18 "NextStep":1 46  "NextScenario":null,
19 } 47  "Media":true,
20 }, 48  "Source":null,
21 "NextScenario":null, 49  "Animation":null,
22 "Media":true, 50  "TriggerName":null,
23 "Source":null, 51  "RekranMain":11",
24 "Animation":null, 52  "RekranSub":22",
25 "TriggerName":null, 53  },
26 "RekranMain":1",
27 "RekranSub":2"
28 },

```

Figure 9. The code for the first two steps of the ".json" file created for "No EQA Communication" scenario.

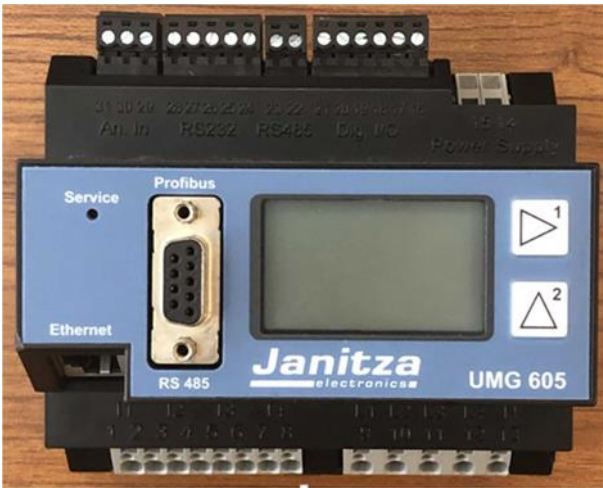
In Figure 10, a rectifier and RTU-DCU automation panels, as well as EQA used in these panels, can be seen in the photograph of a distribution center within SEDAS.

The developed AR application is used on the EQA device in this distribution center, and the scenario of "No EQA Communication" is executed. The EQA image obtained from the mobile device camera used by the operator is shown in Figure 11. Figure 12 shows some of the photographs of the scenario steps obtained when the "No EQA Communication" scenario is started for the device detected by the camera.





**Figure 10.** Automation panels of distribution center a) RTU, DCU and rectifier b) EQA in the panel.



**Figure 11.** EQA image obtained from mobile camera.

The operator switches between scenario steps by following the instructions specified in the scenario according to the fault and terminates the process. When the fault is fixed, the operations performed at each step are recorded with the "Finish/Save" button. On the other hand, when the fault remains unfixed, then this situation is recorded with the "Finish/Save Problem" button.

#### 4. Conclusions

AR is an innovative technology that has the potential to be applied in many different industries. In parallel with the increase in processor capacities in mobile devices and the image quality of cameras and the introduction of smart glasses and wearable AR systems for the end-user, it is predicted that AR applications will be used frequently in the electrical energy sector in the near future, as in other sectors.

Therefore, electrical energy suppliers also need to adapt to AR technology as quickly as possible in order not to lose their competitiveness in the market.

In the proposed study, a Software that works on AR technology-based mobile platforms is developed and used in maintenance and repair processes on protection/control panels and devices in SCADA centers, apart from routine maintenance activities. The main aim of using this Software is to provide task support by quickly detecting faults to field maintenance teams. For this purpose, a software application is implemented for possible fault scenarios that may occur in RTU and DCU automation panels of SCADA cabinets located in distribution centers. The gains from this application that also contributes to digital transformation can be listed as follows:

The fact that the teams of DM Department within SEDAS traveled multiple times to the distribution center where the defective cabin is located for detecting faults and MR operations in the SCADA cabins in the area of responsibility covering four provinces, causing time and budget losses. The ability to have these operations performed by field teams, thanks to the developed software application has minimized the losses. Thus, it is predicted to save approximately 50.000 TL per year. At the same time, with reduced fuel consumption, approximately 7 tons of carbon dioxide emission per year will be prevented and it will contribute to the reduction of the carbon footprint.

As the workload of the staff is reduced in the DM Department, which consists of an expert team, pending jobs can be handled faster.

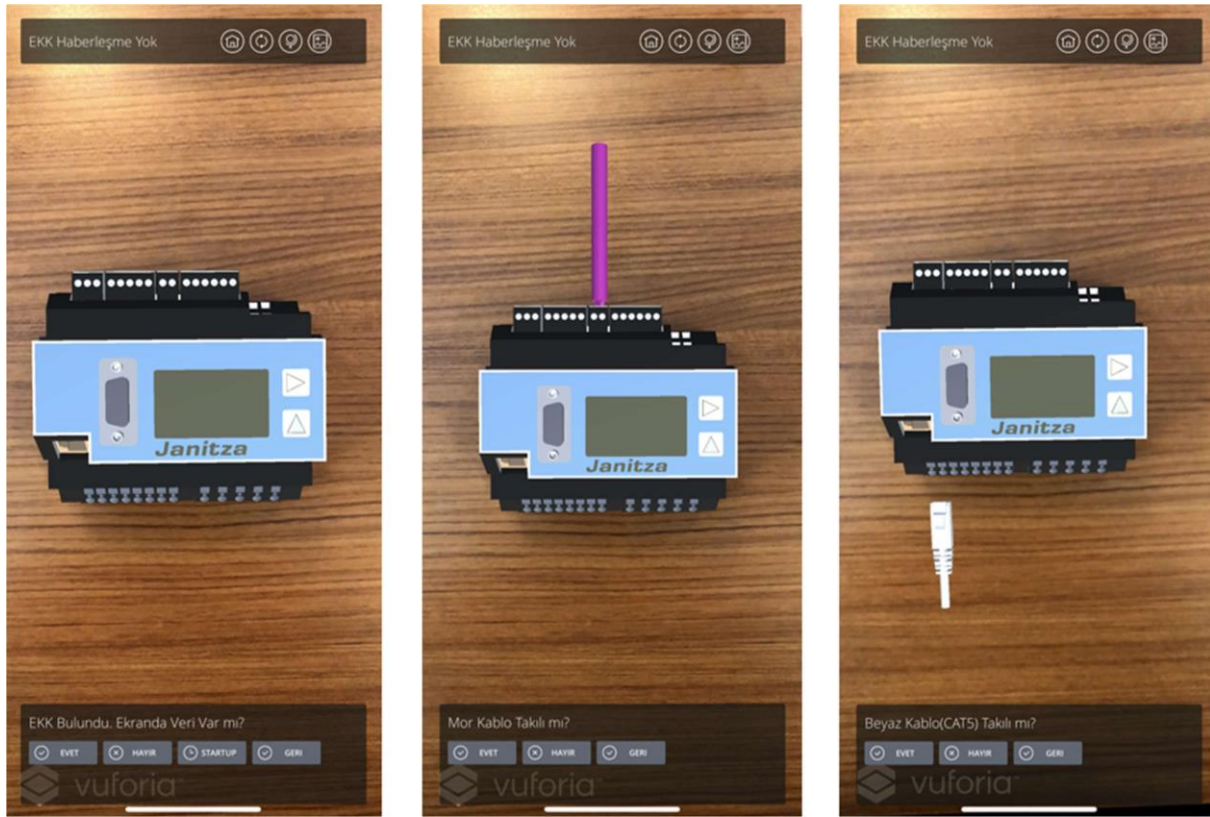
From the perspective of occupational safety, it is guaranteed to reduce the exposure of expert personnel to risks during long journeys. According to the risk assessment, the risk value, which is at the significant risk level, has been reduced from 600 to 150.

Thanks to the developed mobile application, human errors are reduced by following the steps that should be taken to eliminate the failure.

A backup facility, albeit partially, has been created expert personnel and a training portal has been provided for new recruits in the department.

The proposed study constitutes an example of the AR technology applications, which is rare in the electricity energy sector both in our country and in the world.

In short, the advantages of AR technology-based applications are they can be easily used in information transfer. They are highly productive, they have increased efficiency with a low error rate, high quality, and safety. The procedures are simplified, they have effective resource usage and capacity of early adoption of learning that makes the use of this innovative technology important.



**Figure 12.** Some of the images of the “No EQA Communication” scenario steps.

### Declaration of Ethical Standards

The authors of this article declare that the materials and methods used in this study do not require ethical committee permission and/or legal-special permission.

### Conflict of Interest

The authors declare that they have no known competing financial interests or personal relationships that could have appeared to influence the work reported in this paper.

### Acknowledgements

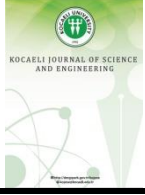
This study was supported by the "Maintenance-Repair and Training Applications in SCADA Operations with Augmented Reality Technology" project by EMRA.

### References

- [1] Porter M.E., Heppelmann J.E., 2017. Why Every Organization Needs an Augmented Reality Strategy. Harvard Business Review Magazine, **95**(6), 46-57.
- [2] AccuVein: <https://www.accuvein.com/why-accuvein/ar>, (05.03.2019)
- [3] Boeing Tests Augmented Reality in the Factory: <https://www.boeing.com/features/2018/01/augmented-reality-01-18.page>, (07.07.2017)
- [4] Hastings E.J., Guha R.K., Stanley K.O., 2009. Automatic Content Generation in the Galactic Arms Race Video Game. IEEE Transactions on Computational Intelligence and AI In Games, **1**(4), 245-263.
- [5] Matsutomo S., Miyauchi T., Noguchi S., Yamashita H., 2012. Real-Time Visualization System of Magnetic Field Utilizing Augmented Reality Technology for Education. IEEE Transactions on Magnetics, **48**(2), 531-534.
- [6] Sheng Y., Yapo T.C., Young C., Cutler B., 2011. A Spatially Augmented Reality Sketching Interface for Architectural Daylighting Design. IEEE Transactions on Visualization and Computer Graphics, **17**(1), 38-50.
- [7] Sirilak S., Muneesawang P., 2018. A New Procedure for Advancing Telemedicine Using the HoloLens. IEEE Access, **6**, 60224-60233.
- [8] Fraga-Lamas P., Fernández-Caramés T.M., Blanco-Novoa Ó., Vilar-Montesinos M.A., 2018. A Review on Industrial Augmented Reality Systems for the Industry 4.0 Shipyard. IEEE Access, **6**, 13358-13375.

- [9] Cheng K.H., Tsai C.C., 2013. Affordances of Augmented Reality in Science Learning: Suggestions for future search. *Journal of Science Education and Technology*, **22**(4), 449-462.
- [10] Rosenbaum E., Klopfer E., Perry J., 2007. On Location Learning: Authentic Applied Science with Networked Augmented Realities. *Journal of Science Education and Technology*, **16**(1), 31-45.
- [11] Pérez-López D., Contero M., 2013. Delivering Educational Multimedia Contents Through an Augmented Reality Application: A Case Study on Its Impact on Knowledge Acquisition and Retention. *The Turkish Online Journal of Educational Technology*, **12**(4), 19-28.
- [12] Parmar D., Pelmahale K., Kothwade R., Badgujar P., 2015. Augmented Reality System for Engineering Graphics. *International Journal of Advanced Research in Computer and Communication Engineering*, **4**(10), 327-330.
- [13] Bozyer Z., 2015. Augmented Reality in Sports: Today and Tomorrow. *International Journal of Science Culture and Sport*, **3**(4), 314-325.
- [14] Serino M., Cordrey K., McLaughlin L., Milanaik R.L., 2016. "Pokemon Go and Augmented Virtual Reality Games: A Cautionary Commentary for Parents and Pediatricians. *Current Opinion in Pediatrics*, **28**(5), 673-677.
- [15] Arroyo E., Arcos J.L.L., 1999. SRV: A Virtual Reality Application to Electrical Substations Operation Training. *Proceedings IEEE International Conference on Multimedia Computing and Systems*, 835-839.
- [16] Arendarski B., Termath W., Mecking P., 2008. Maintenance of Complex Machines in Electric Power Systems Using Virtual Reality Techniques. *Conference Record of the 2008 IEEE International Symposium on Electrical Insulation*, 483-487.
- [17] Cardoso A., et al., 2013. VRCEMIG: A Virtual Reality System for Real Time Control of Electric Substations. *2013 IEEE Virtual Reality (VR)*, 165-166.
- [18] Hernández Y., Ramírez M.P., 2016. Virtual Reality Systems for Training Improvement in Electrical Distribution Substations. *2016 IEEE 16th International Conference on Advanced Learning Technologies*, 75-76.
- [19] Peng Y., Yu G., Ni W., Lv Z., Jiang Y., Chen J., 2017. Design and Development of Intelligent Operation and Maintenance Training System for Substation Based on Augmented Reality. *2017 Chinese Automation Congress*, 4765-4769.
- [20] Cordonnier M., et al., 2017. Contribution of Augmented Reality to the Maintenance of Network Equipment, *International Conference on Electricity Distribution Open Access Proceedings Journal*, **1**, 87-90.
- [21] Martino S., Gonbeau O., Boisseau C., Recapet J., Blanc F., Augustin B., 2017. Enedis Field Experience of Augmented and Virtual-Reality Technologies at the Service of Network Operators. *International Conference on Electricity Distribution Open Access Proceedings Journal*, **1**, 1081-1084.
- [22] Sermet M.Y., Demir I., Kucuksari S., 2018. Overhead Power Line Sag Monitoring through Augmented Reality. *North American Power Symposium*, 1-5.





## A Case Study on the Assumption of Mean Radiant Temperature Equals to Indoor Air Temperature in a Free-Running Building

Mehmet Furkan ÖZBEY<sup>1</sup> , Cihan TURHAN<sup>2,\*</sup> 

<sup>1</sup> Department of Mechanical Engineering, Atılım University, Ankara, 06830, Turkey, **ORCID:** 0000-0002-5813-3514

<sup>2</sup> Department of Energy Systems Engineering, Atılım University, Ankara, 06830, Turkey, **ORCID:** 0000-0002-4248-431X

### Article Info

#### Research paper

Received : November 30, 2020

Accepted : March 15, 2021

#### Keywords

Adaptive Thermal Comfort  
Free Running Building  
Globe Thermometer  
Indoor Air Temperature  
Mean Radiant Temperature

### Abstract

Thermal comfort is basically affected by environmental (mean radiant temperature, indoor air temperature and relative humidity and air velocity) and personal parameters (clothing value and activity level). Mean Radiant Temperature is the most complicated parameter among all thermal comfort parameters due to the difficulty of measurement and calculation processes. Calculation methods are not preferred by the researchers because of the complexity of obtaining angle factors while the measurement methods require very expensive devices such as globe thermometers and radiometers. On the other hand, assumptions are commonly used in thermal comfort studies because of their simplicities. One of the most frequently used assumptions expresses the equality of mean radiant temperature to indoor air temperature. However, the accuracy of this assumption needs further experimental research in order to evaluate thermal comfort, especially in free-running buildings. To this aim, this study proposes to determine the accuracy of the assumption of mean radiant temperature equals to indoor air temperature in a free-running building where Adaptive Thermal Comfort approach is applied in summer condition. Environmental parameters are measured via objective sensors, while adaptive thermal comfort is assessed by a software program. The statistical results show that there are significant deviations between two parameters in summer conditions for a free-running building.

## 1. Introduction

The main concerns on thermal comfort are traditionally assessed with Fanger's Predicted Mean Vote (PMV) and Predicted Percentage of Dissatisfied (PPD) method for air-conditioned and/or mixed-mode buildings [1-3]. However, free-running buildings are without indoor climate control such as heating, cooling and ventilation [4]. Occupants have wider tolerance on their discomfort since windows and/or doors are allowed to be open when an occupant wants to re-satisfy thermal comfort in the indoor environment [5]. For free-running buildings, Adaptive Thermal Comfort (ATC) models are applied by using linear correlations linking an optimal comfort temperature to mean outdoor temperature [6-7]. Thus, obtaining

operative temperature (OT) is vital to obtain accurate thermal comfort for free-running buildings. In the calculation of OT, Mean Radiant Temperature (MRT), Indoor Air Temperature ( $T_i$ ) and Air Velocity ( $v_a$ ) are included [8]. In a free-running building, air velocity is uncontrolled since there is no ventilation controlling. For this reason, MRT and  $T_i$  values generally vary, which makes thermal comfort models difficult to obtain [9].

MRT is defined as "the temperature of a uniform, black enclosure that exchanges the same amount of heat by radiation with the occupant as the actual enclosure" in ASHRAE Standard 55 [1] and measured by globe thermometer, radiometers and constant air temperature sensors. However, the price of the sensors is very high, and the usage of these devices require highly skilled and expert users. On the other hand, calculation methods are very complicated due to determine the angle factors of the occupant [10,11]. Instead of calculation and measurement methods, the researchers prefer to use the assumption of

\* Corresponding Author: [cihan.turhan@atilim.edu.tr](mailto:cihan.turhan@atilim.edu.tr)



the equality of MRT and  $T_i$  [1,12-15]. However, the accuracy of the assumption is always a question mark for free running and/or air-conditioned buildings. To this aim, some researchers compare the assumption of the equality of MRT and  $T_i$ . In the studies, the comparison of the MRT and  $T_i$  values are assessed with an equivalent ratio [16]. For instance, Koch [17] studied the relationship between the MRT and  $T_i$  in ranges of 22.7°C to 29.9°C and 21.2°C to 26.9°C for  $T_i$  and MRT, respectively, in mechanically ventilated buildings with 12 different measurement data. As a result of the study, MRT and  $T_i$  had a difference up to 1.5°C, and the equivalent ratio was found as 0.669. In another study, McIntyre et al. [18] used 33 measurements between a range of 20.8°C to 23.8°C and 24°C to 28.5°C for  $T_i$  and MRT, respectively. The authors found the equivalent ratio as 0.791. Lin et al. [19] conducted research in mixed type buildings that have different heating systems of the radiator, radiant floor heating and all-air heating systems. The results showed that the difference between MRT and  $T_i$  was between -0.5°C to +0.5°C. Catalina et al. [20] handled research in the mixed type test chamber by using radiant ceiling panels and found 0.8°C difference between  $T_i$  and OT. The most blazing research was conducted by Dave et al. [15] that used over 200.000 measurement data in 48 different mechanically conditioned office buildings. The results demonstrated that the median absolute difference between the MRT and  $T_i$  was 0.4°C.

The assumption of the equality of MRT to  $T_i$  causes uncertainty on thermal comfort results. For instance, Chaudhuri et al. [21] investigated the effect of using the equality of MRT and  $T_i$  on the PMV in air-conditioned buildings. The experiments proved that using this assumption cause an error to the PMV value up to 1.54 PMV difference. Furthermore, De Dear and Brager [5] found that this assumption overestimated the occupant responses on ASHRAE 55 scales in high temperatures while using PMV/PPD method, which was originally created for air-conditioned buildings, in free-running buildings.

Even though the studies on the accuracy of the equality of MRT to  $T_i$  are common in air-conditioned buildings, the studies on the accuracy of the assumption are very limited for free-running buildings, especially in temperate climate zone. To this aim, this study investigates the accuracy of the assumption of MRT to  $T_i$  for a free-running building in a temperate climate zone by using ATC approach.

## 2. Materials and Methods

A free-running case-building (4.7m depth x 3.25m width x 2.75m height) was selected in a university campus

in Ankara, Turkey which is located in Csb-type climate zone according to the Köppen-Geiger Climate Classification [22]. The case building includes a large-glazed window (window to wall ratio is 3.6) in the south direction. Since the case building is a free-running building, Heating Ventilating, and Air Conditioning (HVAC) system does not exist, and the building is ventilated naturally. An outlook and architectural drawing of the case building are depicted in Figures 1 and 2, respectively.

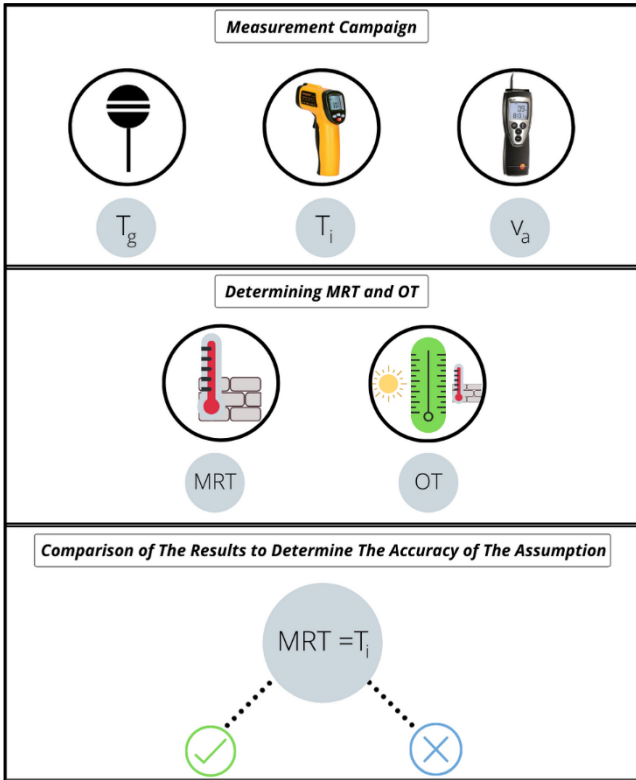


Figure 1. The outlook of the case building.



Figure 2. Architectural drawing of the case building.

The methodology of the study consists of three separate sub-sections, namely, measurements of  $T_i$ ,  $T_g$  and  $v_a$ , determining the MRT and OT via using Eq. (1) and Eq. (2) and comparison of the results to determine the accuracy of the assumption as shown in Figure 3.



**Figure 3.** The methodology of the study.

The MRT,  $v_a$ , and  $T_i$  measurements were taken on weekdays from 09:00 to 12:00 and from 13:00 to 17:00 with a 10-min interval between 15<sup>th</sup> of July 2020 and 6<sup>th</sup> of October 2020 including summer season. During the measurements, one male occupant was seated (metabolic rate value: 1 met) and occupant could open and/or closed the window and door, and the occupant was allowed to freely adopt clothing insulation to ensure thermal comfort since ATC standards were applied [23]. Besides, the outdoor temperature ( $T_o$ ) values were taken from Meteorological Station of the university.

$T_i$  values were taken with an infrared thermometer – EXTECH Measurements 42530 [24] – and  $v_a$  was measured with an anemometer – TESTO 425 [25] – inside the case building. The utilized devices in the measurement campaign and their specifications are indicated in Table 1.

**Table 1.** Utilized devices for measurements of  $T_i$  and  $v_a$ .

Device	Model	Specification
Infrared Thermometer	EXTECH Measurements 42530 [24]	Accuracy $\pm 2\%$ Resolution: 0.1 °C
Anemometer	TESTO 425 [25]	Accuracy: $\pm (0.03 \text{ m/s} + 5\% \text{ of Measured Value})$ Resolution: 0.1 m/s

On the other hand, the MRT values were obtained from a developed Globe Thermometer (GT) by the authors. The developed GT has 135 mm diameter with 0.6mm thick matt-black copper globe and k-type thermometer in the middle of the copper sphere. It is worth to note that the GT was calibrated with an industrial well-known globe thermometer. The MRT was calculated by using the Eq. (1), which is also indicated in ISO 7726 [26].

$$MRT = \left[ (T_g + 273)^4 + \frac{0.25 \times 10^8}{\epsilon_g} \left( \frac{T_g - T_i}{D} \right)^4 (T_g - T_i) \right]^{\frac{1}{4}} - 273 \quad (1)$$

where  $T_g$  represents the globe temperature,  $\epsilon_g$  defines emissivity of the globe, which is 0.95 for matt-black copper [26], and D is the diameter of the globe.

In ATC models, the OT, defined as *the temperatures of a body that can achieve in its natural environment*, was used [1,27,28] and calculated, as shown in Eq. (2).

$$OT = T_i + (1 - A)(MRT - T_i) \quad (2)$$

where A is equal to 0.5 if  $v_a$  is lower than 0.2 m/s, 0.6 if the  $v_a$  is between 0.2 m/s to 0.6 m/s and 0.7 if the  $v_a$  between 0.7 m/s to 1 m/s.

In order to check the accuracy of the assumption, the null hypothesis ( $H_0$ ) and the alternative hypothesis ( $H_1$ ) were constructed as; “There is no difference between the MRT and  $T_i$  in a free-running building ( $MRT=T_i$ )” and “There is a difference between the MRT and  $T_i$  in a free-running building ( $MRT \neq T_i$ )”, respectively.

The determination of the accuracy of assumption was provided with well-known statistical criteria which are Mean Squared Error (MSE) (Eq. (3)) and Determination of Multiple Coefficient ( $R^2$ ) (Eq. (4)) by using the MRT data stem from GT and  $T_i$ .

$$MSE = \frac{1}{p} \sum |z_i - o_i| \quad (3)$$

$$R^2 = 1 - \left( \frac{\sum |z_i - o_i|^2}{\sum o_i} \right) \quad (4)$$

where  $o_i$  represents the output,  $z_i$  defines the target, and p is the number of input-output pairs of  $i^{th}$  data [29,30].

Moreover, two-tailed *t-test* was used in the study in order to check the accuracy of the hypotheses (Eq. (5)). The significance level was selected as 5% [31,32].

$$t = \frac{\bar{x}_a - \bar{x}_b}{\sqrt{\frac{s_a^2}{n_a} + \frac{s_b^2}{n_b}}} \quad (5)$$

where  $\bar{x}_a$  and  $\bar{x}_b$  represents the means,  $S_a^2$  and  $S_b^2$  defines

standard deviation and  $n_a$  and  $n_b$  are the sample sizes of  $T_i$  and MRT, respectively.

In the final step, ATC graphs were drawn in order to compare both cases in different acceptance levels of 80% and 90%. The ATC acceptable upper and lower limits were described in Eqs. (6) and (7) for 80% acceptance limits and Eqs. (8) and (9) for 90% acceptance limits [1,33].

$$\text{Upper Limit}_{80\%} = 0.31 T_{out} + 21.3 \quad (6)$$

$$\text{Lower Limit}_{80\%} = 0.31 T_{out} + 14.3 \quad (7)$$

$$\text{Upper Limit}_{90\%} = 0.31 T_{out} + 20.3 \quad (8)$$

$$\text{Upper Limit}_{90\%} = 0.31 T_{out} + 15.3 \quad (9)$$

### 3. Results and Discussion

The MRT and  $T_i$  data were examined in order to determine the variation between two parameters and to check the accuracy of the null hypothesis, which was identified in Eq. (5). Moreover, Figure 4 represents the comparison of MRT and  $T_i$  data while the results of regression analysis are expressed in Table 2.

Figure 5 depicts the results of  $T_i$ , MRT, OT with respect to  $T_o$  values. Since the study was conducted in the summer season, the MRT values were found higher than  $T_i$  values.

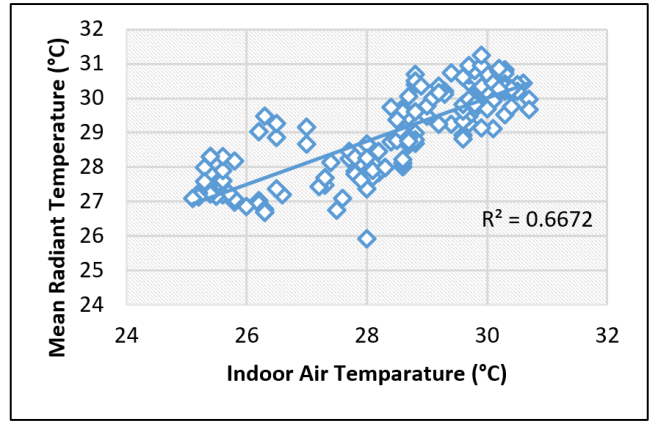


Figure 4. Comparison of measured MRT and  $T_i$  data with linear comparison method.

Table 2. Results of Regression Analysis

<b>Slope</b>	0.63
<b>Intercept</b>	11.08
<b>MSE</b>	1.22
<b>R<sup>2</sup></b>	0.66

The linear comparison analysis demonstrated that MRT and  $T_i$  had exceedingly different values with a  $R^2$  value of 0.66 and MSE of 1.22. MRT is generally bigger than  $T_i$  because the temperature of the glazing surface is greater than  $T_i$  and the short-wave solar radiation is significantly high in the summer season. The equivalent ratio was found as 0.85. In comparison with the mechanically ventilated buildings, the equivalent ratio was found slightly higher.

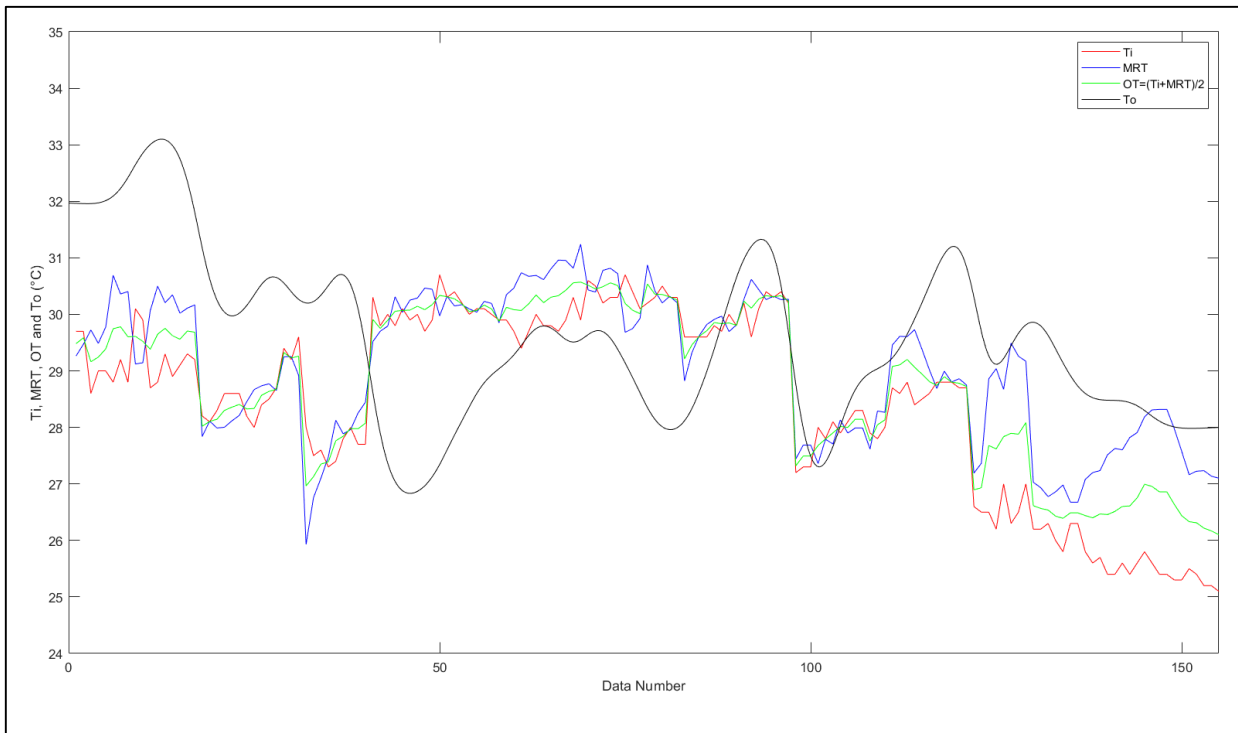


Figure 5. An example of measured values of  $T_i$ , MRT, OT and  $T_o$ .

Table 3 indicates the standard deviations (SD), mean values of MRT and  $T_i$  and t & p values.

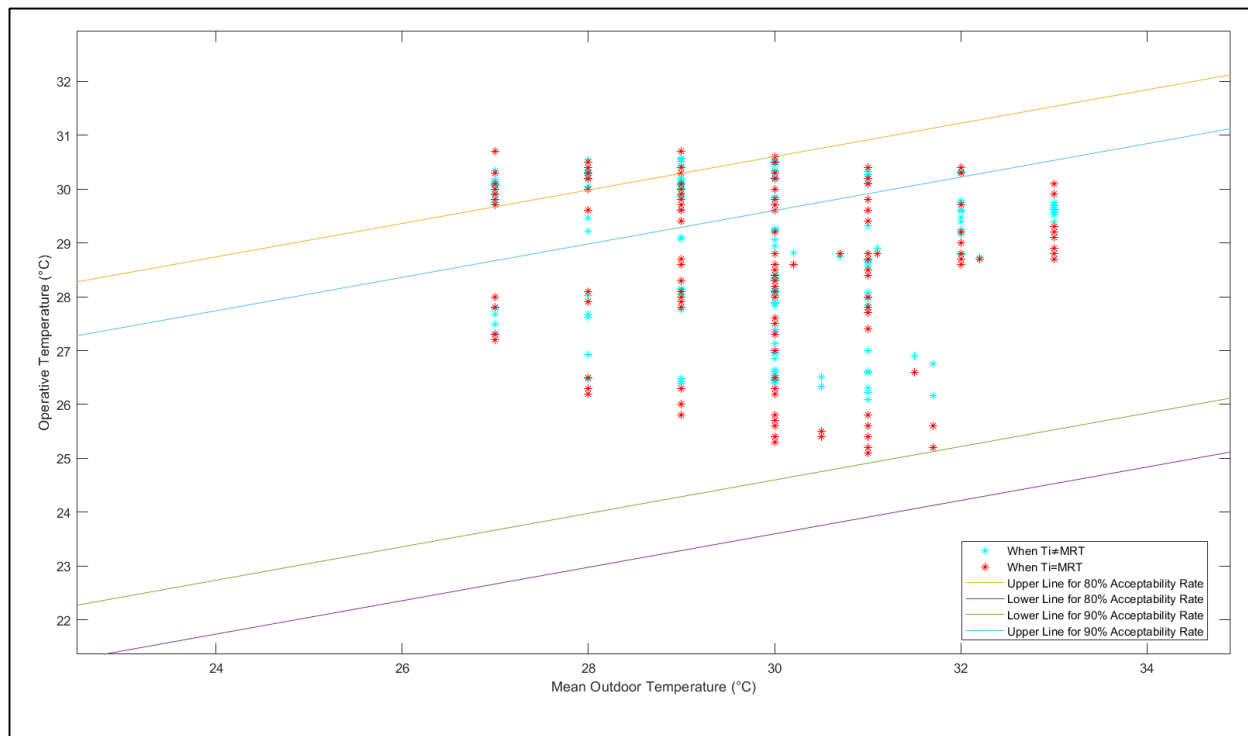
**Table 3.** Statistical values of the study.

	MRT	$T_i$
<b>SD</b>	1.27	1.64
<b>Mean</b>	29.05	28.45
<b>t-value</b>	4.18	
<b>p-value</b>	.001	

The two-tailed *t-test* revealed that the null hypothesis was rejected since the p-value was found lower than the significance value, which was selected .05 in the study.

Therefore, the equality of MRT and  $T_i$  hypothesis was rejected, and the alternative hypothesis was accepted.

Figure 6 depicts the effect of using the assumption of the equality of MRT and  $T_i$  to the ATC standards for acceptable limits of 80% and 90%, respectively. A significant difference was observed in both 80% and 90% acceptable limits. While comparing the OT data for 80% acceptance limit, using assumption changes the OT data of 30.4% to the out of the upper and lower acceptable limits. In the other side, the assumption changes the OT data of 27.4% out of the upper and lower acceptable limits of 90%.



**Figure 6.** Adaptive thermal comfort charts for 80% and 90% acceptance limits with temperature data.

#### 4. Conclusions

The MRT is the most crucial and difficult to obtain one of the environmental parameters which affect thermal comfort. There are three different methods to obtain to MRT in the indoor environment, which are calculation, measurement method and assumptions. The calculation methods are not preferred since its complexity and challenging calculation steps, and measurement methods are not chosen to obtain MRT due to the cost of equipment. Therefore, the MRT values are generally obtained by using the assumption of the equality of MRT and  $T_i$  in various studies because of its easiness. However, using this assumption brings along

the uncertainty about the accuracy of the assumption.

The evidence from this study discussed the accuracy of the assumption. The findings of this study do not support the idea of using the assumption of the equality of MRT and  $T_i$  in summer conditions for free-running buildings by using the linear comparative method and two-sample *t-test* method.

As a result of applied methods,  $R^2$  was found 0.66 and p-value was found .001. Besides, the equivalent ratio was depicted 0.853, which slightly higher than previous findings of mechanically ventilated buildings [16-18].

This study clearly has some limitations. As a first limitation, the occupant, who was inside the case building while taking the measurements, was an



additional heat source to the environment. Therefore, the MRT and  $T_i$  values could be affected from the occupant. Secondly, this study only examined the accuracy of the assumption in the summer season. The result should be discussed for winter condition in a free-running building. In winter conditions, since the radiative heat diffuses from the human body to the outside, the MRT is expected to be lower than the indoor air temperature. Furthermore, solar radiation values will be different as discussed in [1,34].

As future work, further experimental studies will determine the accuracy of the assumption also for the lower values of the MRT and  $T_i$ .

### Declaration of Ethical Standards

The authors of this article declare that the materials and methods used in this study do not require ethical committee permission and/or legal-special permission.

### Conflict of Interest

The authors declare that they have no known competing financial interests or personal relationships that could have appeared to influence the work reported in this paper.

### References

- [1] ASHRAE 55, 2017, Thermal Environmental Conditions for Human Occupancy
- [2] ISO Standard 7730, 1994, Moderate Thermal Environments-Determination of the PMV and PPD Indices and Specification of the Conditions for Thermal Comfort, International Standards Organization, Geneva, Switzerland.
- [3] Fanger, P.O., 1970. Thermal comfort. Analysis and applications in environmental engineering. Thermal comfort. Analysis and applications in environmental engineering.
- [4] Nicol, F. and Humphreys, M., 2010. Derivation of the adaptive equations for thermal comfort in free-running buildings in European standard EN15251. *Building and Environment*, **45**(1), pp.11-17.
- [5] De Dear, R.J. and Brager, G.S., 2002. Thermal comfort in naturally ventilated buildings: revisions to ASHRAE Standard 55. *Energy and Buildings*, **34**(6), pp.549-561.
- [6] Wagner, A., Gossauer, E., Moosmann, C., Gropp, T. and Leonhart, R., 2007. Thermal comfort and workplace occupant satisfaction—Results of field studies in German low energy office buildings. *Energy and Buildings*, **39**(7), pp.758-769.
- [7] Pfafferott, J., Herkel, S., Kalz, D.E. and Zeuschner, A., 2007. Comparison of low-energy office buildings in summer using different thermal comfort criteria. *Energy and Buildings*, **39**(7), pp.750-757.
- [8] CEN EN 15251, 2007. Indoor Environmental Input Parameters for Design and Assessment of Energy Performance of Buildings Addressing Indoor Air Quality. Thermal Environment. Lighting and Acoustics. European Committee for Standardization. Brussels, Belgium.
- [9] Van der Linden, A.C., Boerstra, A.C., Raue, A.K., Kurvers, S.R. and De Dear, R.J., 2006. Adaptive temperature limits: A new guideline in The Netherlands: A new approach for the assessment of building performance with respect to thermal indoor climate. *Energy and Buildings*, **38**(1), pp.8-17.
- [10] Kántor, N. and Unger, J., 2011. The most problematic variable in the course of human-biometeorological comfort assessment—the mean radiant temperature. *Central European Journal of Geosciences*, **3**(1), pp.90-100.
- [11] Wang, Y., Meng, X., Zhang, L., Liu, Y. and Long, E., 2014. Angle factor calculation for the thermal radiation environment of the human body. In *Proceedings of the 8th International Symposium on Heating, Ventilation and Air Conditioning* (pp. 447-455). Springer, Berlin, Heidelberg.
- [12] JOKL, M.V., 2015. 4 New Thermal Comfort Standards of the Czech Republic. *Standards for Thermal Comfort: Indoor air temperature standards for the 21st century*.
- [13] ROWE, D., 2015. 24 Warm and Sweaty: Thermal Comfort in Two Naturally Ventilated Offices in Sydney, NSW. *Standards for Thermal Comfort: Indoor air temperature standards for the 21st century*, p.48.
- [14] Itani, M., Ghaddar, N., Ghali, K. and Laouadi, A., 2020. Development of heat stress charts for older people under indoor environmental conditions. *Energy and Buildings*, **224**, p.110274.
- [15] Dawe, M., Raftery, P., Woolley, J., Schiavon, S. and Bauman, F., 2020. Comparison of mean radiant and air temperatures in mechanically-conditioned commercial buildings from over 200,000 field and laboratory measurements. *Energy and Buildings*, **206**, p.109582.

- [16] Guo, H., Aviv, D., Loyola, M., Teitelbaum, E., Houchois, N., and Meggers, F., 2020. On the understanding of the mean radiant temperature within both the indoor and outdoor environment, a critical review. *Renewable and Sustainable Energy Reviews*, **117**, 109207.
- [17] Koch, W., 1962. Relationship between air temperature and mean radiant temperature in thermal comfort. *Nature*, **196**(4854), pp.587-587.
- [18] McIntyre, D.A. and Griffiths, I.D., 1972. Subjective response to radiant and convective environments. *Environmental Research*, **5**(4), pp.471-482.
- [19] Lin, B., Wang, Z., Sun, H., Zhu, Y. and Ouyang, Q., 2016. Evaluation and comparison of thermal comfort of convective and radiant heating terminals in office buildings. *Building and Environment*, **106**, pp.91-102.
- [20] Catalina, T., Virgone, J. and Kuznik, F., 2009. Evaluation of thermal comfort using combined CFD and experimentation study in a test room equipped with a cooling ceiling. *Building and Environment*, **44**(8), pp.1740-1750.
- [21] Chaudhuri, T., Soh, Y.C., Bose, S., Xie, L. and Li, H., 2016, October. On assuming Mean Radiant Temperature equal to air temperature during PMV-based thermal comfort study in air-conditioned buildings. *IECON 2016-42nd Annual Conference of the IEEE Industrial Electronics Society* (pp. 7065-7070). IEEE.
- [22] Köppen-Geiger Climate Classification, 2009. Retrieved March 3, from <http://koeppen-geiger.vuwien.ac.at/> (Access Date: 30/11/2020)
- [23] EN 16798, 2019. Energy performance of buildings - Part 1: Indoor environmental input parameters for design and assessment of energy performance of buildings addressing indoor air quality, thermal environment, lighting and acoustics.
- [24] Extech Instruments 42530, <http://www.extech.com/display/?id=14256>, (Access Date: 30/11/2020)
- [25] TESTO 425 - Compact Thermal Anemometer, <https://www.testo.com/en-UK/testo-425/p/0560-4251>, (Access Date: 30/11/2020)
- [26] ISO 7726, 1998. Ergonomics of the Thermal Environment-Instruments for Measuring Physical Quantities.
- [27] Camacho, A., Rodrigues, M.T. and Navas, C., 2015. Extreme operative temperatures are better descriptors of the thermal environment than mean temperatures. *Journal of thermal biology*, **49**, pp.106-111.
- [28] Kazkaz, M. and Pavelek, M., 2013. Operative temperature and globe temperature. *Eng. Mech*, **20**(3/4), pp.319-325.
- [29] Allen, M.P., 2004. *Understanding regression analysis*. Springer Science & Business Media.
- [30] Dekking, F.M., Kraaikamp, C., Lopuhaä, H.P. and Meester, L.E., 2005. *A Modern Introduction to Probability and Statistics: Understanding why and how*. Springer Science & Business Media.
- [31] Schechtman, E. and Sherman, M., 2007. The two-sample t-test with a known ratio of variances. *Statistical Methodology*, **4**(4), pp.508-514.
- [32] Rumsey, D. J., 2016. *Statistics For Dummies*, 2nd ed., John Wiley & Sons, Nashville, TN.
- [33] Bughrara, K.S., Arsan, Z.D. and Akkurt, G.G., 2017. Applying underfloor heating system for improvement of thermal comfort in historic mosques: the case study of Salepçioğlu Mosque, Izmir, Turkey. *Energy Procedia*, **133**, pp.290-299.
- [34] Walikewitz, N., Jänicke, B., Langner, M., Meier, F., and Endlicher, W., 2015. The difference between the mean radiant temperature and the air temperature within indoor environments: A case study during summer conditions. *Building and Environment*, **84**, 151-161.



